NTNU

Norwegian University of
Science and Technology

Concept Study and Analysis of a Floating Bridge

Heidi Brede

Marine Technology
Submission date: July 2017
Supervisor: Bernt Johan Leira, IMT
Co-supervisor: Erkan Oterkus, University of Strathclyde

Norwegian University of Science and Technology
Department of Marine Technology

Preface

This thesis is the final project at the end of a five year integrated Master's degree in Marine Technoloy at the Norwegian University of Science and Technology (NTNU). The study was carried out over the course of 26 weeks while in Glasgow on exchange at the University of Strathclyde.

The topic and scope of work for the study was worked out in collaboration with my supervisor, and built in part on a project thesis written previously, *Static and Dynamic Analysis of a Floating Bridge*. The study mainly focused on the dynamic response of a floating bridge in waves, in particular a bridge concept suggested by the Norwegian Public Road Administration. In addition, some basic static responses were considered. All analyses were carried out using ANSYS 17.1.

Since I had worked with the same topic for my project thesis, getting familiar with the problem at hand was relatively quick. Instead, a significant amount of time was spent on creating a detailed model that yielded reasonable results. In retrospect, the choice of using ANSYS may have forced me to spend more time than necessary on making it work, but in the end I am happy with the results. Though not the easiest way, I am convinced I have learned a lot from struggling with the model and from having to calculate and apply everything manually.

Special thanks to supervisor Professor Bernt Leira for semi-regular Skype meetings, helpful advice and good cooperation. I'd also like to thank my co-supervisor Professor Erkan Oterkus for support and for making it possible for me to write my thesis at the University of Strathclyde.

Trondheim

July 23, 2017

Heidi Schjøll Brede

Abstract

A floating bridge is a structure carrying traffic across a body of water and whose supports floats on the surface. The history of the floating bridge goes as far back as around 2000 BCE, when their use was mainly military. Today, several large floating pontoon bridges help relieve traffic in and out of large cities and populated areas. In Norway, the National Public Road Administration (NPRA) have made plans to build floating bridges across two large fjords to replace the ferries that currently ship traffic across. One of these fjords is Bjørnafjorden, for which the NPRA have come up with a few different concept solutions for crossing. One of these concepts was chosen for this study to look closer at static and dynamic responses.

The model of the concept bridge was created in ANSYS 17.1, and several different analyses were performed; modal, static, regular wave and irregular sea state for three storm conditions. The main aim was to determine the dynamic response of the bridge in waves, to ensure traveller's safety and comfort even during certain storm conditions. Criteria included limitations to maximum accelerations in y- and z-direction, and maximum rotations about the x-axis.

The modal analysis showed that some vertical and horizontal eigenfrequencies of the bridge may coincide with environmental loads and could potentially be of concern. The static analyses with environmental and traffic loads showed that the bridge would remain structurally safe for maximum traffic and winds and currents with a 100-year return period. Of some concern were the responses to the regular wave analyses, as the results showed little coherency and were larger than expected. The reason for this was somewhat unclear, and the responses to regular waves should be studied further. The results from the irregular sea states were more consistent and showed that the bridge would be safe for traffic during storms with a 1-year return period. For more severe storms with return periods of 10 and 100 years the extreme responses exceeded the criteria limits, and would therefore not be deemed safe for traffic. This was not considered to be of concern, however, as the NPRA for safety reasons close bridges when wind speeds exceed 25 m/s, which they are likely to do during these storms.

Oppsummering

En flytebro er en konstruksjon som frakter trafikk over et parti med vann, og hvis fundament flyter på overflaten. Historien til flytebroen strekker seg så langt tilbake som 2000 fvt., da bruken stort sett var begrenset til militær. I dag benyttes flytebroer først og fremst til å avlaste trafikk ut og inn av byer og bebygde områder helt eller delvis omringet av vann. I Norge jobber Statens Vegvesen med å bygge flytebroer over to store fjorder for å erstatte fergene som frakter trafikken i dag. En av disse fjordene er Bjørnafjorden, som Statens Vegvesen har kommet opp med noen ulike konsepter for å krysse. Ett av disse konseptene ble valgt til dette studiet for å se nærmere på statisk og dynamisk respons.

Brokonseptet ble modellert i ANSYS 17.1, og flere ulike analyser ble utført; modal, statisk, regulærbølge og irregulær sjøtilstand for tre ulike stormer. Hovedmålet var å finne den dynamiske responsen til broen i bølger, for å forsikre at den er sikker for trafikanter selv i visse stormtilstander. Kriteriene besto av begrensninger på maksimale akselerasjoner i z- og y-retning, samt maksimal rotasjon om x-aksen.

Modalanalysen viste at noen av de vertikale og horisontale egenfrekvensene til broen kan sammenfalle med frekvensen til miljøkreftene og potensielt være grunn til bekymring og videre analyser. De statiske analysene med miljø- og trafikklaster antydet at broen vil beholde strukturell integritet selv for maksimal trafikk og strøm og vind med 100-års returperiode. Noe usikkerhet var knyttet til responsen ved regulærbølger, da resultatene viste liten sammenheng og var større enn forventet. Årsaken til dette var uklar, og responsen ved regulære bølger bør studeres videre. Resultatene fra irregulær sjøtilstand var mer konsekvente og viste at broen vil være trygg for trafikk ved en storm med 1-års returperiode. For sterkere stormer med 10- og 100-års returperiode vil derimot ekstremrespons kunne overstige grensene og dermed ikke anses som trygg for trafikk. Dette ble ikke sett på som et problem da Statens Vegvesen på grunn av sikkerhet stenger broer når vindhastigheten overskrider 25 m/s, hviket den vil ved disse stormintensitetene.

Contents

List of Figures

List of Tables

List of Symbols

This list describes several symbols used later in this thesis, mainly in the theory chapter

Hydrodynamics

α	Mass matrix multiplier for damping
β	Stiffness matrix multiplier for damping
ξ	Damping ratio, $= \frac{c}{c_{cr}} = \frac{c}{2m\omega}$
c	Damping
k	Spring stiffness
m	Mass
$Q(t)$	External force varying with time
u	Displacement
$\dot{u}$	Velocity
$\ddot{u}$	Acceleration

Current and Wind

η	Shielding factor
ϕ	Solidity ratio
ρ, ρ_w	Density of water
ρ_a	Density of air
C_D	Drag coefficient
U_∞	Incident flow velocity
U_c	Current velocity
$U_{T,z}$	Wind velocity averaged over time period T and height z over the sea surface

Wave Theory

ϵ	Phase angle
λ	Wave length
ω	Circular frequency
ω_n	Eigenfrequency
ϕ	Phase shift
ζ	Wave elevation
ζ_a	Wave amplitude
D	Duration of sea state
g	Acceleration of gravity
H_M	Most probable largest wave in sea state
H_s	Significant wave height
H_{m0}	Approximation of H_s
k	Wave number $= \omega^2/g$
T_p	Peak period
T_z	Mean zero crossing period
T_{m02}	Approximation of T_z

Statistics

μ	Statistical mean
σ	Standard deviation
σ^2	Variance

Chapter 1

Introduction

A floating bridge is, as the name implies, a structure floating on a body of water, designed to transport traffic from one edge of the water to the other. Its purpose is often, similarly to any other bridge, to offer a reliable, efficient and safe route of transportation between populated areas and thereby improve infrastructure. In ancient times, floating bridges were used mainly for temporary military purposes, but today they serve mostly to relieve traffic in and out of cities and populated areas surrounded by water. In Norway, floating bridges also serve the purpose of offering a faster means of crossing the deep and wide fjords that are found along the west coast of the country.

Several variations in design of floating bridges exist today, but the main principles are largely the same – pontoons float on the water and provide buoyancy sufficient to hold up the main structure and traffic. Because water does not offer a solid foundation, motions of the bridge have to be constrained in some way, mainly through mooring and/or the geometry and material of the bridge. In order to design a bridge that is safe and comfortable for travellers, detailed analyses of the behaviour of the bridge is of vital importance. These analyses can be done analytically or numerically, but with the advance in computer technology and the finite element method (FEM) over the past decade or so, the numerical analysis is usually more accurate and therefore preferred (Shixiao et al., 2005). Modal, static and dynamic analyses are of particular interest, and together they may provide valuable information about the response of the bridge

when acted upon by a variation of loads.

The National Public Roads Administration (NPRA) in Norway is currently working on a project to improve the Coastal Highway E39 along the west coast. This includes substituting ferry crossings with bridges, and in some cases the only realistic option is a floating bridge. The project has been going on for a few years, and several detailed studies have been carried out on different potential design solutions. One of these design concepts were chosen as the subject for the study in this thesis, and the NPRA's report (Larsen, 2016a) provided a lot of useful information and laid the basis for the study.

The aim of the study was to determine the responses of the bridge concept when subjected to sea states of different intensity and decide on a preliminary level whether the design would be safe for traffic or not. The main interest was translational accelerations and longitudinal rotations of the bridge, as these are important indicators to safety and comfort of road users. Maximum internal forces and stresses were also determined on a large-scale, global level to ensure structural integrity. Responses were determined through analyses in ANSYS for static loads, regular and irregular waves, and sea states with three different return periods.

Chapter 2 contains the history of and some future plans for floating bridges, focusing on the projects involved in the improvement of E39 in Norway. Theory considered important for the study is presented in Chapter 3, such as forces acting on a floating bridge, principles of hydrodynamics, wave theory and the finite element method. In Chapter 4, the model and methods used in the analyses are explained and justified in relation to the aforementioned theory. Chapter 5 contains the most relevant results from these analyses, which are discussed in Chapter 6. Chapter 7 presents the conclusion of the study and Chapter 8 suggests future work.

Chapter 2

Background

2.1 The History of the Floating Bridge

Historic evidence suggests that the floating bridge is not a new invention, but rather has existed in one form or another for about 4000 years. It is believed that an ancient Chinese people made some of the first floating bridges by mooring small wooden boats a few feet apart and placing wooden planks across as early as 2000 BCE. These early bridges were created in order to move armies and military equipment across rivers and lakes. Later, in the mid 5th century BCE, the Greek historian Herodotus mentioned three other important military floating bridges from the Black Sea area. Persian king Darius had two floating pontoon bridges built across the Danube and the Bosphorus at the end of the 6th century BCE. More formidable, however, was the floating bridge his son, Xerxes, built across the Hellespont (today's Dardanelles) in 480 BCE. It crossed a span of more than 1.5 km and contained two rows of about 300 ships each, lashed together with flax and papyrus cables. Wood and soil was laid on top and trodden hard, and railings added to the sides. According to Herodotus, it took seven days and nights for the troops to march across, due to their vast numbers (Watanabe and Utsunomiya, 2003; Brown, 1993).

Since ancient times a lot has changed with regards to technology, materials and design of floating bridges, but the main idea remains the same – floating pontoons (or similar) provide the buoyancy to hold up a girder which carries the traffic. Although temporary floating bridges are

still in use by military today, several permanent bridges for civilian use have been built over the past two centuries.

In 1820 Brookfield in Vermont, USA, got its first tentative floating bridge across the local lake as a reaction to a resident going through the ice and drowning the previous spring. Logs were laid across the ice in winter and bound together, which, when the ice melted in spring, turned into the first floating bridge in the USA. The bridge has since been rebuilt or reinforced several times with more modern materials. The latest version, number eight, opened in 2015 and was the first floating bridge in the world with a foundation of reinforced polymer, which is a material highly resistant to corrosion, stress and strains. The bridge is decked with woodplanks and a wooden railing in order to maintain the traditional look, which was of high importance to the local community (Vermont Agency of Transportation, nd; VtransTV, 2015).

From the mid- to late 1800s, railroad traffic increased around the upper Mississippi River in Iowa and Minnesota, USA, because of the northwards extension of the railways. Crossing the river was a challenge, however, and at first rail cars were shipped across on towed barges. This was slow and inconvenient, and in 1874 a wooden railway bridge was constructed. It crossed the two canals of the river on two 124 m long wooden pontoons, one in each canal, that could be moved to allow waterborne traffic to pass. The bridge was deconstructed in 1961, and trains now cross the Mississippi River in Savanna, Illinois or La Crosse, Wisconsin (Lindeman, 1965).

In 1912, the first floating steel bridge was constructed in Istanbul, Turkey, because the soft bottom of the Golden Horn inlet was deemed unfit to hold regular piers. The Galata Bridge was 460 m long, 25 m wide and consisted of 26 pontoons carrying the traffic deck. It was followed by a similar construction in 1938, the Unkapani Bridge, which was placed only a few hundred meters further up the Golden Horn. Both bridges were replaced in 1993 to meet the high traffic demand of the city. The new bridges are supported on piles, made possible due to new technology (Arda et al., 1996; Shixiao et al., 2005; Watanabe and Utsunomiya, 2003).

The area around Seattle, USA, also experienced an increase in traffic in the early 20th century, which was a challenge due to Lake Washington separating the city from the surrounding areas. In 1940, a concrete bridge was therefore opened across the 2018 m wide lake, making it the largest floating bridge of its time. The Lacey V. Murrow bridge is still in use on the Washington

Lake today, together with two other bridges of similar build, letting hundreds of thousands of commuters pass in and out of the city every day (Lwin, 93).

In the 1960s, the number of commuters along parts of the west coast in Norway got so high in places that ferry crossings were no longer an effective way to cross the fjords. Planning, designing and obtaining permissions to build a feasible solution took several years, but by the early 1990s two floating bridges had been built to overcome the traffic challenge. The first bridge was built across Bergsøysund north of Molde, the other by Salhus just north of Bergen. The bridges consisted of concrete pontoons and unique, innovative steel superstructures, the technology for which came partly from the experience and expertise associated with the booming oil industry in the country (Lwin, 2000; Watanabe and Utsunomiya, 2003). New technologies are presently being developed in Norway in order to meet the increasing traffic demand and crossing fjords deeper and wider than previously possible.

Evidently, the history of the floating bridge extends far in both time and geographical range. Although major improvements have been implemeneted over the last few decades, technology continues to develop and open up for new opportunities. Utilising new technology and knowledge together with concepts that have been in use since the ancient times might just provide the range of expertise needed to come up with innovative new designs literally stretching further than ever before.

2.2 Strengths and Weaknesses of the Floating Bridge

Bridges are usually effective ways of connecting islands and peninsulas with each other and/or the mainland. The societal benefits can be quite substantial, as it improves the infrastructure between cities and surrounding areas, which saves commuting time and may therefore benefit job markets, productivity and competition. However, in some instances a traditional suspension or pillar bridge might not be feasible due to wide or deep water, or because the bottom is too soft to support a pillar bridge foundation. One example is the crossing of Lake Washington in Washington, USA, where the lake bottom consists of deep layers of soft clay. Here, floating bridges were found to be the most cost-efficient way of crossing the water (Lwin, 93). Another

example is the 3.7 km wide and 1.25 km deep Sognefjorden in Norway, the crossing of which is part of the Coastal Highway E39 (Jakobsen, 2013). A pillar bridge is not feasible due to the depth, and a suspension bridge is not achievable with today's technology. Currently the fjord has to be crossed by ferry, which is both time consuming and expesive for travellers. Ferries also use costly fuel and requires regular maintenance. While a floating bridge would be a large one-time investment, they are usually designed for a 75-100 year lifetime and ideally require limited maintenance (Lwin, 2000; Falk-Petersen et al., 2016; Ulstein et al., 2015).

While a floating bridge might be the only or the most economical way to carry road traffic across a body of water, there are certain associated challenges that need to be addressed early on in the design phase. The bridge may create an obstacle for waterborne traffic, in which case a means of crossing needs to be implemented. This could be achieved by elevation or submersion of parts of or the entire structure, or by including movable spans in the design. However, these solutions may create new challenges like loss of stabilisation and increased need of maintenance. Another issue specific to floating bridges occurs due to the movement of the water surface. It is important to design the bridge and its foundations in a way that limits translations and accelerations caused by currents and waves, due to both safety and comfort of the users. In addition, the bridge might be subjected to tidal variations, for which the connections to land at each end need to accommodate. Challenges with regards to corrosion, marine growth and the construction process also needs to be dealt with. The safety of travellers in the event of an accident is another matter of high importance, as immediate evacuation off the structure might not be a possibility. One alternative is to provide safe places along the structure where people can stay safely until evacuation is possible (Watanabe et al., 2004).

2.3 Different Concepts of Floating Bridges

There are several ways in which to design a floating bridge, and the choice of design will depend on environmental conditions like width and depth of water to be crossed and exposure to wind and waves. Other factors may be economy and limitations in existing technology (Statens Vegvesen, 2011). So far only continuous and separated pontoon bridges are in existence, but other

concepts are under development.

2.3.1 Continuous Pontoon Bridge

This type of floating bridge consists of a number of pontoons rigidly joined together at the ends to form one long girder. The traffic can be carried either directly on the pontoons or on a structure built on top. The pontoons can either be identical or of different lengths to accommodate certain environmantal factors and/or design requrements, and they need to be moored with anchors to be able to withstand transverse forces. Usually, the pontoons are divided into several watertight compartments in order to be able to remain afloat in the event of a collision or other accidents. The bridges on Washington Lake in the USA are all examples of continuous pontoon bridges (Lwin, 2000)

2.3.2 Separated Pontoon Bridge

A separated pontoon bridge consists of a bridge beam supported by floating pontoons that are not directly connected to each other. The bridge girder is most commonly a steel superstructure, and needs to be sufficiently strong and stiff to maintain relative position to the pontoons. The pontoons can either be moored individually, or the bridge can be shaped like an arc and anchored at each end to resist transverse forces. Two examples of the latter are the Nordhordland and Bergsøysundet bridge in Norway (Lwin, 2000).

2.3.3 Suspension Bridge With TLP Foundations

A third option for a floating bridge, the feasability of which is currently being studied by the NPRA in Norway, is the suspension bridge with tension leg platform (TLP) foundations. This type of bridge has few, long spans held up by suspension cables. These cables are in turn held up by towers resting on TLPs, which stay afloat because their buoyancy is greater than the gravity of the structure. They are tethered to the sea floor through anchors, and these tethers are kept at

a constant tension, which creates both vertical and horizontal stiffness. When sufficiently pre-tensioned, the tethers will virtually remove all heave, roll and pitch motion as well as counteract horizontal displacements (Statens Vegvesen, 2016a).

2.3.4 Submerged Tunnel

Although commonly not called a bridge, submerged tunnels provide the same service as a bridge – carrying traffic from one edge of a body of water to the other. Some options were looked into by the NPRA in the 1990s for crossing Høgsfjorden, and again more recently as an alternative for crossing Bjørnafjorden and Sognefjorden. A submerged tunnel consists of either one or two concrete and steel tubes through which the traffic can pass. The tubes can either be held afloat by pontoons floating on the surface, or the tunnel can have positive buoyancy and be moored to the bottom. Safety with regards to ship collisions and other accidents is of high importance, and more analyses and tests need to be conducted before this kind of construction can become reality (Falk-Petersen et al., 2016; Statens Vegvesen, 2011).

2.3.5 Temporary Military Bridges

As previously mentioned, floating bridges have been used for military purposes since ancient times. A lot has happened over the course of the 20th century, however, with lighter material and higher load capacity as well as shorter construction time and less personnel required to set it up. The U.S. military's floating bridges generally consist of pontoon modules that can be combined and locked together to form a temporary bridge. The improved ribbon bridge (IRB), invented in 2003, can accommodate two-way traffic, is air transportable and can be installed as a floating bridge or used as a ferry. The U.S. military also makes use of floating causeways, i.e. connections from ship to shore to transport supplies to troops on land. These are created similarly to the bridge by combining modules, and one prototype consists of an aluminium deck resting on lightweight pneumatic floats (Russell and Thrall, 2013).

2.4 Floating Bridges in Existance Today

Several large, permanent floating bridges can be found around the world today in North America, Europe and Asia. Although there are variations in design solutions, they are all pontoon bridges, of either the continuous or separated kind.

2.4.1 Lake Washington Bridges

Lake Washington in the US separates the big city of Seattle from other city areas to the east. Already in the early 1920s it was evident that an expanded east-west transportation system was needed across Washington state. The traffic on the existing roads was heavy, especially during winter time when some roads had to be closed for the season. Due to the deep layer of soft mud on the bottom of Lake Washington, a conventional bridge structure was estimated to be more challenging and expensive than a floating bridge. Lake Washington was also ideal for a floating bridge because the water level was regulated and there were no currents, drift or ice to take into consideration (WSDOT, 1990).

Figure 1: Construction of the Lacey V. Murrow Bridge (Washington State Archives, nd)

In July 1940 the largest floating bridge of its time, the Lacey V. Murrow Bridge (Figure 1), was opened to traffic. It is made up by 25 continuous pontoon sections up to 107 m long, 18 m

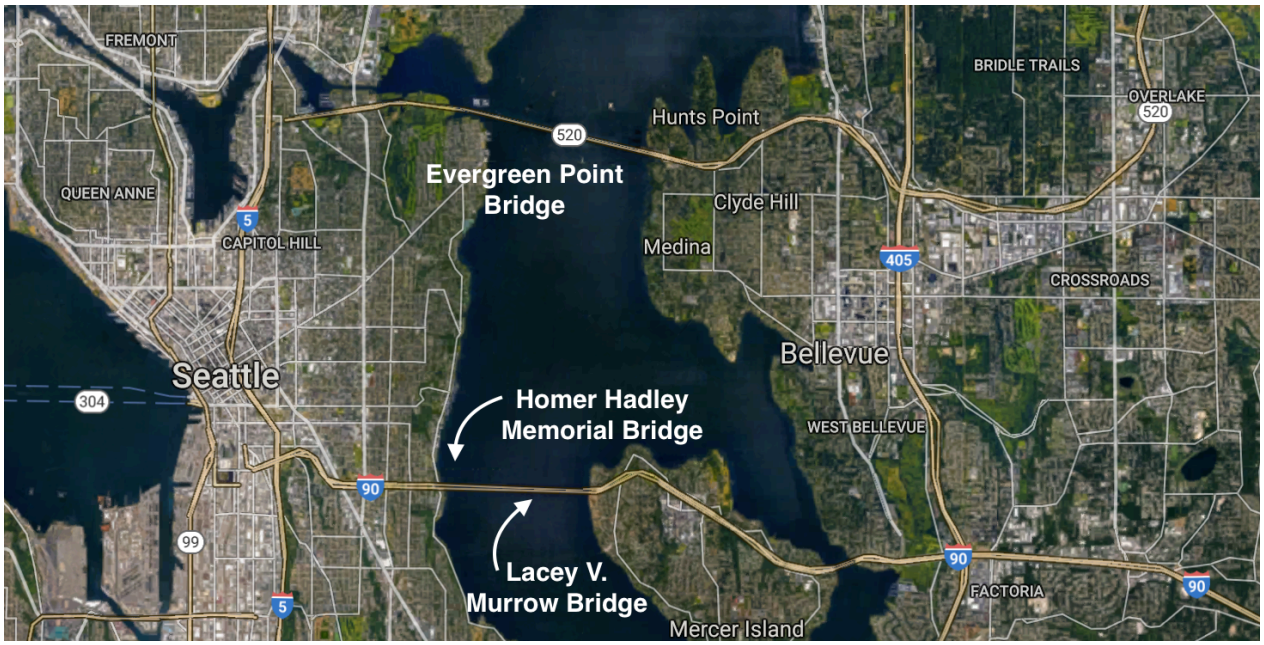

Figure 2: Lake Washington with the existing bridges named and marked (Google Maps, nd)

wide and 4.4 m deep that consist of twelve watertight compartments. The pontoons are rigidly connected end to end, essentially creating a 2018 m long girder across the lake. For stability, cables are attached to the pontoons and secured to the bottom with anchors (Lwin, 2000). Unfortunately, during renovation work in November 1990, one of the pontoons took in water and started sinking, soon dragging the other pontoons with it. The bridge disappeared under water, but was later rebuilt and is still there today (History.com, 2010).

In 1989 an additional bridge, the Homer Hadley Memorial Bridge, was built next to the Lacey V. Murrow bridge to accommodate for the increase in traffic. It is of similar construction as the first bridge, but is 22 m wide and was by that the widest floating bridge in the world at the time of its construction (WSDOT, 2003). Two other floating bridges have also been built across Lake Washington, further north. The Evergreen Point Floating Bridge, shown on the map in Figure 2, was the second bridge to be built on the lake, in 1963. It was 2310 m long, 18 m wide and consisted of 33 continuous pontoons held in place by 58 anchors. It was replaced when the new bridge with the same name opened in April 2016. The new bridge is 2349 m long, consists of 77 continuous pontoons and is almost twice as wide as the old bridge, with an extra high occupancy vehicle lane in each direction (WSDOT, 2016).

2.4.2 Bergsøysundet Bridge

Bergsøysundet bridge was opened in 1992 and was the first floating bridge in Norway. It connects two islands along the E39, an important coastal road in the Norwegian national road system. The fjord between the islands reaches a depth of 320 m, making it inconvenient to build a bridge resting on the sea floor (Watanabe and Utsunomiya, 2003). The bridge is 914 m long, with a floating span of 845 m. The seven pontoons are 20 m wide, 34 m long and 5.8 m high. The bridge is shaped like an arc with a radius of 1300 m, which results in lateral wind and current forces being transferred as axial loads to the stationary foundations in each end. Mooring of the pontoons is therefore superfluous, which may prove economical and time saving for the construction of a floating bridge as it is fastened by the foundations at each end only (Johs.holt, nd).

Figure 3: The Bergsøysundet bridge, with the steel superstructure clearly seen resting on the oval pontoons (Johs.holt, nd)

2.4.3 Nordhordland

The plans for a bridge across the Salhus fjord started in the late 1960s because of the large number of commuters that needed to be ferried across each year (1,683,000 vehicles in 1993). After

many years of planning, the Nordhordland bridge was opened in 1994, making it easier for thousands of people in the nearby areas to travel between the islands and the coast. The bridge is 1614 m long, out of which the floating part comprises 1246 m. In the south end, a 369 m long cable bridge connects with the floating bridge, creating a 32 m high underpass for vessels. The rest of the bridge floats on ten pontoons and is shaped like an arc with radius 1700 m, similar to the bridge at Bergsøysund, to avoid the challenge of mooring lines. The pontoons are 42 m long, 20.5 m wide, 4.3-5.6 m deep and placed 113 m apart. They are divided into nine watertight compartments, to maintain buoyancy even if one side is damaged by a colliding ship, for example. The bridge is held in place by a foundation at 30 m depth at the southern end, and a foundation on land in the northern end. On top of the pontoons rests the steel box girder, which is a continuous steel construction with an octagonal cross section, uniform apart from reinforcements at the pontoons and bridge ends. For most of the length of the bridge, vehicles, cyclists and pedestrians are transported directly on the steel girder. For the last 414.5 m in the southern end, a viaduct and the cable bridge leads the road up from 11.0 to 34.4 m above sea level (see Figure 4) (Statens Vegvesen, 1994).

Figure 4: View of the Nordhordland bridge with the cable bridge, underpass and arced shape visible (Broer.no, nd)

2.4.4 Osaka Bay

In July 2000 a 410 m long floating swing bridge with a long-spanned separated foundation was built in Osaka Bay, Japan. The Yumemai bridge was the first of its kind and consists of two steel pontoons 280 m apart that are moored to moveable reaction walls. These reaction walls can detach when needed to swing the bridge around its pivot point and let large ships pass (see Figure 5). This operation takes place only a few times a year, as most vessels can pass under the span of the bridge. The bridge accommodates three traffic lanes in each direction, and connects two islands to the main road network in the area (Watanabe and Utsunomiya, 2003).

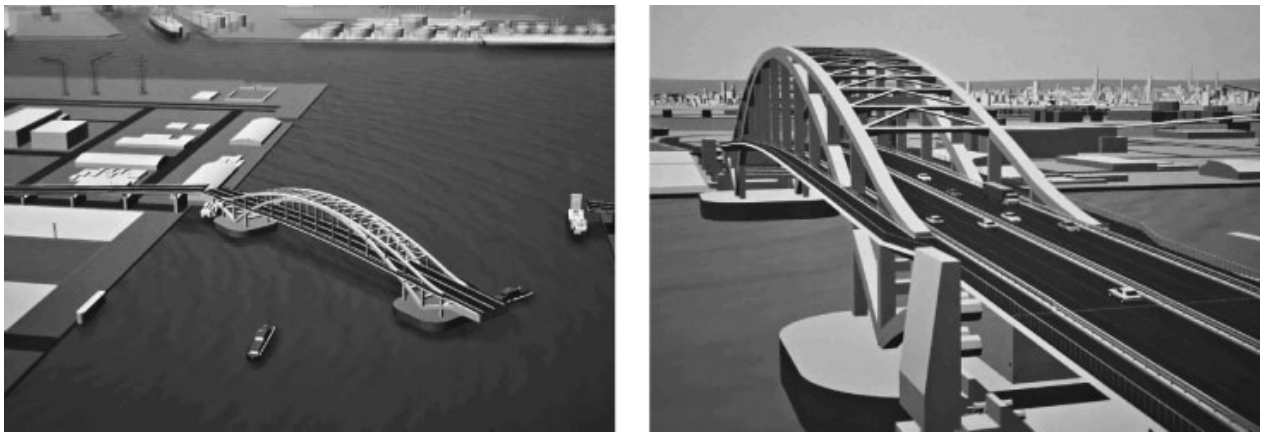

Figure 5: The Yumemai Bridge in Japan (Watanabe and Utsunomiya, 2003)

2.5 "Ferjefri E39" in Norway – Connecting the West Coast

Norway, although a relatively small country, has one of the longest coastlines in the world. According to Statistics Norway (2013) the coastline stretches 83,281 km, without accounting for Svalbard and Jan Mayen. This is largely because of the high number of islands and fjords along the Norwegian coast, and especially the west coast holds many deep and wide fjords. This poses challenges to local infrastructure as roads have to be built around the edges of the fjords, adding substantially to travel time, or bridges and ferry crossings have to carry traffic across the fjords, adding to costs and maintenance time.

The Coastal Highway E39 is the main road connecting the larger cities along the Norwegian

Figure 6: Map over E39 from Kristiansand to Trondheim with today's ferry crossings marked (Falk-Petersen et al., 2016)

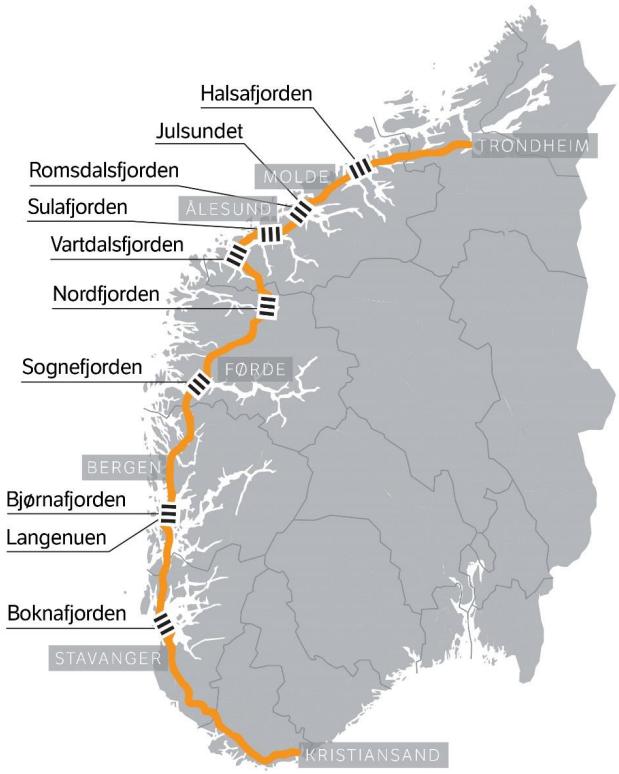

south- and west coast, and it stretches 1068 km from Kristiansand in the south to Trondheim in the middle of Norway. With today's seven ferry crossings and winding, narrow roads, travelling this distance takes about 21 hours with an average speed just above 50 km/h. This is highly inefficient and time consuming for people and businesses situated along the west coast, which ultimately affects the economies and job markets all over the country (Ulstein et al., 2015). To improve the infrastructure and productivity along the coast, the Norwegian Parliament confirmed in the National Transport Plan (NTP) for 2014-2023 that the E39 is to become free of ferry crossings within twenty years. The roads are also to be improved in general, to two- and four lane highways, allowing for higher average speeds. Through these measures, the Norwegian Public Road Administration (NPRA), who are in charge of the project, aims to shorten the total travel time to just over 10 hours (Falk-Petersen et al., 2016).

The project is still largely in the planning phase, where the aim is to come up with feasible, cost-effective solutions for crossing the fjords and improving the roads. In many cases, tunnels

under or suspension bridges over the fjords are the most realistic options. These technologies are already well-known, and therefore relatively easy to implement. For example has it been decided by the NPRA that Boknafjorden and Romsdalsfjorden will be crossed by tunnels under the sea, and Langenuen, Nordfjorden and Julsundet by suspension bridges. In the latter cases, the fjords are just narrow enough to make suspension bridges a possibility with existing technology. Other fjords, like Halsafjorden, Sulafjorden, Sognefjorden and Bjørnafjorden, are so wide (wider than a few kilometres) that existing technology does not offer any solutions. In these cases, the NPRA together with engineering companies in Norway are working to develop new technology, including new concepts for floating bridges (Falk-Petersen et al., 2016). At this point in time, the passages over Sognefjorden and Bjørnafjorden are the most developed, and will be discussed in more detail below.

2.5.1 Socioeconomic Benefits of a Ferry Free Highway

Because of the shape of the land and quality of the roads, even driving short distances along E39 can take a lot of time. This, together with the added time spent waiting for and crossing fjords with ferries, means that commuting large distances along the west coast is tedious and time consuming. In general, people are willing to commute to work if they live within one hour of their work place (So et al., 2001), which on the west coast of Norway means the job markets are geographically limited. Improving the quality of the roads and creating reliable, safe and shorter travel options across the fjords may significantly benefit job markets and society in general (Statens Vegvesen, 2015b). The NPRA are working together with experts in macroeconomics and economic analysis to quantify and qualify the effects of a ferry free and improved E39. Norman and Norman (2012) looked at the effect of an improved E39 on the job market in Møre og Romsdal, a county on the west coast of Norway. In the study they identified four larger job markets within the county, with little or no integration amongst them. By assuming a ferry free and improved coastal highway, the study concluded that the county could gain 1.3 billion NOK per year. This result was a simplified estimate, and would be reached only if and when the market was fully integrated. Nevertheless, the study suggests there could be a significant benefit of an improved infrastructure and accessibility in the county, and it may be safe to assume

this sort of effect could apply elsewhere too. So et al. (2001) similarly concluded that improving means of transportation into metropolitan areas may boost the economy in surrounding rural areas. Therefore, substituting ferries with bridges and expanding the road network is not just money spent on shortening commuting and travel times, but also an investment into the future economy and society.

2.5.2 Environmental Consequences

Expanding and developing the Coastal Highway E39 is likely to have some effect on the environment, both with regards to aesthetics, flora and fauna, and pollution. The goal is to increase the speed limits along the highway, which means making the roads wider and straighter. This change will lay claim to large areas and could in some places greatly affect the landscape. Alterations in the landscape may affect the wildlife and historic sites, and obstruct recreational activities for locals or tourists. The NPRA is focused on avoiding conflict where possible, partly by designing roads and bridges of "high architectural quality" (Falk-Petersen et al., 2016, p. 37). This is especially relevant with regards to the bridges that are to replace the ferries, as many will be prominent features in the landscape and potential eye-sores.

The effect on nature is important to consider when expanding and improving road systems. Habitats of species on the Norwegian redlist (Henriksen and Hilmo, 2015) may need to be carefully avoided, or wildlife may pose a threat to vehicles. The NPRA has done extensive research and planning in the areas that will be affected, and reports for the different sections of E39 can be found on their website (www.vegvesen.no). Rådgivende Biologer (English: Advisory Biologists. Todt et al., 2015) did a detailed investigation of the marine environment between Stord and Os, including Bjørnafjorden. The resources in the fjord were found to have little to moderate value, and the impact of different bridge designs on the marine life was assessed. A floating tunnel with pontoons was found to have the least impact, with an arced floating bridge coming second. This is the concept that will be analysed closer in this thesis.

Pollution is another issue that should be addressed when developing roads, with special interest in CO_2-emissions. Table 1 contains a list of factors that will change with the "Ferry Free E39"

Table 1: Effects of an improved E39 on net emissions (Falk-Petersen et al., 2016, p. 38)

Increased traffic	increased emissions
Improved geometry	decreased emissions
More consistent speeds	decreased emissions
Higher speeds	increased emissions
Construction, operation and maintenance of fjord crossings	increased emissions
Construction, operation and maintenance of roads	increased emissions
Fewer ferries	decreased emissions
Less air traffic	decreased emissions
Less express boat traffic	decreased emissions

project, and how they will affect net emissions over time. According to the National Transport Plan (Falk-Petersen et al., 2016), total CO_2-emissions are expected to decrease substantially in a 40-year perspective. The emissions could potentially be lower with no E39 improvements, however, as the NPRA expects all ferries in Norway to run on biodiesel by 2030. Nevertheless, the socioeconomic benefits of a ferry free highway are likely to outweigh this difference.

2.5.3 Sognefjorden

Sognefjorden is the world's second longest fjord, measuring 205 km long, and Norway's deepest fjord with a maximum depth of 1308 m (Askheim and Thorsnæs, 2016). The fjord's ferry crossing is 5.5 km long, and takes about 20 minutes from one side to the other (Norled, nd). The same distance by car, assuming an average speed of 80 km/h, would take just over 4 minutes. Sognefjorden is 3.7 km wide and 1.25 km deep at the planned location of the bridge. In a study first presented in 2012, Jakobsen mentions that finding a solution to crossing a fjord of this width and depth may also solve similar problems for other fjord crossings. Hence, finding a feasible way of crossing Sognefjorden could be crucial in realising the project of a ferry-free coastal highway in Norway. According to a status report from Statens Vegvesen (2015b), the possibility studies carried out for Sognefjorden around 2012 confirmed that crossing a wide and deep fjord is possible with either a floating pontoon bridge, a floating suspension bridge or a submerged tunnel. This was further backed up through analyses of bridge concepts for Boknafjorden and Bjørnafjorden. A few different design concepts were proposed, some of which are presented below. The NPRA has not yet settled on a design, and have scheduled the construction start as late as 2031.

Arced Pontoon Bridge with Mid-Span

Similarly to the two existing bridges in Norway, this design consists of a horizontally arced bridge girder supported by several pontoons. Differently, however, the span under which large ships are allowed to pass is placed at the middle of the bridge rather than close to land. Two pontoons are larger than the others and placed at the middle of the bridge, a few hundred meters apart. Each pontoon supports a tower from which cables hold up the bridge span. The bridge concept can be seen in Figure 7. The arced shape of the bridge means mooring of the pontoons is unnecessary, which is convenient when the fjord is as deep as Sognefjorden. This solution is relatively cost and time efficient compared to other solutions, but limits marine traffic somewhat because of the low elevation for most of the bridge's length (Jakobsen and Larsen, 2012).

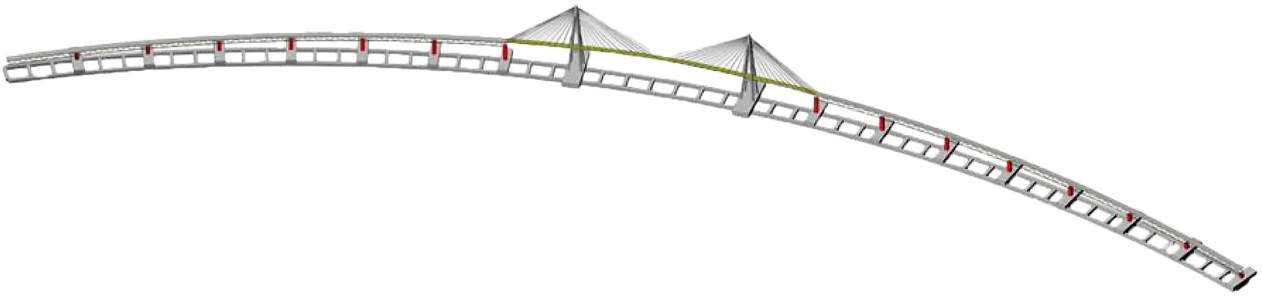

Figure 7: Arced pontoon bridge with mid-span (Jakobsen and Larsen, 2012)

Straight Pontoon Brigde with Multiple Spans

This bridge design consists of several large pontoons with a tower resting on each. Cables are connected to the top of the towers and hold the bridge beam up in the same way as a conventional cable-stay bridge (See Figure 8). The pontoons have to be moored in order to withstand lateral forces as well as rotations. This solution allows ships to pass along the entire length of the bridge, but requires the development of new technology (Jakobsen and Larsen, 2012)

2.5.4 Bjørnafjorden

Bjørnafjorden is a fjord on the west coast of Norway, roughly 30 km south of Bergen. Today, people travelling along E39 have to cross the fjord by a ferry between Sandvikvåg in the south and

Figure 8: Straight Pontoon Bridge with Multiple Spans (Jakobsen and Larsen, 2012)

Halhjem in the north. The 20 km long journey takes about 40 minutes (Fjord1, nd), which comparatively would take 15 minutes in a car travelling at 80 km/h. Bjørnafjorden is approximately 4.6 km wide at the point where the future bridge crossing will be, with depths down to 550 m. A passage this wide and deep cannot be crossed with conventional bridge technology, and it has been decided that the fjord will be crossed by a floating bridge. The project of coming up with a feasible design started in 2009, and it has since become apparent that new technologies will have to be developed. Data on winds, currents, waves and vessel traffic are presently being gathered and mapped in Bjørnafjorden in order to provide accurate information for use in designing the bridge (Statens Vegvesen, 2016b). Because of the wide range of research topics surrounding the design and development of the bridge, expertise from many different fields is required. As per December 2016, about 50 PhD and post-doc projects had been embarked upon, spanning from ship collisions and modelling of floating bodies to execution strategies and graphene enhanced asphalt (Statens Vegvesen, 2016c,d). Several potential designs have been worked out for crossing Bjørnafjorden by a floating bridge, and the NPRA has decided to move forward with three different concepts.

Multispan Cable Bridge with Floating TLP Towers

This bridge concept makes use of known cable stay bridge technology together with offshore tension leg platform (TLP) technology. Two towers floating on pontoons tethered to the ocean floor are connected by cables to each other and a tower on land in each end. Top cables are

required to keep the floating towers from listing. Suspension cables will be attached to the main cables to hold the bridge girder up and contribute to the vertical stiffness of the bridge (see Figure 9).

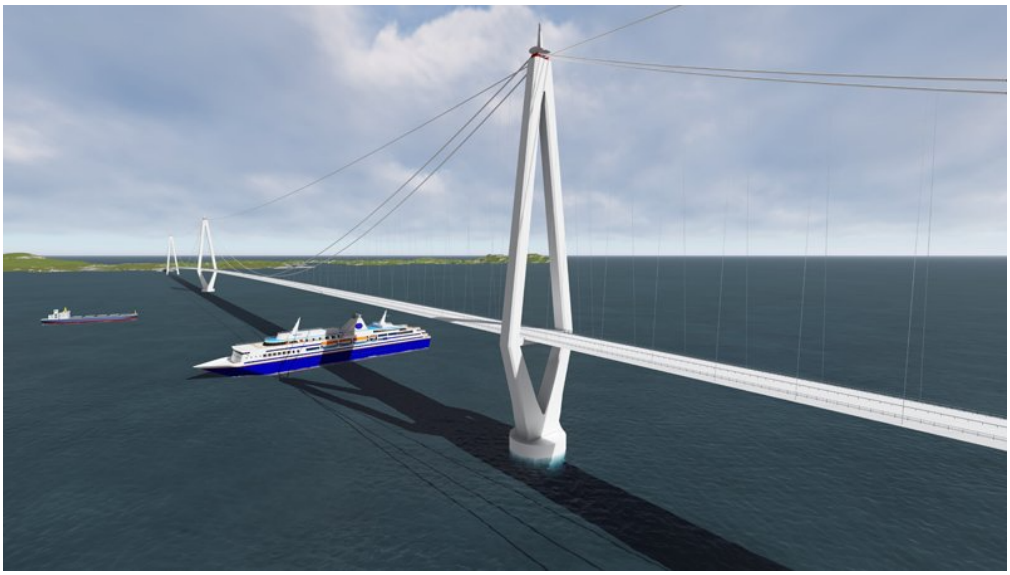

Figure 9: Design concept for crossing Bjørnafjorden, TLP bridge (Statens Vegvesen, 2016b)

Arced Pontoon Bridge

This bridge concept is very similar to the one already in use at Nordhordland and Bergsøysundet. The bridge girder is a horizontal arc floating on oval pontoons evenly spaced along the length of the bridge, with a cable bridge in one end for larger ships to pass underneath. Because the bridge is arced, transverse loads are absorbed throught arc action, and no mooring is necessary along the length of the bridge to prevent large horizontal displacements. The bridge beam consists of two parallell boxes connected by cross beams at approximately 40 m intervals, with a smaller box in the middle for pedestrians and cyclists (see Figure 10). The pontoons are placed 197 m apart, supporting the bridge through two colums each (Larsen, 2016a). Although the technology for this kind of bridge already exists, a bridge across Bjørnafjorden would have to be more than twice as long as the one in Nordhordland. This makes the design more challenging partly due to greater environmental and internal loads.

Figure 10: Design concept for crossing Bjørnafjorden, arced bridge (Statens Vegvesen, 2016b)

Straight Pontoon Bridge with Anchors

Similar to the previous design, the bridge girder for the straight pontoon bridge is floating on evenly spaced oval pontoons and is elevated by cables at the south end, as can be seen in Figure 11. The bridge is not shaped as an arc like the previously mentioned concept, however, and will therefore require mooring to restrict sideways motions. The bridge beam consists of one hexagonal box which is 6.5 m high and 31 m wide. The 18 pontoons are spaced 203 m apart, and three of them (pontoons 3, 9 and 15) are moored to the ocean floor by six mooring lines each (Larsen, 2016b).

2.6 Similarities and Differences Between the Bridges

The selection of floating bridges presented in this thesis is limited, as there are and have been other floating bridges around the world. Many of these are smaller and less significant from an engineering point of view, however, and were not considered explicitly relevant for this study. The bridges mentioned in Chapters 2.4 and 2.5 are of similar build and regarded as useful background information for this study. They have in common that they are, or possibly in the future will be, significant engineering achievements of their time. Designing and constructing these

Figure 11: Design concept for crossing Bjørnafjorden, straight bridge (Statens Vegvesen, 2016b)

bridges pushed the limits of what was possible with existing knowledge and technology, and the result was great structures that will hopefully last and be beneficial to society for a long time.

When it comes to the structural design and purpose of the floating bridges, some similarities are rudimentary, but still crucial for a well-functioning structure. Firstly, the bridges all aim to improve the infrastructure of the area in which they are located by providing a reliable and quick transportation route. Secondly, the buoyancy of the structures is provided by pontoons, although their shape, size and numbers differ. The pontoons are comprised of several watertight compartments for improved safety and redundancy in the case of an accident caused by e.g. a ship collison or extreme weather. The pontoons for all but the Yumemai bridge are made of concrete, which is strong, relatively light and experiences low to no corrosion in sea water (Moe, 1997). The Yumemai bridge avoids corrosion of the pontoons by lining the sides with titanium plates (Watanabe and Utsunomiya, 2003). Thirdly, because the bridges are floating on a dynamic surface, the pontoons and the bridge girder must be designed in such a way that vertical and horizontal motions and accelerations are restricted as much as possible. The bridges should be safe and comfortable for road users during all common weather situations, and maintain structural integrity even in unlikely weather scenarios. Horizontal motions are restricted either by mooring lines or by arc action, and vertical motions are resticted mainly by the stiffness and

weight of the bridge, or by tension cables in the case of the TLP bridge.

One important aspect in which the bridges differ, is the environment they were built for. The Lake Washington bridges were built for a relatively calm lake with limited currents and regulated water level. The bridges in Norway, however, often stretch across fjords that are subject to heavy storms every year as well as daily tidal variations of several meters and need to be able to accomodate these load changes. In Japan, earthquakes are common and might be assumed a regular load, while in Norway it would be considered an unlikely accidental load (Moe, 1997). Varying temperature, ice loads and rate of marine growth are other environmental aspects that might have an impact depending on location, as well as size and frequency of traffic loads. Evidently, the same design might be insufficiently strong or over-dimensioned for different sites.

Chapter 3

Theory

3.1 Loads Acting on a Floating Bridge

All bridges are almost constantly subject to a number of forces due to environment, gravity and/or traffic. The forces may vary depending on the size and design of the structure and the environment in which it is situated, but their nature is largely the same regardless. Common forces are the self-weight of the structure, wind forces, and vehice loads. For a floating bridge, the water inflicts additonal hydrostatic and hydrodynamic forces on the pontoons due to wave and current action that must also be taken into consideration. Less frequent loads may include traffic accidents, earthquakes and rock slides. Even though events like these are less likely and may never occur in the lifetime of the bridge, it must be able to maintain structural integrity should an accident occur. For a floating bridge this means staying afloat, even in the case of flooding of one or several pontoons. Table 2 contains a list of some of the more important loads to consider when designing a floating bridge. Only the first five load types were considered in this study, but all are described in more detail below. Wave loads are discussed separately in Chapter 3.5.

Table 2: Loads to be considered on a floating bridge (Watanabe and Utsunomiya, 2003)

Current loads
Wind loads
Traffic loads
Wave loads
Self-weight
Hydrostatic water pressure
Marine growth and water absorption in concrete
Ice/snow loads
Traffic accidents, including effects from fire/explosion
Collision loads
Loss of buoyancy
Effect of tsunami
Effect of earthquake
Rock/clay slides affecting bridge foundations or creating waves
Loading during the construction and installation phases
Water-level variations (tides, etc.)

3.1.1 Steady Current and Wind Loads

Recommended practice for environmental conditions and environmental loads on marine structures can be found in a document from DNV GL (former DNV) from 2010 (DNV, 2010). For the purpose of this study, current and wind loads were considered to be static loads.

The general expression for a steady current load is given by

$$F = C \cdot U_c^2 \tag{3.1}$$

where C is the current coefficient and U_c is the velocity of the current. The current coefficient has to be found empirically through model test, which was not an option for this study. Instead, the expression for the drag force can be used:

$$F_D = \frac{1}{2}\rho_w C_D A U_\infty^2 \tag{3.2}$$

where ρ_w is the water density, C_D is the drag coefficient, A is the projected area perpendicular to the current and U_∞ is the incident flow velocity (Fjeld, 2013).

Although pontoons and TLPs are considered large-volume structures, they may be treated as slender bodies in the case of calculating pure current loads, according to DNV. Interaction between structural parts may occur if one part is placed in the wake of another, which may affect the drag coefficient and therefore the size of the force acting on the part. This effect should not be neglected for structural parts that are close together, but the pontoons and TLPs in this study were considered to be far enough apart to not experience this behaviour.

In the same document from DNV basic, steady wind pressure is expressed as

$$q = \frac{1}{2}\rho_a U_{T,z}^2 \tag{3.3}$$

where ρ_a is the density of air and $U_{T,z}$ is the wind velocity averaged over a time period T at a height z over the surface. From this, the general static wind force can be found to be

$$F_W = CqS\sin\alpha \tag{3.4}$$

where C is the shape coefficient, S is the projected area of the structure normal to the direction of the wind force, and α is the angle between the wind direction and axis of the exposed structure. The angle was chosen to be 90°for this study, as only the maximum forces were of interest.

Similarly to current loads, structural parts close together may result in interaction and variations in the wind forces. If several parts are situated in the same plane normal to the wind direction, a *solidification effect* must be taken into account. Essentially the force is multiplied by a solidity ratio, ϕ, which is the area of the structure divided by the area enclosed by the structure. This effect was included to find the wind force on the pedestrian bridge beam, as it had a smaller geometry than the two main beams.

If two or more parts of a structure are located behind one another relative to the wind direction, a *shielding effect* may occur. The shielding effect can be expressed as

$$F_{W,SHI} = F_W\eta \tag{3.5}$$

where η is the shielding factor and depends on the solidity ratio ϕ and the shape and distance

between the two parts. Where two or more members are placed in line with the wind direction after the first part of the structure, the force on the following members should be equal to the force on the second member (DNV, 2010).

3.1.2 Traffic Loads

The ultimate purpose of a floating bridge is to transport traffic from one side of a body of water to the other. The bridge should therefore be dimensioned to carry the maximum possible amount of traffic without any chance of failure. In Europe, standards regarding various loads on structures are provided in a set of *Eurocodes*, and traffic loads are handled specifically in Eurocode 1, Part 2 (CEN, 1991). Similarly, the NPRA in Norway has its own handbook addressing design and loads on bridges, which builds on the Eurocodes (Statens Vegvesen, 2009). The Eurocode mentioned above (BS EN 1991-2:2003), with corresponding National Annex (British Standards, 2008) were used to determine the traffic load cases for load spans shorter than 500 m.

The bridge girder consists of three beams - one for each traffic direction and one for pedestrians and cyclists. The span between each pontoon is less than 500 m, so the regulations from CEN (1991) were applied. The carriageway on each of the two beams carrying vehicles is 10 m wide. According to Eurocodes, this corresponds to three notional lanes (see Table 3), each 3 m wide, with a remaining area of 1 m, because:

$$n_1 = Int\left(\frac{10}{3}\right) = 3 \qquad \text{and} \qquad 10 - 3 \times 3 = 1$$

Table 3: Number and width of notional lanes (CEN, 1991)

Carriageway width w	**Number of notional lanes**	**Width of notional lane w_l**	**Width of the remaining area**
$w < 5.4$ m	$n_1 = 1$	3 m	$w - 3$ m
5.4 m $\leq w < 6$ m	$n_1 = 2$	$\frac{w}{2}$	0
6 m $\leq w$	$n_1 = Int\left(\frac{w}{3}\right)$	3 m	$w - 3 \times n_1$
NOTE for example, for a carriageway width equal to 11 m, $n_1 = Int\left(\frac{w}{3}\right) = 3$, and the width of the remaining area is $11 - 3 \times 3 = 2$ m			

Load model 1 is intended to model "flowing, congested or traffic jam situations with a high percentage of heavy lorries" (CEN, 1991, p. 36), which is a reasonable, large traffic load along the E39. It consists of uniformly distributed loads, $\alpha_q q_k$, and concentrated loads, $\alpha_Q Q_k$, where α_q and α_Q are adjustment factors. The adjustment factors can often be set to unity when nothing else is specified. In the case from the NRPA, all adjustment factors were set to 1.0, except for α_{q1}, which was set to 0.6 according to the National Annex. The concentrated loads appear in pairs, but when looking at global reactions, they can be considered one load of twice the size for simplicity. The size of the different loads can be seen in Table 4. The resulting load condition can be seen in Figure 12. The total distributed load is 66.2 kN/m, and the three concentrated loads had to be joined into one load of 1200 kN due to the nature of the model in ANSYS.

Table 4: Characteristic values for load model 1 (CEN, 1991)

Location	**Tandem system TS**	**UDL system**
	Axle loads Q_{ik} (kN)	q_{ik} (**or** q_{rk}) (kN/m^2)
Lane number 1	300	9
Lane number 2	200	2.5
Lane number 3	100	2.5
Other lanes	0	2.5
Remaining area (q_{rk})	0	2.5

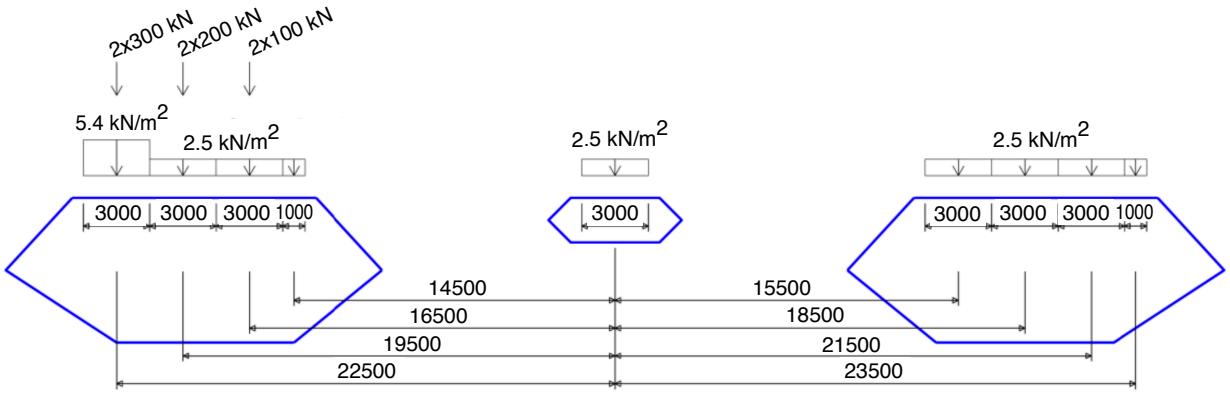

Figure 12: Load model 1 for the pontoon bridge. Dimensions in millimetre (Larsen, 2016a)

3.1.3 Hydrostatic Water Pressure and Self-weight

A floating bridge large enough to cross Bjørnafjorden in Norway will necessarily be substantial in size and weight. The pontoons or TLPs need to be large enough to provide buoyancy for the entire structure, and this buoyancy is a result of the hydrostatic water pressure pushing the floating device upwards (Watanabe and Utsunomiya, 2003). In addition to the floating devices keeping the bridge afloat, the bridge beam itself must be designed so that it is strong and stiff enough not to buckle under its own weight. This self-weight is important to account for in both dynamic and static analysis, and it has a substantial effect on the eigenfrequencies of the system (see Chapter 3.6.5).

3.1.4 Loads From Marine Growth and Ice/Snow

The occurance of marine growth such as seaweed and barnacles on the submerged parts of a structure is practically inevitable, and might in some geographical locations grow up to 0.3 m in thickness. The growth adds to the diameter and volume of a structure, and it increases roughness and therefore drag. The result is an increase in wave forces on the structure, which might be accounted for by adjusting the diameter and mass of the submerged body (Chandrasekaran, 2015). Although marine growth will have an effect on submerged structures, this effect is assumed too small to account for in the case of a 4 km long floating bridge when the aim is to determine global responses.

Ice and snow loads may affect a structure in different ways, and are classified as either gobal or local. Global ice loads affect the stability and motions of the structure, while local ice loads influence the behaviour at connections between structural parts. Such loads may for instance result in creep, cracking and buckling that would not appear otherwise. How to account for these effects is described in Chandrasekaran (2015), but will not be further described in this thesis as they are outside the scope of this study.

3.1.5 Accident Loads

Assuming the lifespan of a floating bridge is about 100 years, it is relatively likely that an accident will occur and affect the bridge at some point during its lifetime. Traffic accidents may occur between vehicles travelling on the bridge, and ships may collide with the floating devices keeping the bridge buoyant. The latter may result in loss of buoyancy and stability, in which case the bridge should be able to remain afloat. Environmental accidents like tsunamis, earthquakes and rock slides may cause large waves and damage the foundations. Although important to consider in an overall design of a floating bridge, the loads caused by such accidents are not assumed relevant to the scope of this study.

3.1.6 Construction and Installation Loads

Floating bridges are often built in parts in dry docks before the parts are transported to the installation site (Lwin, 2000). This means that not only must the final bridge structure be strong enough to resist forces like self-weight and wind, but also the individual parts by themselves. The segments might also need to be dragged, upended and lifted into place, which it should be able to sustain without damage (Chandrasekaran, 2015).

3.1.7 Tidal Variations

A bridge floating on the sea will have to be able to accommodate for regular variation in sea level due to changing tides. The difference between high and low tide will vary from place to place and from day to day, and the bridge needs to allow for maximum change in water level. Bearings and hinges at the connections with land foundations might be necessary, which is the case for the Nordhordland and Bergsøysundet bridges in Norway. These bridges experience daily changes in water levels of about ±2 m (Moe, 1997). This study evaluated responses at mean water level only, since the difference in global responses between varying tide levels was assumed negligible.

3.2 Permitted Load Response

Handbook N400 (Statens Vegvesen, 2009) by the NPRA was created in accordance with EU standards and contains guidelines and regulations related to bridges. Chapter 5.1 in this handbook covers requirements to the response of a bridge when subjected to static and dynamic loads. In particular should vertical displacements not exceed L/350 for 70% of maximum traffic loads, where L is the length of the relevant span. Maximum accelerations should be limited to 1.0 m/s^2 for bridges without pedestrian traffic and 0.6 m/s^2 for bridges where pedestrian traffic is considerable. If a bridge is likely to have some pedestrian traffic, an intermediate value should be assumed. The accelerations should be calculated for a load combination estimated to be exceeded no more than 100 times during the life time of the bridge. Assuming a life span of about 100 years, finding the accelerations for a storm with 1-year return period should be suitable.

These requirements apply to common bridge types only, however, and special requirements may apply to more advanced structures like cable-stay bridges with very long spans, moveable bridges, and floating tunnels and bridges. For floating bridges, Handbook N400 states that limit values should be determined for the individual project. The motion criteria as given in the NPRA's report (Larsen, 2016a) are given in Table 5.

Table 5: Most relevant motion criteria (Larsen, 2016a)

Motion	**Load**	**Criterion**
Vertical deflection due to traffic	0.7 x traffic	approx. 1 m
Rotation about bridge axis (roll) due to traffic	0.7 x traffic	1 deg
Rotation about bridge axis (roll) due to environmental loads	1 year storm	1.5 deg
Vertical acceleration	1 year storm	0.5 m/s^2
Horizontal acceleration	1 year storm	0.6 m/s^2

One reason why the criteria from N400 cannot be used directly for a floating bridge is that it might be difficult to clearly define a span because of the moving pontoons. Still, the criteria may be used to verify resonable results for deflections of the bridge beam relative to the deflections of the pontoons.

The criteria given above only refer to extreme response during a 1 year storm. For stronger

storms, or when wind speeds exceed 25 m/s, the bridge will be closed to traffic due to safety considerations (Johansen, 2016). Nevertheless, responses should not be too great even when the bridge is closed, as this may lead to structural damage and limit fatigue life. The fatigue life of the structure was not considered in this study, but will be an important aspect to evaluate before choosing the final concept.

3.3 Shear Forces and Bending Moments in Beams

Two basic principles in structure mechanics are shear forces and bending moments. Knowing the size of shear and bending forces is important when designing a structure, as it has to be able to withstand these internal forces. The bridge in this study was approximated as a beam, and the distribution of shear forces and bending moments for two beams with different boundary conditions can be seen in Figure 13. The expressions for the shear and bending for the fixed beam are

$$M_{max} = \frac{wl^2}{12} \qquad M_1 = \frac{wl^2}{24} \qquad V_{max} = \frac{wl}{2} \tag{3.6}$$

Although these expressions are too simple when assessing complex structures like a 4 km long floating bridge, they can give a rough estimate of values, which can be useful early on in a design phase.

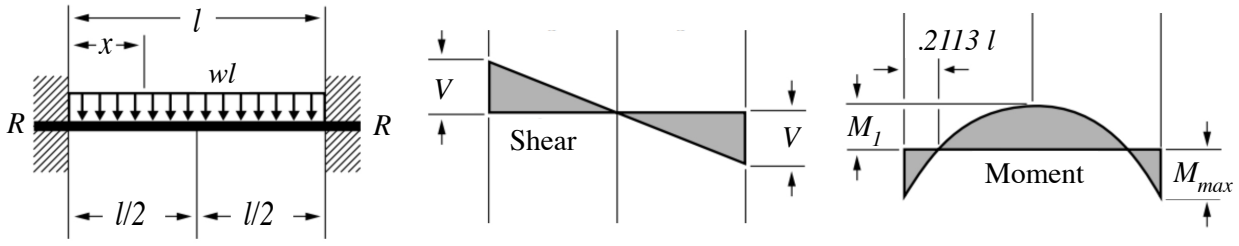

Figure 13: Shear forces and bending moments for a fixed beam with evenly distributed load (American Wood Council, 2007)

3.3.1 Arc Action

As mentioned, a beam with a lateral load will experience shear forces, V, and bending moments, M. If insufficiently stiff, the lateral forces may cause the beam to buckle and fail. In a straight floating bridge beam, sideways motions due to currents, waves and winds must therefore be prevented by mooring or tethering, as the water does not provide any substantial horizontal restrictions. An arced beam, however, works differently. In addition to the shear forces and bending moments, a concentric axial compression acts in the beam due to the restrictions at each end of the arc. The result is an axial compressive force (traced as the "C" line in Figure 14) which adds to the bending moment in the beam. The stress distribution can be seen in Figure 15(b-e).

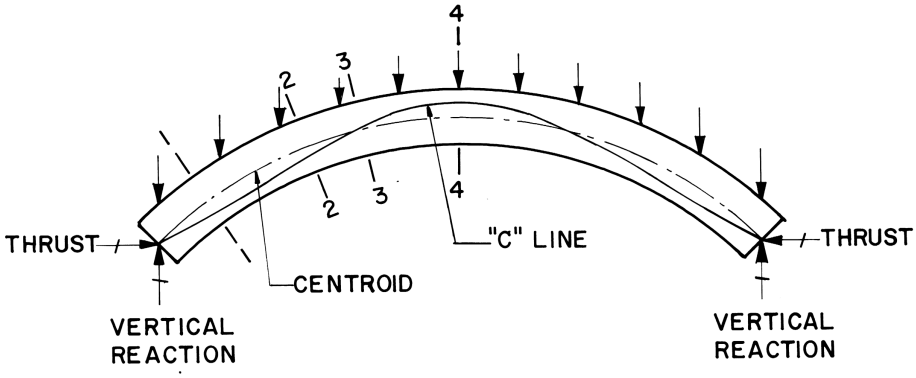

Figure 14: Arced beam with distributed load (Zallen, 2008)

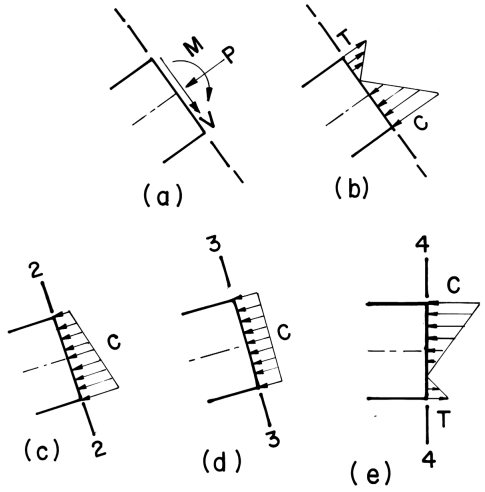

Figure 15: Stress distribution at different points in an arced beam (Zallen, 2008)

3.4 Static Nonlinearity

In a static analysis, the problem to be solved can be expressed as

$$\boldsymbol{K}\boldsymbol{r} = \boldsymbol{R} \tag{3.7}$$

where $\boldsymbol{K}$ is the stiffness matrix for the system, $\boldsymbol{r}$ is the response vector and $\boldsymbol{R}$ is the load vector. This relation holds for elastic, linear materials and small deformations, and can be used in many situations. In the case of large deformations, however, the stiffness is not a constant, but rather changes with displacement. Three factors affect the stiffness in this case: geometry, material properties and boundary conditions (Moan, 2003).

3.4.1 Geometric Nonlinearity

Geometric nonlinearity is accounted for when the change in geometry is considered in equilibrium and strain calculations. Equation (3.7) then becomes

$$\boldsymbol{K}(\boldsymbol{r})\boldsymbol{r} = \boldsymbol{R} \tag{3.8}$$

$\boldsymbol{K}$ is called the secant stiffness. This equation can sometimes be solved analytically to find the displacement $\boldsymbol{r}$ corresponding to a given $\boldsymbol{R}$. Generally, however, this is not the case and the use of iterative methods is necessary. Equation (3.8) can therefore be rewritten on a differential form as

$$\mathrm{d}\boldsymbol{R} = \frac{\mathrm{d}}{\mathrm{d}\boldsymbol{r}}\big(\boldsymbol{K}(\boldsymbol{r})\boldsymbol{r}\big)\mathrm{d}\boldsymbol{r} \tag{3.9}$$

or

$$\mathrm{d}\boldsymbol{R} = \boldsymbol{K}_I \mathrm{d}\boldsymbol{r} \tag{3.10}$$

where $\boldsymbol{K}_I$ is the tangent stiffness. $\boldsymbol{K}_0$ is the initial, linear stiffness and $\boldsymbol{K}_G$ is the geometric stiffness.

3.4.2 Material and Boundary Condition Nonlinearity

The stress-strain relationship for elastic materials can be expressed by Hooke's law:

$$\sigma = E\epsilon \tag{3.11}$$

When nonlinearity in the material is taken into account, this no longer holds, and E_T is introduced. This is called the tangent modulus, which depends on the stress σ, and therefore needs to be determined iteratively.

Boundary condition nonlinearity is when boundary conditions change when a load is applied, usually due to large deformations. The boundary conditions of a structure will for example change if it deforms and hits a wall or the ground.

3.5 Waves

A significant part of the study for this thesis revolved around the effect of waves on a floating structure. There are different ways to simulate waves, and the accuracy and complexity of the wave simulation often dictates how accurate and realistic the response of the structure will be.

3.5.1 Regular Waves

In mathematics, waves of any sort can be described as a function of sine or cosine. Ocean waves are no exception, and the profile of a regular wave can be expressed as

$$\zeta = \zeta_a \sin(\omega t - kx) \tag{3.12}$$

where ζ_a is the wave amplitude, ω is the circular wave frequency, and k is the wave number ($k = \omega^2/g$ for deep water). t is the time variable and x is the horizontal position along the direction of wave propagation. This linear representation of an ocean wave is often not completely accurate,

as wave crests are steeper and wave troughs deeper than for a regular sinusoidal wave. Other theories exist to better estimate this shape, but they require more computational time and do not necessarily offer a much better model for long-crested waves (Faltinsen, 1993). Linear wave theory is therefore assumed sufficient for this study.

3.5.2 Irregular Waves

The ocean surface does not move in regular sinusoidal waves. Most of the time, it looks like a chaos of crests and troughs with no apparent pattern. While this may be true, it is possible to model an approximation of an irregular sea state by superpositioning a large number of different regular waves:

$$\zeta = \sum_{j=1}^{N} A_j \sin\left(\omega_j t - k_j x + \epsilon_j\right) \tag{3.13}$$

where A_j, ω_j, k_j and ϵ_j are the wave amplitude, circular frequency, wave number and phase angle, respectively, of wave component j. The phase angles are random and uniformly distributed between 0 and 2π. This expression for the surface elevation applies to *long-crested* irregular sea, i.e. a sea state where all waves are propagating in the same direction. Sometimes, a sea state will more accurately be modelled by waves moving in different directions, called *short-crested* irregular sea. This can be obtained by adding another sum to Equation 3.13, and including a random variable between 0 and 2π for direction of propagation (Faltinsen, 1993). This will not be explored further in this thesis, however, as only long-crested waves were of interest for this study.

3.5.3 Standardised Wave Spectra

A sea state will never consist of an equal number of waves of all frequencies. Instead, waves of certain frequencies and amplitudes will be common, while others are less likely to occur. Data like wave height and wave periods are therefore recorded over time in an area and analysed to create a spectrum of frequencies. This could be done individually for each particlar site of interest, but that would require a large amount of equipment and take a lot of time. Therefore, stan-

dardised parametric spectra have been developed to describe sea states of different types. One of the more widely used spectra in the North Sea is the JONSWAP (JOint North Sea WAve Project) spectrum from 1973, which builds on spectra formulated by Phillips in 1957 and later adjusted by Pierson-Moscowitz in 1964. The JONSWAP spectrum takes into account the effect of wind with limited fetch (the distance the wind blows over the sea), whereas the Pierson-Moscowitz (PM) spectrum assumes unlimited fetch and the Phillips spectrum does not account for wind speed (Fréchot, 2006). The expression for the JONSWAP spectrum is

$$S_J(\omega) = A_\gamma S_{PM}(\omega)\gamma^{exp\left(-0.5\left(\frac{\omega-\omega_p}{\sigma\cdot\omega_p}\right)^2\right)} \tag{3.14}$$

S_{PM} = Pierson-Moskowitz spectrum
γ = non-dimensional peak shape parameter
σ = spectral width parameter
$\sigma = \sigma_a for \omega \leq \omega_p$
$\sigma = \sigma_b for \omega > \omega_p$
A_γ = $1 - 0.287\ln(\gamma)$

$$S_{PM}(\omega) = \frac{5}{16}\cdot H_s^2\omega_p^4\cdot\omega^{-5}\exp\left(-\frac{5}{4}\left(\frac{\omega}{\omega_p}\right)^{-4}\right) \tag{3.15}$$

where H_s is the significant wave height and ω_p is the peak frequency, related to the peak period T_p by $\omega_p = 2\pi/T_p$. Average values for JONSWAP found through experiements are γ = 3.3, σ_a = 0.07 and σ_b = 0.09. The JONSWAP spectrum is assumed to be an acceptable model for $3.6 < T_p/\sqrt{H_s} < 5$ (DNV, 2010).

The wave spectrum for a sea state can be used to determine a variety of parameters, two important ones being the significant wave height and mean wave period. These parameters can be derived using the moments of the spectrum, where moment n is expressed by

$$m_n = \int_0^\infty \omega^n S(\omega)\mathrm{d}\omega \qquad n = 0, 1, 2, ... \tag{3.16}$$

The significant wave height can be approximated as

$$H_s = H_{m0} = 4\sqrt{m_0} \tag{3.17}$$

and the mean zero crossing period as

$$T_{m02} = 2\pi\sqrt{\frac{m_0}{m_2}} \tag{3.18}$$

A zero-crossing is defined as every time the wave elevation crosses the mean water level. A zero crossing period is measured from a zero crossing in one direction (upwards or downwards) to the next of the same direction (Myrhaug and Lian, 2009).

Another useful piece of information is the most probable larges wave height in a sea state, which is approximated by

$$H_M = H_{m0}\sqrt{\frac{\ln N}{2}} \tag{3.19}$$

when N is large. N is the number of waves in a sea state given by

$$N = \frac{D}{T_z} \tag{3.20}$$

Here, D is the duration of a sea state in seconds, and T_z is the mean zero-crossing period which can be approximated as T_{m02} as mentioned previously.

3.5.4 Wave Forces

When a wave moves along a structure in water, several forces are acting on the structure at once. One part of this is the added mass, damping and restoring terms discussed in Chapter 3.6. The other part is the excitation forces, consisting of Froude-Kriloff and diffraction forces. These can be calculated based on the movement of the water and the properties of the structure. Since the pontoons in this study were simplified as rectangular boxes in head waves, the focus will be on this particular case. The coordinate system can be seen in Figure 16.

Froude-Kriloff Forces

As a regular sine wave passes a structure in water, the pressure will vary along the length of the structure. The dynamic pressure in deep water for a wave propagating along the positive x-axis

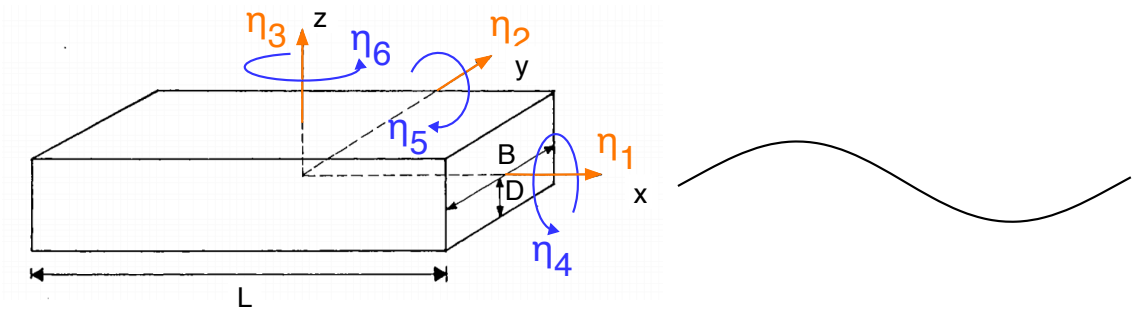

Figure 16: Definition of coordinate system and dimensions for a barge (Faltinsen, 1993, edited)

is expressed as

$$p_D = \rho g \zeta_a e^{kz} sin(\omega t - kx) \tag{3.21}$$

where z is the water depth at the point of interest. Integrating this expression gives the resulting total hydrodynamic pressure on the structure:

$$F_{FK} = \iint_S p_D \vec{n}\, ds \tag{3.22}$$

where S is the average wetted surface and $\vec{n}$ is the unit vector normal to the body surface.

When looking at vertical forces on the barge in Figure 16 in head waves, Equation 3.22 becomes

$$F_{FK,3} = \int_{-L/2}^{L/2} \rho g \zeta_a e^{kz} \sin(\omega t - kx) B\, dx \tag{3.23}$$

This is assuming the pressure is uniform along the y-axis, which is the case for regular waves propagating in the x-direction (Faltinsen, 1993). The expression for the Froude-Kriloff forces in surge motion is found in a similar way, but integrated over the draught at x=-L/2 and x=L/2. The force in pitch, rotations about the y-axis, can be found by multiplying the expression for heave force with -x and integrating over the length of the barge.

The three expressions then become

$$
\begin{aligned}
F_{FK,1} &= \left(\rho g \zeta_a B\right)\left(2\sin\left(\frac{2L}{2}\right)\cos(\omega t)\right)\left(\frac{1-e^{kz}}{k}\right) \\
F_{FK,3} &= \left(\rho g \zeta_a B e^{kz}\right)\left(\frac{2}{k}\sin\left(\frac{kL}{2}\right)\sin(\omega t)\right) \\
F_{FK,5} &= \left(\rho g \zeta_a B e^{kz}\right)\left(\frac{L}{k}\cos\left(\frac{kL}{2}\right) - \frac{2}{k^2}\sin\left(\frac{kL}{2}\right)\right)
\end{aligned}
\tag{3.24}
$$

Diffraction Forces

While Froude-Kriloff forces are caused by the undisturbed pressure field around the floating structure, diffraction forces are the forces that arise when structure motions cause the pressure field to change. This force is related to the acceleration of the fluid, which in the vertical direction in deep water can be expressed as

$$a_3 = -\omega^2 \zeta_a e^{kz} sin(\omega t - kx) \tag{3.25}$$

The diffraction force can then be written as

$$F_{D,3} = A_{33} a_3 \tag{3.26}$$

where A_{33} is the proper added mass in heave. Again the force has to be integrated over the surface of the body to find the total force. In heave and pitch, acceleration is found at the middle of the draught, $z_m = z/2$. For surge, the acceleration is found at the middle of the length, i.e. $x = 0$. The expression for heave force becomes

$$F_{D,3} = -\omega^2 A_{33}^{(2D)} \zeta_a e^{kz_m} \int_{-L/2}^{L/2} \sin(\omega t - kx) \tag{3.27}$$

The integrated expressions in surge, heave and pitch for head sea are:

$$
\begin{aligned}
F_{D,1} &= \left(\omega^2 \zeta_a A_{11}^{(2D)}\right)\left(\frac{1-e^{kz}}{k}\right)\cos(\omega t) \\
F_{D,3} &= \left(-\omega^2 A_{33}^{(2D)} \zeta_a e^{kz_m}\right)\left(\frac{2}{k}\sin\left(\frac{kL}{2}\right)\sin(\omega t)\right) \\
F_{D,5} &= \left(-\omega^2 A_{33}^{(2D)} \zeta_a e^{kz_m}\right)\left(\frac{L}{k}\cos\left(\frac{kL}{2}\right) - \frac{2}{k^2}\sin\left(\frac{kL}{2}\right)\right)
\end{aligned}
\tag{3.28}
$$

When the hydrodynamic forces and coefficients have been found, they can be inserted into the equations of motion to find the response of the system.

3.6 Dynamic Behaviour

The vibration of a structure appears as a result of the mass and elasticity of the system. If an external force is applied momentarily to the structure, the structure will be deformed and the internal forces will act to bring the system back to its original form. The elastic energy in the system is converted into kinematic energy at equilibrium, causing the structure to deform in the opposite direction. Again the internal forces will act to regain the original position, and the cycle is repeated. This results in vibratory motions, which in theory could go on indefinitely if no damping occurs in the system. The frequency and amplitude of the vibration depend on the dynamic properties of the system as well as the nature of the external force. Having knowledge about a system's behaviour under the influence of different forces, either transient, harmonic or static, is important in order to make sure the structure remains safe and structurally intact at all times.

3.6.1 Equation of Motion

A dynamic system with mass, a spring and a damper is in equilibrium when

$$
Q(t) - m\ddot{u} - c\dot{u} - ku = 0 \tag{3.29}
$$

or

$$m\ddot{u} + c\dot{u} + ku = Q(t) \tag{3.30}$$

where $Q(t)$ is the applied force, m, c and k are the mass, damping factor and spring stiffness, and u, $\dot{u}$ and $\ddot{u}$ are the displacement, velocity and acceleration of the system (Bergdahl, 2009). For a body with six degrees of freedom subjected to steady-state sinusoidal waves, the equation becomes:

$$\sum_{k=1}^{6} \left[\left(\boldsymbol{M}_{jk} + \boldsymbol{A}_{jk} \right) \ddot{\eta}_k + \boldsymbol{B}_{jk} \dot{\eta}_k + \boldsymbol{C}_{jk} \eta_k \right] = \boldsymbol{F}_j e^{-i\omega_e t} \qquad j = 1, 2, \ldots, 6 \tag{3.31}$$

Here, $\boldsymbol{M}$, $\boldsymbol{A}$, $\boldsymbol{B}$ and $\boldsymbol{C}$ are the 6x6 matrices for mass, added mass, damping and stiffness, respectively. For a floating body, $\boldsymbol{A}$ and $\boldsymbol{B}$ will usually be frequency-dependent. η and its derivatives are 6x1 vectors with displacements, velocities and accelerations in three directions and three rotations. $\boldsymbol{F}$ is a 6x1 vector containing the amplitudes of the exciting forces (Faltinsen, 1993; Bergdahl, 2009).

Equation 3.31 can be solved in two ways – either in the time domain or in the frequency domain. If all the coefficients are constant, i.e. do not depend on the frequency of the motions, the equation can be solved directly by integration in the time domain for any arbitrary load. The response is found as a function of time, which means that the total response is found instantly for each point in time. If the added mass and/or damping coefficients are frequency dependent, the equation of motion cannot be solved so easily, and special convolution technology must be adopted and solved in the frequency domain. However, an irregular sea state can often be approximated by a linear superposition of a series of harmonic functions. In this case, the response for each frequency component is calculated, and the total response is found as a sum of the individual responses. This approach relies on statistical data and wave information rather than actual measured wave forces, and is looked at further in Chapter 3.5.

3.6.2 Added Mass

The added mass loads of a structure are hydrodynamic forces and moments caused by changes is the pressure field around a body moving in fluid (Faltinsen, 1993). The body is forced to move, which causes the fluid surrounding it to oscillate. This creates the impression that the body is

"heavier" than it really is, and moving it requires more force than it would in a less dense fluid or in air. The size of the added mass depends on size and geometry of the body as well as density of the fluid. The NPRA had in their report (Larsen, 2016a) calculated accurate values for the added mass of the pontoons for the bridge, and these plots were used to find polynomial expressions for the added mass in heave, roll and sway. This was done through regression in Microsoft Excel by reading off the graphs, plotting the points and adding a trendline (See electronic appendix *addmass_NPRA.xlsx*). For most of the graphs the trendline was too inaccurate to be of use on the whole range of periods from 0-30 s, which the NPRA had provided. Instead a smaller range was chosen, with periods from 1-12 s, within which all probable periods for the relevant JONSWAP spectra could be found. In some cases, the graph was divided and two different expressions were found for increased accuracy. The expressions were later used in MATLAB in order to calculate the excitation forces on the floating pontoons. This is discussed in Chapter 4.3.

3.6.3 Damping

Hydrodynamic damping can be divided into two terms, radiation damping and viscous damping. The radiation damping occurs as a result of waves being created as a structure is forced to move in still water, and this damping is equivalent to the energy in the radiating waves. The radiation damping is frequency dependent and is of different magnitude in different directions (Ashton et al., 2009). Similarly to the added mass, the radiation damping of the pontoons was given in the NRPA's report. This damping was accounted for through springs with dampers in the ANSYS model. The viscous damping is caused largely by friction between the surface of the structure and the fluid.

In addition to hydrodynamic damping, internal friction causes structural damping which may need to be accounted for. Structural and viscous damping can be approximated as proportional damping, or Rayleigh damping, on the form

$$\boldsymbol{C} = \alpha \boldsymbol{M} + \beta \boldsymbol{K} \tag{3.32}$$

where

$$\alpha = \frac{2\omega_1\omega_2}{\omega_2^2 - \omega_1^2}(\xi_1\omega_2 - \xi_2\omega_1)$$
$$\beta = \frac{2(\omega_2\xi_2 - \omega_1\xi_1)}{\omega_2^2 - \omega_1^2} \tag{3.33}$$

and

$$\xi_i = \frac{c}{c_{cr}} = \frac{c}{2m\omega} \tag{3.34}$$

which means that if the damping ratio is known for two frequencies, α and β can be calculated (Langen and Sigbjörnsson, 1979). Rayleigh damping can be implemented in dynamic analyses in ANSYS by specifying α and β.

3.6.4 Restoring Forces

For a structure floating freely on the surface, restoring forces will occur when a rotation or displacement is forced on the structure and then released. The buoyancy forces will act to restore the system to equilibrium, which results in an osciallatory movement depending on the damping terms. For a structure symmetrical about the x-z plane, restoring forces occur for heave, roll and pitch motions. The two expressions relevant for this study were:

$$C_{33} = \rho g A_{WP} \tag{3.35}$$

and

$$C_{55} = \rho g V \overline{GM}_L \tag{3.36}$$

Where A_{WP} is the area of the waterplane, V is the displaced volume and $\overline{GM}_L$ is the longitudinal metacentric height (Faltinsen, 1993). The restoring forces can be modelled as springs, which is discussed in Chapter 4.2.3.

3.6.5 Eigenfrequencies

The eigenfrequencies, or natural frequencies, of a system are "natural properties of the system when it is allowed to vibrate freely without any external excitation" (Chopra, 2007, p. 41). The natural frequency depends solely on the ratio of mass and stiffness of the system, and the relationship for the circular eigenfrequency is expressed as

$$\omega_n = \sqrt{\frac{k}{m}} \tag{3.37}$$

where k is the total stiffness and m is the total mass of the system. Equation 3.37 indicates that an increased stiffness results in higher natural frequencies and increased mass gives lower frequencies. The expression can be derived from the equation of motion for the free vibration of an undamped system with a single degree of freedom:

$$m\ddot{u} + ku = 0 \tag{3.38}$$

which can be solved as a differential equation:

$$u = sin(\omega t) \tag{3.39}$$

and

$$\ddot{u} = -\omega^2 sin(\omega t) \tag{3.40}$$

gives

$$(k - m\omega^2) sin(\omega t) = 0 \tag{3.41}$$

which, when solved for ω, results in Equation 3.37. The natural period for a system is expressed as

$$T_n = \frac{2\pi}{\omega_n} \tag{3.42}$$

3.6.6 Modal Analysis

Since about the 1980s, modal analysis has become a powerful tool to obtain information on and improve the dynamic characteristics of a structural system. Modal analysis can be applied in a wide range of engineering fields where vibrations and dynamic behaviour is of particular concern, and where certain demands to weight, safety and reliability need to be met. Performing a modal analysis with a finite element analysis computer program and combining it with modern experimental techniques makes it possible for engineers to determine dynamic properties like eigenfrequencies, damping factors and modal shapes with high accuracy. Together, a set of these properties describes one of the *modes* of a system. Similar to the way an irregular wave can be expressed as a combination of many regular waves, the total dynamic behaviour of a system can be expressed as a combination of many modes. To what degree each mode participates to the total behaviour is determined by the mode shape as well as the nature of the external forces (He and Fu, 2001). This is a popular way of determining the dynamic response of a system due to its effectiveness and high accuracy when used correctly.

For this study, a full transient analysis was carried out instead of modal superposition to determine the responses to a dynamic load. A modal analysis was still performed in order to determine the range of eigenfrequencies for the bridge. This was to ensure that no resonance would occur in the structure for common wave and wind frequencies. Resonance in a lightly damped system appears when the external loads have the same frequency as the system's eigenfrequency, at which point the responses may become increasingy large and erratic with each oscillation. This may lead to damage and sometimes total failure, which of course is undesirable. Resonance should therefore be avoided where possible, for example by making sure the eigenfrequencies of the system are not within a typical range of frequencies of environmental loads.

3.7 The Finite Element Method (FEM)

In the field of engineering, most physical phenomenon can be modelled by differential equations of varying complexity. These equations or systems of equations quickly become very challenging to solve when the phenomenon is complex, and this is where the finite element method comes in. FEM is a numerical tool used to find the approximate solutions to the differential equations by dividing the body in question into smaller elements, over which the differential equations are assumed to be valid (Ottosen and Petersson, 1992, pp. 27-35). These elements can be either one, two or three dimensional, and together they form what is called a finite element mesh. When the problem is meshed, boundary conditions such as external loads and deflection constraints can be applied and the differential equations solved over each element.

3.7.1 Steps in FEM

The procedure presented in this chapter is general for all problems to be solved using the finite element method, but is exemplified by the simple spring problem in Figure 17. The following example with theory and figures was found from Ottosen and Petersson (1992, pp. 27-35).

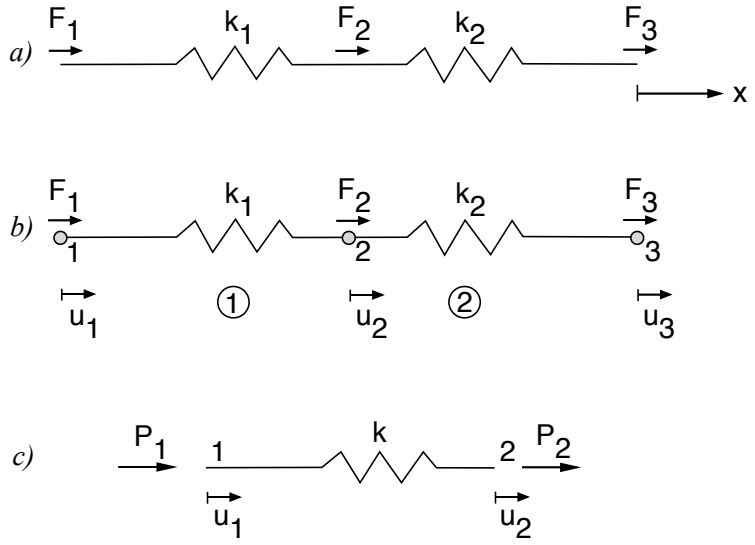

Figure 17: a) Two springs with external load. b) Discretized system with nodes, elements, local displacements and forces. c) One element with nodes, displacement and local forces

Discretization of the System

The structure or part to be analysed is divided into elements, and the stiffness for each element is established. Figure 17c gives

$$P_2 = k(u_2 - u_1)$$

which, in order to have equilibrium, means

$$P_1 = k(u_1 - u_2)$$

Combination of these result in

$$\begin{bmatrix} k & -k \\ -k & k \end{bmatrix} \begin{bmatrix} u_1 \\ u_2 \end{bmatrix} = \begin{bmatrix} P_1 \\ P_2 \end{bmatrix} \tag{3.43}$$

or

$$\boldsymbol{K}^e \boldsymbol{a}^e = \boldsymbol{f}^e$$

where $\boldsymbol{K}^e$ is the element stiffness matrix, $\boldsymbol{a}^e$ is the nodal displacement vector and $\boldsymbol{f}^e$ is the element force vector.

Establish Connectivity

A meaningful relationship needs to be established to connect the elements with each other. The relationships of interest will vary with problem formulation and degrees of freedom (DOF), but for this example only the displacement in the x-direction is of importance. Hence, each local displacement is related to the global displacements by

$$u_1^1 = u_1\,, \qquad u_2^2 = u_3 \qquad \text{and} \qquad u_2^1 = u_1^2 = u_2 \tag{3.44}$$

where u_i^j is the displacement at node i of element j. These relationships can now be translated back to the element matrices, which can be expanded to include the DOFs of the whole system as

$$\begin{bmatrix} k_1 & -k_1 & 0 \\ -k & k & 0 \\ 0 & 0 & 0 \end{bmatrix} \begin{bmatrix} u_1 \\ u_2 \\ u_3 \end{bmatrix} = \begin{bmatrix} P_1 \\ P_2 \\ 0 \end{bmatrix} \tag{3.45}$$

or

$$\boldsymbol{K}_1^{ee}\boldsymbol{a} = \boldsymbol{f}_1^{ee}$$

$\boldsymbol{K}_i^{ee}$ and $\boldsymbol{f}_i^{ee}$ are the expanded element stiffness matrix and expanded element force vector for element *i*, respectively, and $\boldsymbol{a}$ is the nodal displacement vector for the whole structure. Here, the global displacements are introduced as defined in Equation (3.44).

Establish Equilibrium Conditions

The global forces are determined by demanding equilibrium at each node, i.e. the external forces must be equal to the sum of local forces acting on a node (see Figure 18). This gives us

$$\begin{bmatrix} F_1 \\ F_2 \\ F_3 \end{bmatrix} = \begin{bmatrix} P_1^1 \\ P_2^1 \\ 0 \end{bmatrix} + \begin{bmatrix} 0 \\ P_1^2 \\ P_2^2 \end{bmatrix}$$

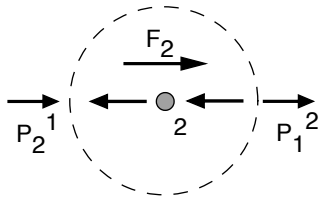

Figure 18: Forces acting on a nodal point

Assemble the Global Matrices

Now that the relations and equilibrium have been established, the global system matrices can be assembled:

$$\begin{bmatrix} k_1 & -k_1 & 0 \\ -k_1 & k_1+k_2 & -k_2 \\ 0 & -k_2 & k_2 \end{bmatrix} \begin{bmatrix} u_1 \\ u_2 \\ u_3 \end{bmatrix} = \begin{bmatrix} F_1 \\ F_2 \\ F_3 \end{bmatrix} \tag{3.46}$$

or

$$\boldsymbol{K}\boldsymbol{a} = \boldsymbol{f}$$

Introduce Boundary Conditions

$\boldsymbol{K}$ will always be a symmetrical matrix, and its determinant will therefore be equal to zero. Hence, the system in Equation (3.46) is not possible to solve. To mend this, boundary conditions need to be introduced. For the simple spring system with one DOF, constraining one of the nodes to translations in the x-direction will suffice, i.e. setting $u_1 = 0$. Now the first row can be removed as it will not provide any useful information, as well as the first column, since these values will be multiplied with u_1 and therefore disappear. This leads to

$$\begin{bmatrix} k_1+k_2 & -k_2 \\ -k_2 & k_2 \end{bmatrix} \begin{bmatrix} u_2 \\ u_3 \end{bmatrix} = \begin{bmatrix} F_2 \\ F_3 \end{bmatrix} \tag{3.47}$$

which consists of two equations, has two unknowns and is invertible. This system can now be solved.

Solve the System of Equations

When external forces and the stiffness matrix are known, the displacement vector can be found by

$$\boldsymbol{a} = \boldsymbol{K}^{-1}\boldsymbol{f}$$

and the problem at hand is solved.

3.7.2 FEM for a Beam

The steps in the previous chapter are essentially valid for any FE formulations, but determining the stiffness matrix is more complex for larger systems. Since the floating bridge in this report was modelled as a beam, this is the formulation to be looked at closer in this section. Again the theory is obtained from Ottosen and Petersson (1992). The deflection along the beam is:

$$w = \boldsymbol{N}\boldsymbol{a}$$

where

$$\boldsymbol{N} = \begin{bmatrix} N_1 & N_2 & \cdots & N_n \end{bmatrix} \qquad \text{and} \qquad \boldsymbol{a} = \begin{bmatrix} u_1 \\ u_2 \\ \vdots \\ u_n \end{bmatrix} \tag{3.48}$$

Here, n denotes the number of unknowns (not the number of nodes), and N_i is a shape function. When defining

$$\boldsymbol{B} = \frac{\mathrm{d}^2\boldsymbol{N}}{\mathrm{d}x^2} \tag{3.49}$$

the stiffness matrix, boundary vector and load vector are given, respectively, as

$$\begin{aligned} \boldsymbol{K} &= \int_a^b \boldsymbol{B}^T EI\boldsymbol{B}\mathrm{d}x \\ \boldsymbol{f}_b &= \left[\boldsymbol{N}^T V\right]_a^b - \left[\frac{\mathrm{d}\boldsymbol{N}^T}{\mathrm{d}x}M\right] \\ \boldsymbol{f}_l &= \int_a^b \boldsymbol{N}^T q\mathrm{d}x \end{aligned} \tag{3.50}$$

where

$$M = -EI\frac{\mathrm{d}^2 w}{\mathrm{d}x^2}, \qquad V = \frac{\mathrm{d}M}{\mathrm{d}x} \qquad \text{and} \qquad q = -\frac{\mathrm{d}V}{\mathrm{d}x}$$

M is the moment, V is the shear force and q is the distributed axial load. The system to be solved is now

$$\boldsymbol{K}\boldsymbol{a} = \boldsymbol{f}_b + \boldsymbol{f}_l$$

The rest of the steps are the same as for the previous example.

Chapter 4

Methods

4.1 About ANSYS

ANSYS is a powerful finite element analysis (FEA) software released for the first time in 1971. It is built up by more than 100,000 lines of code, and can perform a wide range of analyses such as static, dynamic, heat transfer, fluid flow and electromagnetic. The software is in use in many fields of engineering, and can perform highly advanced analyses and solve intricate problems. ANSYS uses the steps of the finite element method as explained in Chapter 3.7.1, but can solve problems of much greater complexity than realistically possible through hand calculations (Moaveni, 2015). Since ANSYS can be applied to a vast range of problems, not all aspects can be detailed in this thesis. The steps relevant for the analyses executed in this study are described in some detail below.

4.1.1 Preprocessing

In this step the model geometry is created, materials defined and loads applied. The geometry can either be created *bottom-up* or *top-down*. Bottom-up modelling is done by defining key-points, lines, areas and volumes, in that order. The alternative, top-down modelling, is when a three-dimensional object is created directly using volume primitives provided in ANSYS. When

the geometry is complete, each part has to be assigned an element type (beam, shell, spring etc.), material properties (Young's modulus, thermal conductivity, density etc.) and real constants (spring stiffness, cross-section area etc.). Which types of properties have to be defined depends on the type of analysis and what type of element is being used. Once the attributes have been defined, the model can be discretized, i.e. divided into elements. The size or number of elements for each part can be manually dictated by the user or automatically set by ANSYS default settings. Lastly in preprocessing, loads, boundary conditions and initial conditions are defined. In static and dynamic structural analysis the most relevant loads are pressure, forces and moments. Boundary conditions generally dictate how much an edge or point is allowed to move and/or rotate, and initial conditions include position, velocity and acceleration at the initiation of the analysis.

4.1.2 Solve

After the model in its entirety has been created and sufficiently constrained, the analysis can be carried out. There are different types of analyses to choose between, and several options within each. A static analysis can for example either be linear (small displacements) or nonlinear (large displacements), and a modal analysis can be performed using different methods (Block Lanczos, unsymmetric, supernode etc.). When the suitable analysis and options have been selected, the problem in question can be solved. For the main part of this study a full transient analysis was carried out to determine the response of the bridge when subjected to irregular waves over a period of time.

4.1.3 Post-processing

Once the analysis has been run, the relevant information can be collected. This may be maximum deflection, stress distribution, reaction forces etc. ANSYS can create contour plots showing how the relevant parameter changes over the geometry of the model, or list the same results for any number of chosen elements or nodes.

4.1.4 ANSYS Parametric Design Language

All of the steps mentioned above, from creating keypoints to plotting results, can be done step-by-step by communicating with ANSYS through the Graphical User Interface (GUI). By clicking through the right menu options and filling in the right numbers where needed, the whole process can be performed directly without having any particular knowledge of the ANSYS commands. This is easy and quick for simple models, but can be time-consuming and difficult for a more complex geometry. Instead, ANSYS Parametric Design Language (APDL) can be used to create a string of commands that ANSYS understands and executes. This is useful for instance when creating repetitive geometries as ANSYS understands loops that are repeated a given number of times. This means that instead of spending several minutes or hours creating hundreds of keypoints by manually entering each keypoint's coordinates, a "do-loop" can do the same in seconds when coded right.

All analyses in this study were carried out through APDL commands, and the strings of commands and additional necessary files can be found in the electronic appendices. The text from the different .txt-files can be copied into the command window in ANSYS to run the analysis. In order for the analyses to be carried out successfully, the ANSYS database has to be in the same folder as the *sections* folder, as well as some analysis-specific files mentioned below. *addmass.txt* and *damping.txt* are common for all except the modal analysis.

modal.txt runs the modal analysis and lists the eigenfrequencies of the first 30 modes. The frequency region, as will be explained in Chapter 4.7.2, needs to be specified as an integer between 1 and 6. Element size and time step must also be specified. *damping_modal.txt* is called during the command run and must be located in the same folder as the ANSYS database.

static.txt carries out the different static analysis. Element size and environmental loads can be specified at the beginning of the code. If the whole list of commands is run, both wind, current and traffic loads are applied.

regularanalysis.txt performs the simulation of a regular wave acting on the bridge. Wave period, element size, time step and wave amplitude must be specified. The commands also find the extreme values of accelerations in the last 40 s of the simulations, when only the steady-state

responses remain. The values are stored as parameters and can be read when the analysis is finished. The file *regular_delay.txt* is called during the analysis, as well as the files containing the regular wave forces in heave, sway and roll. These files must be located in the same folder as the ANSYS database.

dynamic_seastate.txt runs the irregular sea state with 1-hour duration, and finds the extreme accelerations and stores them as parameters. Element size, time step and approximate peak period must be specified, as well as file names of the .csv-files containing the forces to be applied. These files must therefore be located in the same folder as the ANSYS database. The forces are calculated using MATLAB codes, described later in Chapter 4.3.

4.2 Description of the ANSYS Model

The model of the bridge concept was created in ANSYS through a list of commands written in APDL, as mentioned previously. It consisted of three parallel beams arced in the horizontal plane, with transverse beams approximately every 40 m. Columns were placed at evenly spaced intervals of about 200 m. Half of the cable-stay bridge was included for improved accuracy of the boundary conditions at this end. The other half of the cable-stay bridge was assumed to have little effect on the relevant properties. This was because the tower holding the cables was assumed infinitely stiff and the bridge girder was assumed fully fixed at the connection with the tower. The bridge was made of S460 grade steel, with yield strength 440 MPa for plate thickness between 16 mm and 40 mm (British Standards, 2004). The density and young's modulus were 7850 kg/m^3 and 210 GPa, respectively. Figure 19 shows the model in ANSYS.

4.2.1 Coordinate System

In Chapter 3.5.4 the theory for wave forces uses the coordinate system presented in Figure 16. In the ANSYS analysis, however, it was convenient to establish a global coordinate system for both the bridge and the pontoons. This coordinate system can be seen in Figure 20, and the relationship between the two coordinate systems are displayed in Table 6.

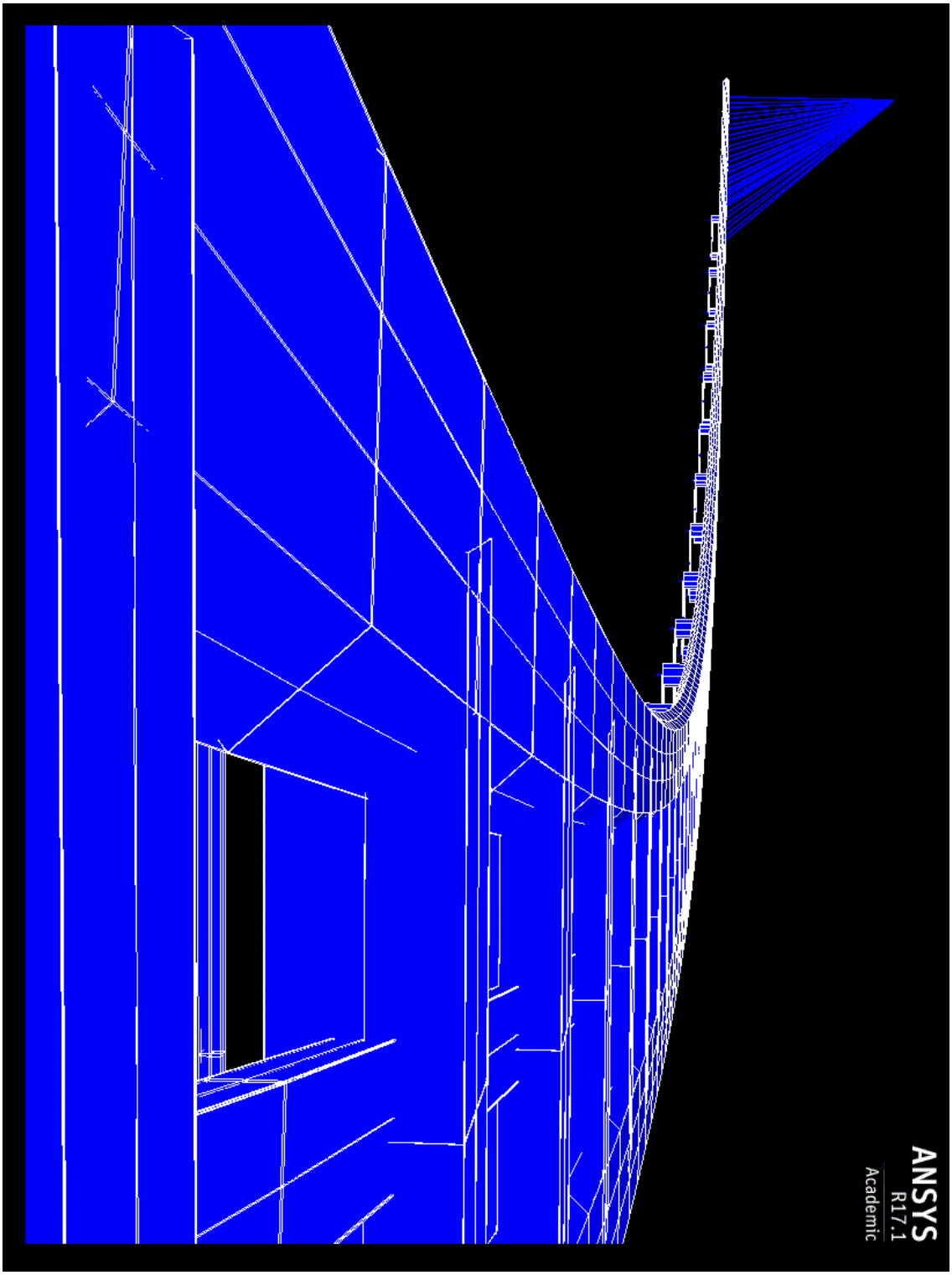

Figure 19: The bridge model in ANSYS seen in perspective from the northern end

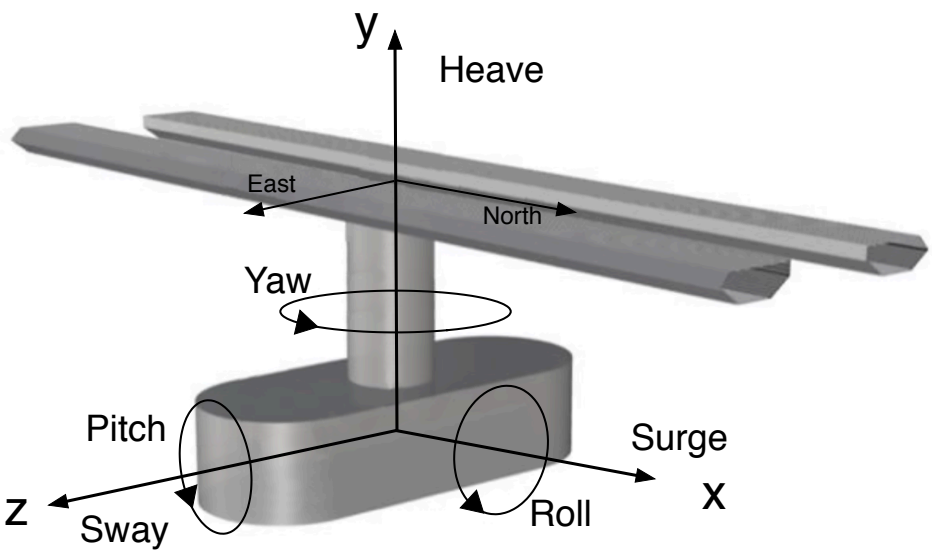

Figure 20: Coordinate system to be used in the analyses (Larsen, 2016a, edited)

Table 6: Relationship between local coordinate system for pontoon motions and global coordinates

Local Coordinates		**Global Coordinates**	
η_1	surge	η_{uz}	sway
η_2	sway	η_{ux}	surge
η_3	heave	η_{uy}	heave
η_4	roll	$\eta_{\theta z}$	pitch
η_5	pitch	$\eta_{\theta x}$	roll
η_6	yaw	$\eta_{\theta y}$	yaw

4.2.2 Geometry

The aim of the analyses in ANSYS was to get relevant and accurate results that could reveal the static and dynamic behaviour of the bridge. One step to achieve this was to create geometries as realistic as possible, as this would give the model structural properties similar to the actual bridge. The bridge is shaped like an arc with radius 5000 m, and the direct distance from the tower of the cable-stay bridge in the south to the abutment in the north is 4322 m. The other half of the cable bridge (between axes 1 and 2 in Figure 21) was not modelled as it was assumed to have little effect on the global responses due to the boundary conditions at the tower (see Chapter 4.2.3). The first 490 m of the bridge are held up by cables while the remaining 3743 m are held afloat on 19 pontoons evenly distributed along the arc length. In the design concept

from the NPRA the pontoons are instead distributed evenly along the x-axis, which will result in slightly different span lengths. This difference is minimal however, and the approximation is assumed accurate enough.

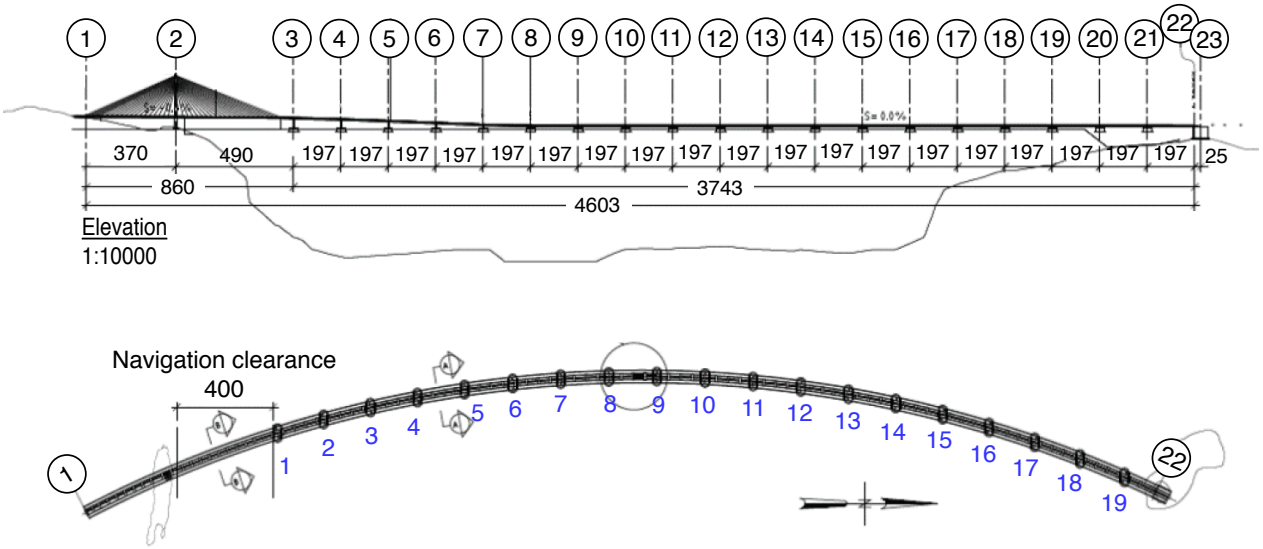

Figure 21: The NPRA's concept illustration for crossing Bjørnafjorden with an arced pontoon bridge. The black, circled numbers indicate axis numbers, and the blue indicate pontoon numbers. All dimensions in metres (Larsen, 2016a, edited)

Another difference between the concept and the ANSYS model is the extra elevation at the southern end for big ships to pass underneath. Figure 21 shows that the bridge has an upward slope from the floating part up towards the tower of the cable-stay bridge. However, the main interest for the analyses were the overall response of the bridge girder, and this was assumed not to be affected greatly by the slope. For more detailed local analyses of stresses and strains in bridge parts, this simplification migth not be valid.

Main Bridge Girders

When creating a beam model in ANSYS, the beams have to be assigned cross-sections that give the beam certain properties like stiffness and toughness. ANSYS have some built-in sections, but they were too simple for the complex geometry of the bridge girder. Therefore, the cross-sections for the two main girders were created separately as meshed areas in ANSYS and saved as .SECT files. Six different ones were created; one section each for inner and outer side of the

arc for the spans, at columns and for the high bridge. The main dimensions were the same for all six (see Figure 23), but the thicknesses differed along the length of the bridge as according to the NPRA design concept (see Figure 22). Table 7 shows the sectional properties for each cross-section, where inner and outer beams are identical but mirrored. The plate thicknesses are not the actual dimensions of the girder plates, but rather equivalent thicknesses after accounting for stiffeners in longitudinal and transverse direction. These values were obtained from the NPRA's report (Larsen, 2016a), and were used to create a simplified model that should still yield valid results.

Table 7 uses average values for the cable-stay bridge, as this part consists of three different cross-sections. This is a weighted average on the form

$$H = \frac{H1 \cdot 330 \text{ m} + H2 \cdot 125 \text{ m} + H3 \cdot 35 \text{ m}}{490 \text{ m}} \tag{4.1}$$

where *H1*, *H2* and *H3* are the properties of interest for the three different sections and H is the weighted average. This was done to save time when creating the model and was considered accurate enough as the main interest was the properties of the main bridge and not the high bridge span.

Pedestrian Lane

The pedestrian lane was modelled as a rectangle with dimensions 5x2 m and plate thickness 55 mm. Because of its limited size compared to the two main beams, it would have little effect on the stiffness of the bridge. However, due to the model being less detailed than the one from the NRPA, some extra weight was needed in order to obtain the same properties. Therefore, the plates of the pedestrian lane were made quite thick to add the extra mass needed. The calculations of the mass per unit length can be found in the electronic appendix *bridgemass.m*.

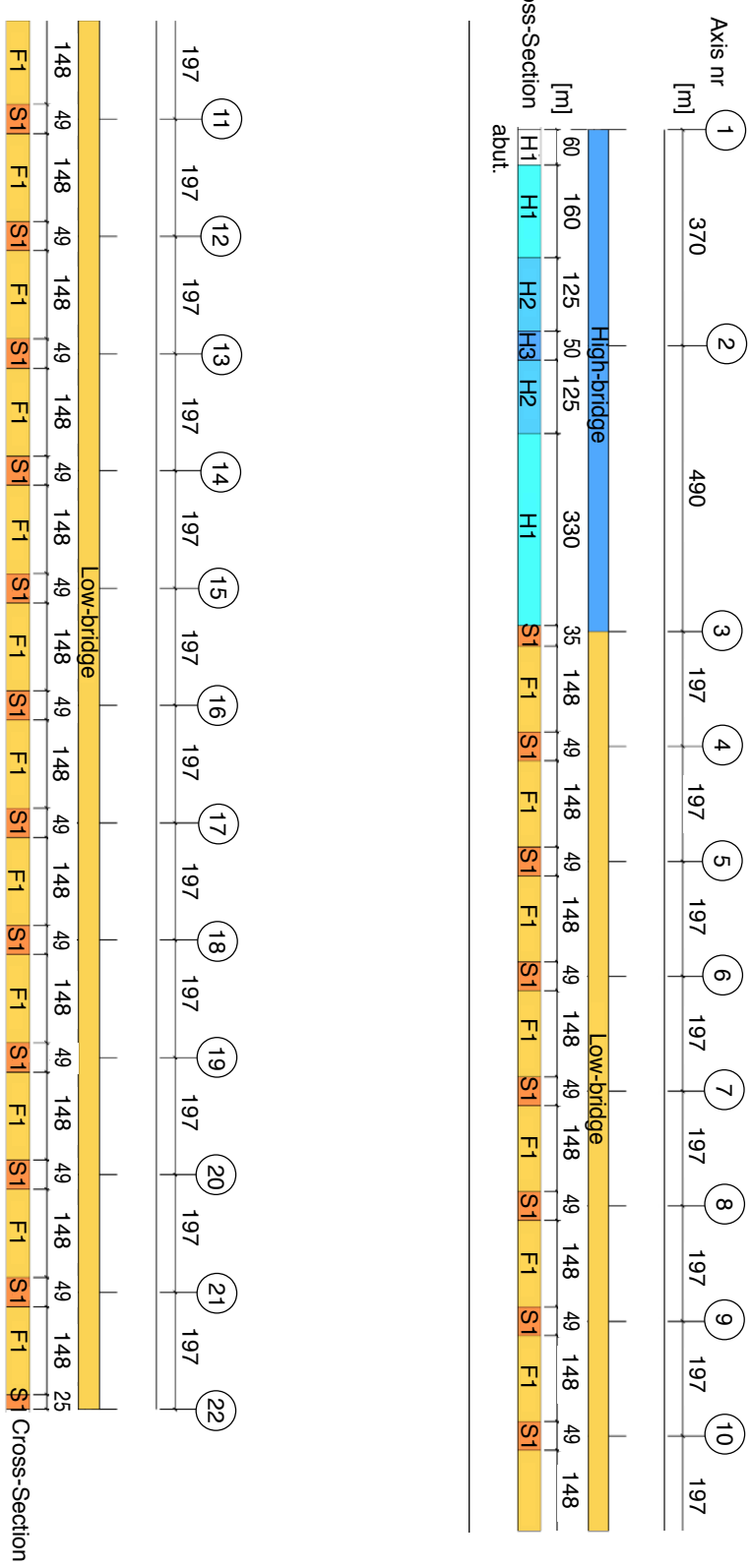

Figure 22: Cross-section distribution over the length of the bridge (Larsen, 2016a)

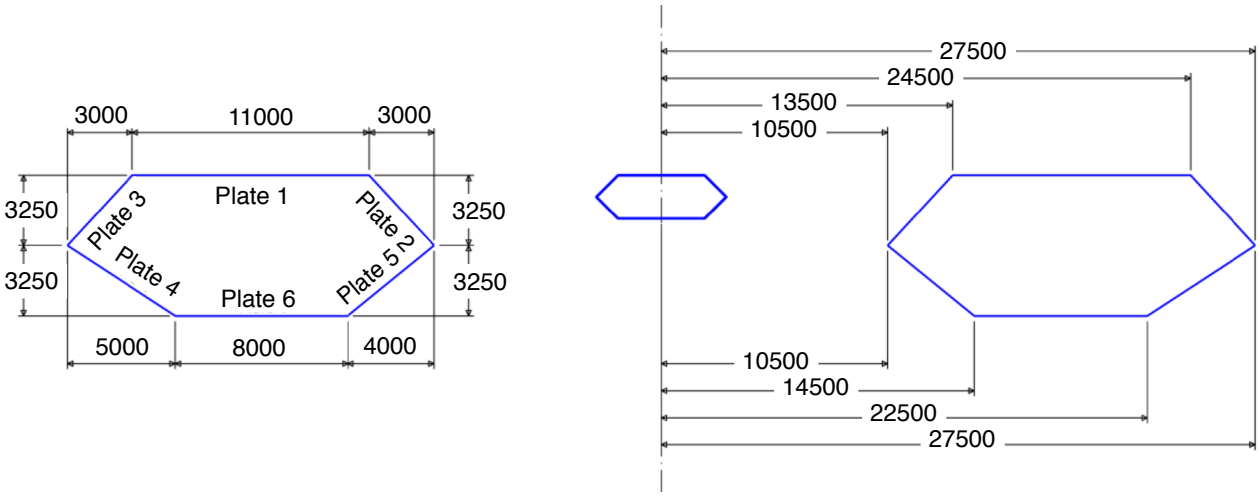

Figure 23: Cross-section of the beam girder with dimensions in millimetres (Larsen, 2016a)

Table 7: Sectional properties for the girders as given by the NPRA and as used in the ANSYS analysis (Larsen, 2016a)

	Cable-stay bridge (H)		**Support section** (S1)		**Span section** (F1)	
	NPRA avg.	ANSYS	NPRA	ANSYS	NPRA	ANSYS
Equivalet plate thickness [mm]						
Plate 1	29.6	25	36	46	25	35
Plate 2	21.4	20	20	20	20	20
Plate 3	23.1	25	36	36	25	25
Plate 4	23.1	25	36	36	25	25
Plate 5	21.4	20	20	20	20	20
Plate 6	26.1	25	36	36	25	20
Area [m^2]						
Twin box	1.71	1.85	2.5	2.72	1.85	2.07
Permanent loads [kN/m]						
Girder weight	197.2	254.6	255	311.9	205	261.8
Asphalt, railings etc.	57	–	57	–	57	–
Total	254.2*	254.6	312	311.9	262	261.8

**the average from the NPRA report was 253.9, but this was assumed to be a typographical error (see Appendix A)*

Cross Beams

The dimensions of the cross beams were taken from Larsen (2016a), similarly to the dimensions of the main beams. The cross beams were modelled as beams with a rectangular cross-section, with height 6.5 m and width 8.0 m (see Figure 24). The equivalent thickness when accounting for stiffeners was 0.03 m for the walls and 0.02 m for the top and bottom plate.

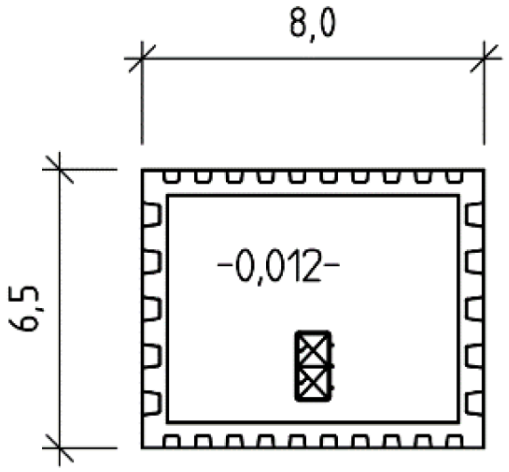

Figure 24: Cross-section of cross beams (Larsen, 2016a)

Cables

The cable-stay bridge has 21 cables attached to each main girder on either side of the tower, but as previously mentioned, only half of the cable bridge was modelled. The length, cross-section area and effective Young's modulus for the different cables are given in the NPRA's report (Larsen, 2016a). The spring stiffness, k, was found for each cable by k=EA/L and averaged over the 21 cables in order to simplify the code for the analysis. Although this may yield slight inaccuracies in the response of the cable bridge, it was thought accurate enough when focusing on the response of the main bridge. A pretension load was also added to the cables, based on the self-weight of the bridge carried by each cable. The high bridge weighs 255 kN/m, resulting in a pretension load of approximately 3 MN per cable when the bridge is 490 m long. The cable part of the bridge is shown in Figure 25.

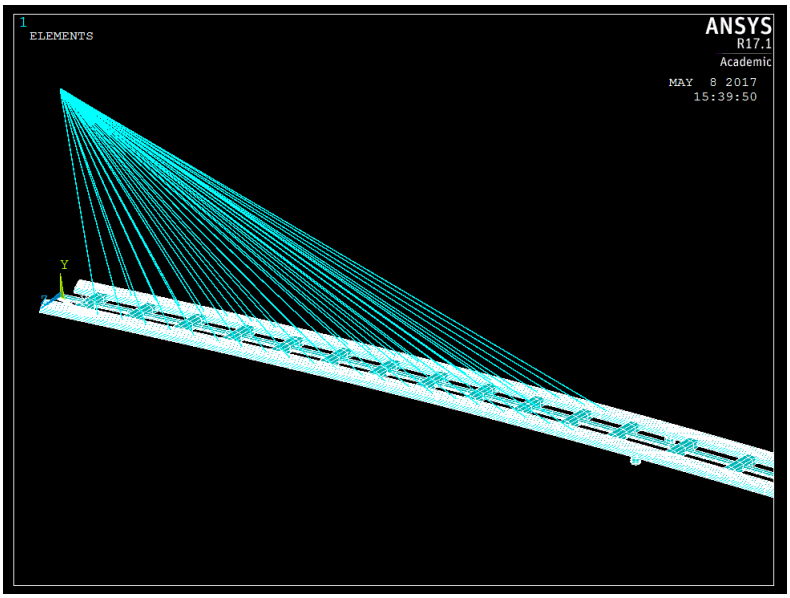

Figure 25: Bridge held up by cables, model in ANSYS

Pontoons

The pontoons were not explicitly modelled in ANSYS, as the interest was on the response of the bridge girder and not on the effect on the pontoons. Nevertheless, the geometry of the pontoons was important in order to calculate the forces acting on the bridge caused by waves and current hitting the pontoons. Figure 26 shows the main dimensions of the pontoons. The flange at the bottom is 5 m wide, and is attached mainly to increase added mass in heave (Larsen, 2016a). The draught is 10.5 m and the radius of the rounded sides is 14 m. This results in a water line area of 1,735.8 m^2.

Although the pontoons were not modelled in ANSYS, the mass and buoyancy of the pontoons had to be included to get accurate responses. A massless beam with very high stiffness connected each pair of beams, with a node at the centre. Added mass and wave forces on the pontoons were applied at these nodes in the analyses in order to get realistic responses. The added mass was frequency dependent and found from the NPRA's report. The values used in the analysis can be found in Appendix B. For the regular wave analyses the appropriate values were used, but for the irregular sea states the added mass was assumed constant and at a value corresponding to a frequency close to the peak frequency. Static buoyancy forces were also applied, which were found from a static analysis of the model without any external forces working on it.

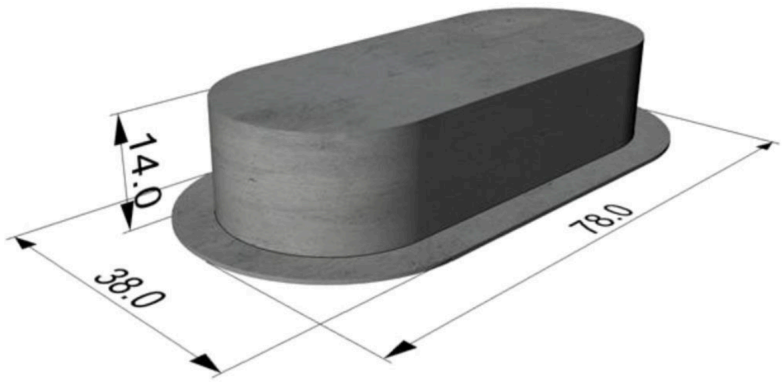

Figure 26: Pontoon geometry (Larsen, 2016a)

4.2.3 Boundary Conditions

One important aspect to make a finite element model accurate is the implementaion of boundary conditions. Boundary conditions are typically applied to edges and/or corners of a structure, and dictate, in a structural analysis, in which directions the point or edge is allowed to move and rotate. The model with boundary conditions can be seen in Figure 27.

Southern End

The southern end of the ANSYS model ends in the middle of the cable bridge, where the tower is placed on a grounded foundation. In accordance with the NPRA's design concept, the connections between the tower and bridge girders were assumed fully fixed. There are several benefits to this solution, including less maintenance (no bearings), more robustness and lower material costs (Larsen, 2016a). When assuming that the tower is infinitely stiff, the tower did not have to be modelled. Instead the bridge girders could be fully fixed at the end and the top point of the cables could be fixed in all translations.

Northern End

At the northern end, the bridge is connected to a caisson structure firmly founded at 40 m depth. The structure is 52 m long, 45 m wide and 50.5 m high and filled with saturated sand for ballast.

As with the tower in the south end, this structure is assumed infinitely stiff and the bridge girders are fully fixed in translations and rotations.

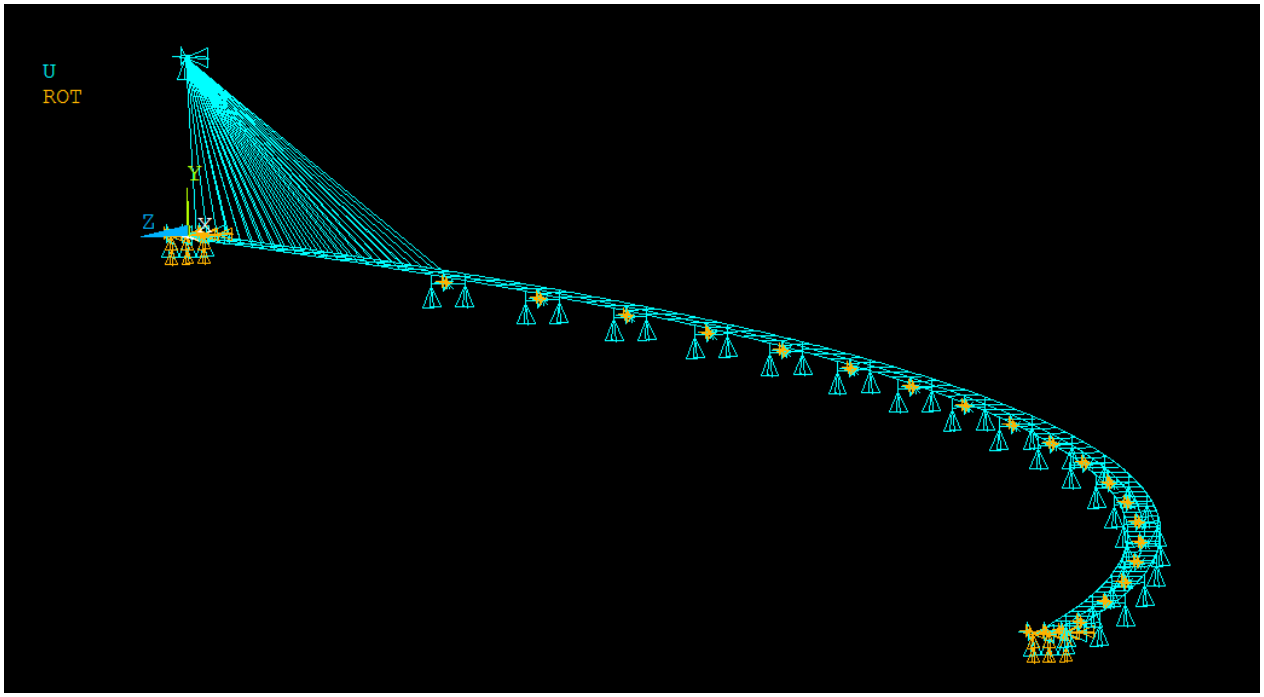

Figure 27: The model with applied boundary conditions

Pontoons

The pontoons of the bridge did not have to be moored because of the arced shape as discussed earlier. Vertical motions, however, were restricted by increase and decrease in buoyancy when the pontoon moves downwards and upwards, respectively. These restrictions are not absolute, and some movement in the vertical plane is allowed. To simulate the effect of the change in buoyancy, i.e. the restoring forces, a vertical spring was attached to the bottom of each column with spring stiffness $k/2$. k is the spring stiffness of the pontoon and can be expressed as the restoring term C_{33} described in Chapter 3.6.4. The spring stiffness had to be halved because the springs in the model were attached in parallel directly to the columns, of which there were two for each pontoon. The reason they were attached separately and not as one spring with stiffness k at the mid-node of the pontoon beam was to increase rotational stiffness and prevent large rotations in a similar way to what the pontoon would. The springs were fixed in the vertical direction only, as the water would not prevent translations in the horizontal plane.

In addition to the vertical springs, a torsional spring was added to each pontoon. The stiffness was found from the NPRA's report, calculated in accordance with the expression for C_{55} in Chapter 3.6.4, and set to 5700 MNm/rad. The end of this spring was fixed in the x-direction and in rotations about the x-axis. Together, the two springs simulated the restoring forces of the pontoons. A third spring hindering rotations about the z-axis was deemed unnecessary due to symmetry of the bridge. Horizontal translations and rotations about the y-axis does not provide any restoring forces and did not have to be accounted for. To simulate the radiation damping of each

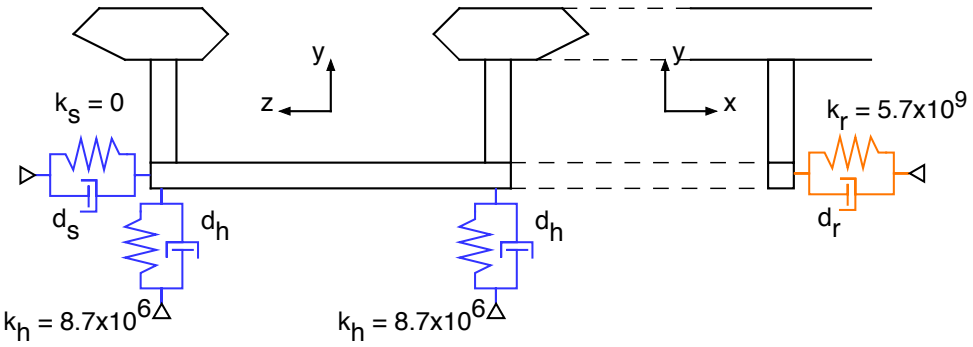

Figure 28: Illuastration of the spring/dampers on the pontoons. Blue indicates translational spring/damper and orange indicates rotational spring/damper. Spring stiffnesses are constant and shown in the figure, while damping is frequency dependent and only indicated by a symbol.

pontoon, a damper was added to the springs in heave and roll. Additionally, a spring/damper system was added in the z-direction with zero spring stiffness and therefore only damping effect. As with added mass, the damping in the different directions were found in NPRA's report and were frequency dependent. For the regular waves, the damping was found for the relevant frequency, but for the irregular sea state this was not an option. Instead the damping was assumed constant and with values corresponding to a frequency close to the peak frequency. An illustration of the boundary conditions on the pontoons is shown in Figure 28, and the damping values for different frequencies can be found in Appendix B.

4.2.4 Rayleigh Damping

The Rayleigh damping of the system was found from the theory in Chapter 3.6.3 and implemented in the dynamic ANSYS analyses through simple commands. Different alphas and betas were briefly experimented with, but seemed to have little to no effect on the results apart from

when they were neglected. Finally, a damping ratio of 2% was assumed for periods of 1 s and 10 s, corresponding to circular frequencies of 6.28 rad/s and 0.63 rad/s, respectively. This resulted in

$$\alpha = 0.02285 \qquad \text{and} \qquad \beta = 0.005787$$

which were the values used in the final analyses.

4.3 MATLAB

MATLAB is a convenient and easy-to-use programming tool often used to solve engineering problems. For this study, MATLAB was used mainly to calculate the forces acting on the pontoons which would then be implemented in ANSYS. This was done using four different scripts; *jonswap.m*, *addedmass.m*, *pontforce.m* and *regularforce.m*. All four were created by the author specifically for this project and can be found in the electronic appendices.

jonswap.m calculates the spectrum and wave amplitudes for three different sea states and saves the values in arrays. This is done for a series of wave frequencies from 0.5 to 6 rad/s as the spectra lie within this region. According to DNV (2010), the minimum number of frequencies should be at least 1000 for a short term sea state. $\Delta\omega$ was therefore set to 0.005, resulting in 1100 frequencies within the region.

addedmass.m uses the expressions for added mass from the Microsoft Excel sheets (see Chapter 3.6.2) to calculate the added mass in heave and sway for the same range of frequencies as mentioned above. The values are saved in arrays.

pontforce.m calls the two previous functions and uses the spectra and added masses to calculate the forces and moments in heave, sway and roll on a pontoon over time for three sea states. The resulting forces are written to excel sheets.

regularforce.m calls function *addedmass.m* and uses this to calculate the forces on a pontoon in heave, sway and roll for regular waves. The forces are calculated for wave periods from 2-13 s with unit amplitude, and are then written to excel sheets.

4.4 Wave Loads

As previously explained in Chapter 3.5.2, an irregular sea state can be modelled by a linear superposition of many regular sinusoidal waves. The sea state can be statistically described through a spectrum, and the JONSWAP spectrum, wich is widely used in the North Sea, relies on two variables – significant wave height H_s and peak period T_p. Buoys were placed at several locations on Bjørnafjorden at the beginning of 2015 to measure these and other values (Statens Vegvesen, 2015a), and the results by November 2016 can be seen in Table 8. The data used in the analyses are marked in the table, and the resulting JONSWAP spectra are shown in Figure 29. This information was received by email from the NPRA (H. K. Fuhr, personal communication, November 29, 2016).

Table 8: Parameters for wind generated waves in Bjørnafjorden, data received through personal communication with the NPRA. The values to be used in the analyses are marked with a box.

Return period	**1 year**		**10 years**		**100 years**		**10 000 years**	
Sector	Hs [m]	Tp [s]	Hs [m]	Tp [s]	Hs [m]	Tp [s]	Hs [m]	Tp [s]
345°- 75°	0.8	4.0	1.1	4.5	1.5	5.0	2.3	5.9
75°- 105°	1.6	5.3	2.2	5.9	2.8	6.6	3.9	7.6
105°- 165°	1.1	4.4	1.3	4.8	1.6	5.3	2.3	6.1
165°- 225°	1.2	4.4	1.5	4.9	1.9	5.3	2.7	6.1
225°- 315°	1.3	4.6	1.8	5.3	2.4	5.9	3.3	6.8
315°- 345°	1.5	5.1	1.9	5.6	2.5	6.2	3.5	7.2

As mentioned in Chapter 3.5.3, the JONSWAP spectrum is only valid for certain T_p and H_s ratios. Table 9 shows that the JONSWAP spectrum is a valid approximation for all three sea states to be looked at in this study.

4.4.1 Wave Load Phase Shift

Because the bridge is arced in the horizontal plane, waves will not hit the pontoons with the same force simultaneously. Instead, there will be a delay in the force between the different

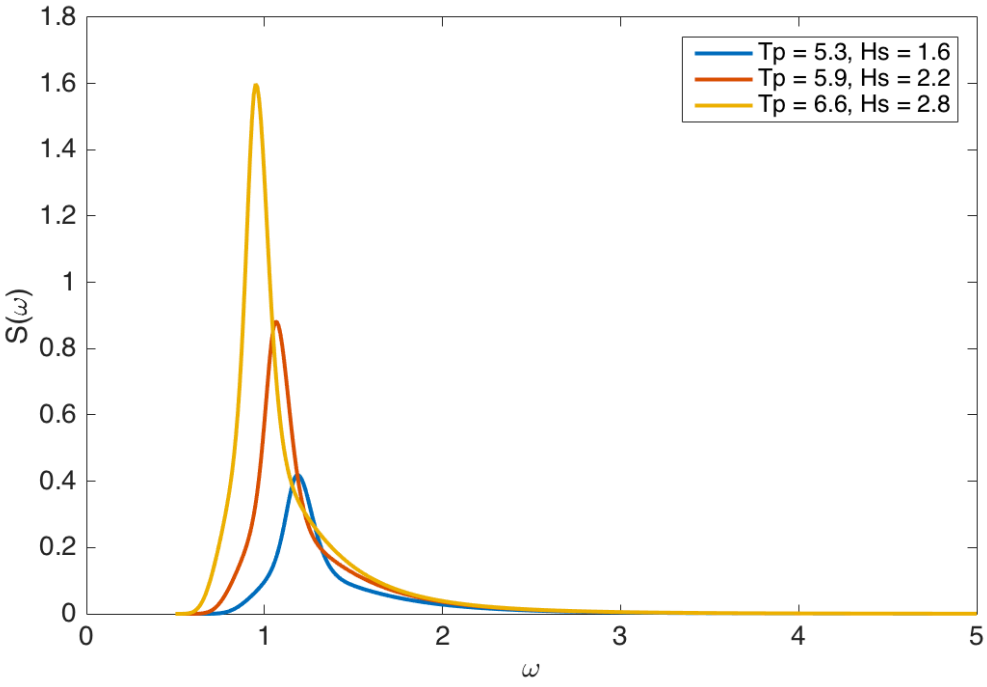

Figure 29: The JONSWAP spectra for the three sea states used in the analyses

Table 9: Determining whether or not the JONSWAP spectrum is valid for the given sea states

H_s	T_p	$\frac{T_p}{\sqrt{H_s}}$	$3.6 < \frac{T_p}{\sqrt{H_s}} < 5$
1.6	5.3	4.19	OK
2.2	5.9	3.98	OK
2.8	6.6	3.94	OK

pontoons, which depends on the position of the pontoons. This delay can be implemented by adding a phase shift to the oscillation term of the force. As a way of saving preparation and computation time, it was decided that the pontoons would be paired together and the same forces would act on the two pontoons at the same time. This was thought to be a reasonable approach as the waves in the relevant sea states hit the bridge at an angle between 75 °-105°, which would be the case for these waves. Paired together would be pontoon 1 and 18, 2 and 17 etc., and only pontoon 19 would not be paired. See Figure 21 on page 59 for pontoon numbering.

In order to determine the phase shift at the different pontoons, the distance between the pontoons had to be determined. The positions of the pontoons were found in ANSYS and plotted in excel, and are shown in Figure 30 as blue crosses. Then, pontoon number 9 and 10 were set as

the reference point as a wave propagating in the positive z-direction would hit these pontoons first. The average position of the paired pontoons were found and are plotted as red dots in Figure 30.

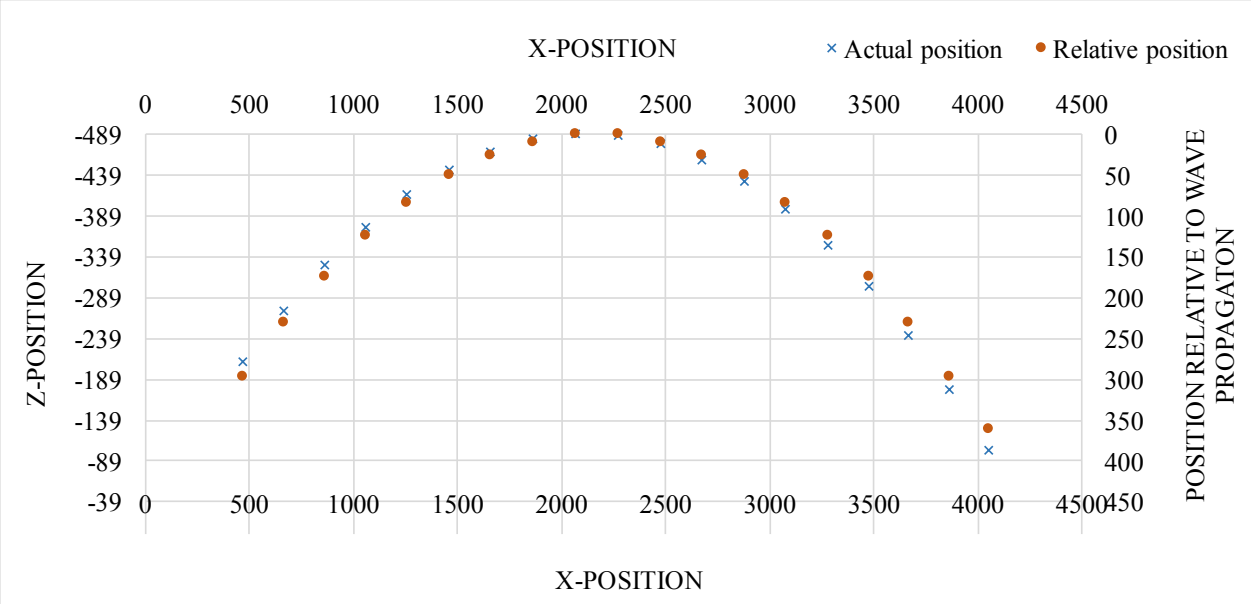

Figure 30: Actual pontoon position in the xz-plane and position relative to waves propagating in the z-direction at a slight angle

The phase shift for each wave component was found as

$$\phi_i = 2\pi \frac{L}{\lambda} \tag{4.2}$$

where L is the distance between the reference pontoons and the relevant pontoon pair in the wave propagation direction. λ is the wave length found by $\lambda = \frac{2\pi g}{\omega^2}$

4.5 Wind Loads

For this study, wind loads were assumed to be static loads, and the mean wind speeds were found from the NPRA's report (Larsen, 2016a). In their analyses wind speeds at 52 m above mean water level were assumed, so slightly smaller values were used in the wind load analyses for this thesis. The values provided by the NPRA were considered conservative even for the

given height, so the wind speeds used in this study are assumed to be quite conservative as well. More detailed data on the wind climate in Bjørnafjorden should be collected and used in further studies.

Because of the geometry of the bridge, with three beams parallell in the horizontal plane, shielding effects of the wind force had to be taken into account. Due to the difference in size, also solidification effects had to be included for the force acting on the pedestrian beam. See theory in Chapter 3.1.1. The wind speeds used in the analyses with resulting forces can be seen in Table 10. The coefficients used were found either from the NPRA report or from DNV's rules (DNV, 2010).

Table 10: Wind speeds used in the analysis, and the resulting wind forces acting on the different parts of the bridge

Return period		**1 year**	**10 years**	**100 years**
Wind speed [m/s]		25	30	38
Wind force [kN/m]	Outer beam	2.75	3.96	6.35
	Ped. beam	0.53	0.77	1.23
	Inner beam	0.53	0.77	1.23

C = 1.04, $\phi = 0.31$, $\alpha = 3$, $\beta = 0.6$, $\eta = 0.63$

4.6 Current Loads

The buoys placed in Bjørnafjorden measuring wave elevation also measured current speeds at different depths, and the resulting values can be found in Table 11. These values came from data sets of poor quality, and the NPRA stated in the personal communication that they used these numbers as extreme values only in their analyses. Since the aim of this study was to determine maximum response, these values fit the nature of the analyses well. Because the pontoons had a draught of 10.5 m, a uniform current speed slighly less than the speed at the surface was assumed. The forces on the pontoons were calculated according to the theory in Chapter 3.1.1, and can be seen in Table 12.

Table 11: Current speeds at various depths in Bjørnafjorden, data received through personal communication with the NPRA

Return period	**1 year**	**10 years**	**100 years**
Depth [m]	Current speed [m/s]		
0-5	1.00	1.20	1.40
15	0.60	0.80	0.95
25	0.40	0.50	0.60
50	0.35	0.45	0.55
100	0.20	0.25	0.30

Table 12: Uniform current speeds and current forces per pontoon used in the analyses

Return period	**1 year**	**10 years**	**100 years**
Current speed [m/s]	0.9	1.1	1.3
Current force [kN]	122.0	182.3	254.6

4.7 The ANSYS Analyses

In order to get an impression of the response of the bridge in different load cases, various analysis types were carried out. Together the results will hopefully give a comprehensive understanding of the behaviour of the bridge as well as potential problem areas and shortcomings in the design or method.

4.7.1 Convergence Study

Often when doing analyses using the finite element method, a lot of time can be saved by dividing the model into larger and fewer elements, by taking larger time steps, or by doing a linear instead of non-linear analyis. Often, however, saving time could mean losing accuracy, which is undesirable. Convergence studies can therefore be carried out to find the point where the analysis is time efficient and yields sufficiently accurate results. In this study, a few simple convergence studies were carried out for element size, linearity versus nonlinearity and for time step length.

The element size convergence was determined through a static analysis where approximate ele-

ment size was set between 2 m and 55 m. In order to get relatively large deflections and therefore possibly better see the difference for different element sizes, maximum traffic load was applied on the bridge beams. The results of interest were maximum vertical deflection, bending moments and shear forces of the bridge beams. A change of less than a few percent was deemed acceptable. After the analysis with changing element size had been run through, it was repeated with an additional setting allowing for large deformations.

To determine the effect of time step, several dynamic analyses were run through with the same regular wave load. Time steps of 0.1, 0.2, 0.4 and 0.6 s were used. For each run of the analysis, maximum and minimum deflection, velocity and acceleration were recorded for a node placed in the middle between two columns. Element size and linearity was chosen according to the results form the previous two convergence studies.

4.7.2 Modal Analysis

The modal analysis was performed for two reasons. The first reason was to make sure the eigenfrequencies of the bridge model were close to the eigenfrequencies determined by the NPRA, as this would be a good indicator that the dynamic properties of the model were acceptable. The second reason was to determine the eigenfrequencies of the modes that were likely to occur when the bridge is acted upon by waves, in particular in heave direction. Ideally the eigenfrequencies should lie outside the common range of wave frequencies in order to avoid resonance. Low-frequency horizontal modes were also of interest as these may become dominant in certain wind conditions.

Because the added mass of the pontoons was frequency dependent, six different added mass combinations where used to find the first 30 eigenfrequencies. The added masses for different frequency ranges can be seen in Table 13. The divisions were somewhat arbitrary, but chosen at intervals within which the added mass changed little and assumed to be accurate enough. The results for the different combinations were so similar that this assumtion was considered valid. The reason only the first 30 modes were found was that the NPRA had determined eigenfrequencies in their report, and all heave modes were amongst these modes.

Table 13: Added mass in x, y and z-translations and rotations for different frequencies (F) as used in the modal analysis. Mass values in kilotonnes [$10^6 kg$] and inertia values in kilotonnes times metres squared [$10^6 kg{\cdot}m^2$]

	F < 0.05	**<**	**F < 0.067**	**<**	**F < 0.1**	**<**	**F < 0.119**	**<**	**F < 0.132**	**<**	**F < 0.17**
$M_{a,x}$	20		22.5		28		26		15		5
$M_{a,y}$	43		39		34		33.5		34		36
$M_{a,z}$	5		5.7		6.4		6		5		3
$I_{a,xx}$	11 450		11 470		11 450		11 500		11 600		11 660
$I_{a,yy}$	3 000		3 000		3 500		4 300		4 800		4 900
$I_{a,zz}$	3 500		3 600		3 800		3 900		3 600		3 900

4.7.3 Static Analysis

Static analyses were carried out to make sure the bridge could withstand both its own self-weight and other static loads without excessive deflections and stresses. Deflections and internal loads were found for the model first without any external loads, and then with static current, wind and traffic loads acting on it. The effects were found from the loads separately and combined. Traffic loads were applied according to load model 1 presented in Chapter 3.1.2, although the concentrated loads were largely omitted. One static analysis was run with a concentrated load of 1200 kN at the middle of each span between pontoons, but the effect was found to be limited and neglected for the remaining analyses.

4.7.4 Regular Wave Analysis

Regular wave analyses were performed for waves with periods of 2-13 s, therefore spanning all periods likely to occur for all three sea states based on the JONSWAP spectrum. Since the analyses were performed using linear theory the response was found for a wave with unit amplitude and then later scaled to a more appropriate amplitude. Damping and added mass was adjusted for each period to match the values given by the NPRA. The regular force acting on each pontoon in heave for the different periods are found in Figure 31. The same forces for roll and sway are found in Appendix C.

For simplicity, instead of creating ten different loads for the ten pontoon pairs, the phase shift

was implemented as a time delay calculated based on distance between pontoons and the wave speed. This was more efficient and still valid as the waves were regular and therefore propagating at a uniform speed for each wave period. These calculations can be seen in the electronic appendix *pontoon_delay.xslx*. The analyses were carried out over 5 minutes, when the transient response had subsided and only the steady-state response remained. Then a series of APDL commands were used to find maximum translations and accelerations for this steady state.

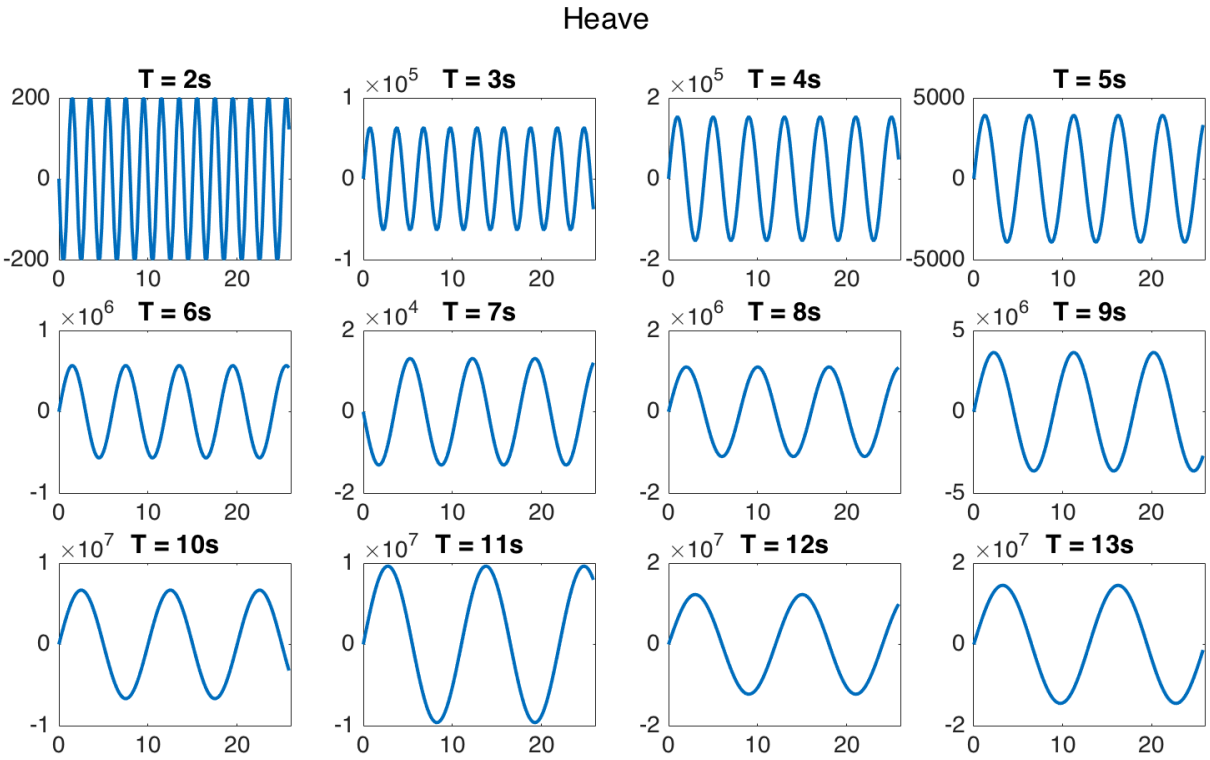

Figure 31: Force in heave for regular waves with periods from 2-13 s. Units are newton on the y-axes and seconds on the x-axes

The amplitudes for the different regular waves were found partly from the spectrum for the sea state with a 1-year return period, partly from the NRPA's report and partly through educated estimation. From Equation 3.19 the most probable largest wave height for the spectrum was found to be 2.94 m, resulting in approximate amplitude of 1.5 m, for a sea state with a 1 hour duration and mean zero-crossing period 4.12 s. The moments needed to find the period, m_0 and m_2, were found by integration in MATLAB (See electronic appendix *jonswap_int.m*. The JONSWAP spectrum (Figure 29 on page 70) has very low values for periods longer than 8 s, which means

their contribution to the total wave elevation and therefore total wave force is practically negligible. Therefore, for waves with longer periods, the amplitudes were set to half of the significant wave height used in NPRA's report. The final amplitudes used in the analyses are presented in Table 14.

Table 14: Amplitudes for regular waves

Period [s]	**Amplitude** [m]	**Period** [s]	**Amplitude** [m]
2	0.2	8	1.5
3	0.3	9	0.1
4	0.5	10	0.1
5	0.8	11	0.1
6	1.1	12	0.2
7	1.4	13	0.2

4.7.5 Irregular Sea State Analysis

The irregular sea states were the main analyses, where the aim was to determine extreme responses of the bridge when exposed to three different storm intensities. Ideally, this would be found by running an analysis of a full storm duration, but as a storm can last for days this is not practically possible. Instead, short-term wave statistics are employed to find the most probable largest response. Sea state durations up to three hours are common, and long durations could potentially yield more reliable results than short. For this study, a three hour sea state would take considerably more time to run than a one hour sea state, presumably without providing significantly improved results. Therefore, the bridge was subjected to six sea states, each with one hour duration.

The sea states were all derived from the same JONSWAP spectrum, but with different random phase shifts for each wave component. Hence, the total force at any point in time will be different for the different sea states, as will the extreme values. For each of the sea states the extreme values for translations and accelerations were found, and from this the mean, variance, and standard deviation were determined. Assuming the extreme responses are normally distributed, 95.45% of the values will be within $\pm 2\sigma$ of the mean (Weisstein, nd). Although the extremes may not be perfectly normally distributed and six data sets are not necessarily enough

to get accurate information about the mean and variance of the extreme responses, it should be good enough to provide a useful estimate. After results were found for a storm with a 1-year return period, similar simulations were run for storms with 10-year and 100-year return periods. These sea states were run 3 times each to find an average, before an upper limit was found by adding two standard deviations, in percentage, as found from the 1-year storm. This was done due to time considerations, and is likely to provide sufficiently viable results.

To determine the precision of the ANSYS analyses, one sea state was run four times and the extreme response values compared. Since the FEM is an approximate method, it is not unlikely that ANSYS will give small variations in results, especially when some settings are set to automatic and may therfore by chance vary slightly each run. Determining the magnitude of the variations was important, as large differences might require some modifications in use and interpretation of results.

Chapter 5

Results

5.1 Convergence Study

The convergence study was carried out for element size, linearity/non-linearity and time step, and results can be found in Tables 15 and 16. Extreme bending moments and shear forces were not affected by accounting for nonlinearities, and the effect on maximum deflection in the y-direction was negligible. Therefore, it was assumed accurate enough to proceed with linear solutions for the remainder of the analyses. When choosing the linear solution, the difference between 2 m and 55 m element length was most significant for extreme bending moments, with a 6% difference. When decreasing the element size to 30 m, the difference is less than 1%. This was assumed sufficiently accurate, and an element size of 30 m was used for the simulations of long durations in order to save computational time. For some of the shorter analyses, element size 16 m was used for marginally improved accuracy.

A quick convergence test was also carried out for different element sizes for a regular dynamic analysis. A regular wave with a period of 5 s was run, with element size 8 m and 30 m. The difference between the responses for the two simulations was less than one percent for all but translations in the z-direction. For these translations, the difference was around 3%, so the result was assumed satisfactory with large element size for the dynamic analyses as well.

While the element size had limited effect on the results, the length of the time step used in the

Table 15: Results from convergence study of element size and nonlinearity. F1, S1 and H can be seen from Figure 22 on page 61

Element length (Ca.)		[m]	2	4	8	12	16	20	30	55
Number of elements	F1		26	13	7	5	4	3	2	1
	S1		13	7	4	3	2	2	1	1
	H		11	6	3	2	2	2	1	1
Linear	$U_{y,max}$	[m]	−1.3017	−1.3016	−1.3017	−1.3013	−1.3009	−1.3009	−1.3009	−1.2996
	$M_{z,min}$	[10^8 Nm]	−7.26	−7.26	−7.26	−7.25	−7.24	−7.24	−7.19	−7.19
	$M_{z,max}$	[10^8 Nm]	2.69	2.69	2.70	2.70	2.70	2.72	2.71	2.86
	$V_{y,min}$	[10^7 N]	−2.91	−2.91	−2.91	−2.91	−2.91	−2.91	−2.91	−2.91
	$V_{y,max}$	[10^7 N]	2.80	2.80	2.80	2.80	2.80	2.80	2.81	2.80
Non-linear	$U_{y,max}$	[m]	−1.3052	−1.3051	−1.3052	−1.3049	−1.3044	−1.3044	−1.3044	−1.3032
	$M_{z,min}$	[10^8 Nm]	−7.26	−7.26	−7.26	−7.25	−7.24	−7.24	−7.19	−7.19
	$M_{z,max}$	[10^8 Nm]	2.69	2.69	2.70	2.70	2.70	2.72	2.71	2.86
	$V_{y,min}$	[10^7 N]	−2.91	−2.91	−2.91	−2.91	−2.91	−2.91	−2.91	−2.91
	$V_{y,max}$	[10^7 N]	2.80	2.80	2.80	2.80	2.80	2.80	2.81	2.80

dynamic analyses significantly affected the results. The extreme accelerations in the y-direction from the analysis with time step 0.6 s were only about 67% of the same results with time step 0.1 s, which was not acceptable, especially since this is on the unconservative side. With time step 0.2 s, the difference was less than 5%, which was acceptable when considering the amount of computation time would be saved in the irregular sea state simulations. This was therefore chosen as the default time step for the remainder of the analyses.

Table 16: Convergence study of time step

Time step	[s]	0.1	0.2	0.4	0.6
$U_{y,min}$	[m]	-0.2985	-0.2951	-0.2833	-0.2751
$U_{y,max}$	[m]	-0.0946	-0.0951	-0.1004	-0.1136
$A_{y,min}$	[m/s^2]	-0.1610	-0.1530	-0.1292	-0.1070
$A_{y,max}$	[m/s^2]	0.1586	0.1543	0.1299	0.1071

5.2 Modal Analysis

The modal analysis was performed in order to determine the eigenfrequencies of the system. The first 30 eigenfrequencies and eigenmodes were determined and can be seen in Appendix D. Modes 6-16, 18-22, 24-25 and 27 were the vertical modes with frequency ranging from 0.584-0.869 rad/s. This corresponds to periods from 7.23-10.75 s, and this range of periods is shown in Figure 32 together with the JONSWAP spectra for the three sea states. For a storm with 1-year return period, the eigenperiods in heave were largely outside the range of the wave spectrum and resonance is therefore unlikely to occur. For the two larger storm sea states, however, the eigenperiods overlapped with some of the longer periods of the spectrum, and the chance of resonance is greater.

The five first horizontal modes have low frequencies and long periods, the first two having periods of 53.6 s and 31.1 s. According to the NPRA (Larsen, 2016a), these two modes are the most dominant and contribute 75% and 15% to the dynamic response, respectively. Due to lack of reliable wind data for Bjørnafjorden it is unclear whether these periods are within a common range of wind oscillation periods. It is likely, however, that one or more of the lower frequencies might coincide with some wind frequencies, and this should be studied more closely in the future.

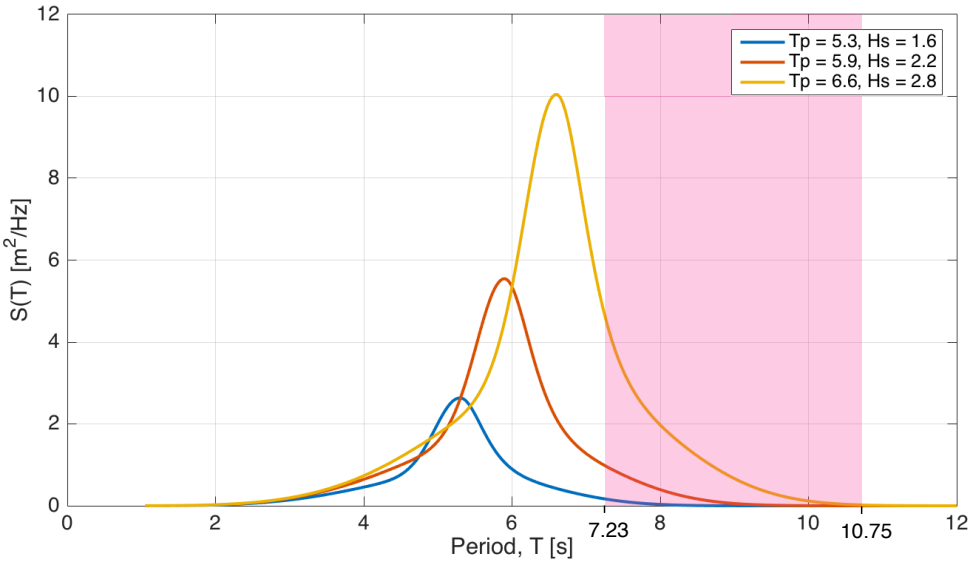

Figure 32: The JONSWAP spectra for three sea states with respect to period with the range of eigenperiods in heave marked with pink

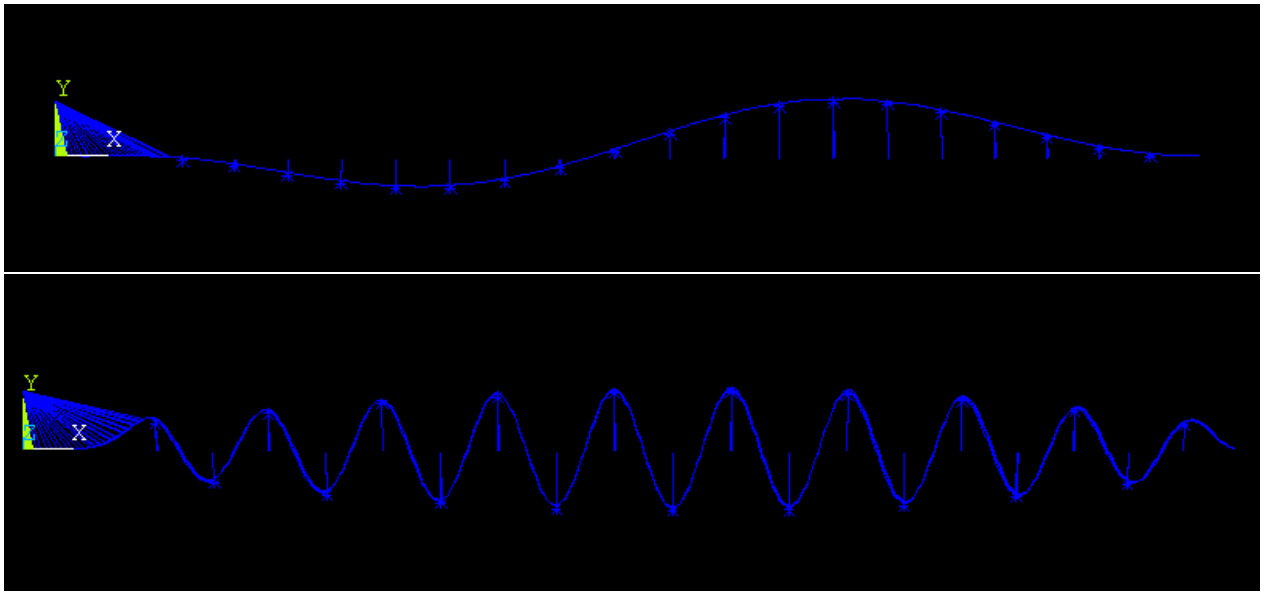

Figure 33: The vertical modes with the longest (top) and shortest (bottom) eigenperiods, respectively 10.75 s and 7.23 s

5.3 Static Response

The vertical deflections of the bridge with no external loads can be seen in Figure 34. Extreme values for the cable bridge was -0.56708 m, and approximately -0.36 m at each of the spans of the main bridge. The first span had a slightly larger deflection at -0.43 m. According to Hand-

book N400 (Statens Vegvesen, 2009), maximum vertical deflection should be less than L/350. The lengths of the cable bridge and spans are 505.9 m and 203.4 m, respectively, which means maximum deflections should be less than 1.45 m and 0.58 m. For self-weight only, the vertical deflections are well within this limit. Although no external horizontal forces were applied to the bridge at this stage, small horizontal deflections can be seen in Figure 35. This was caused by the cables in the southern end which exerted a tension force both vertically and horizontally towards the point of attachment at the tower due to pretension.

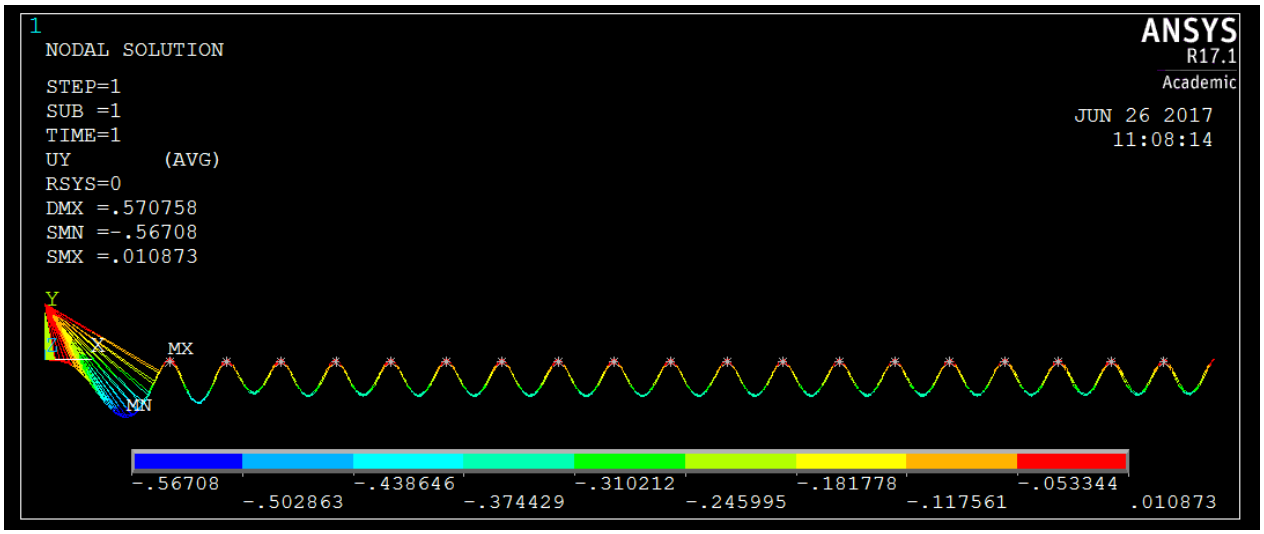

Figure 34: Deflections in the y-direction due to self-weight

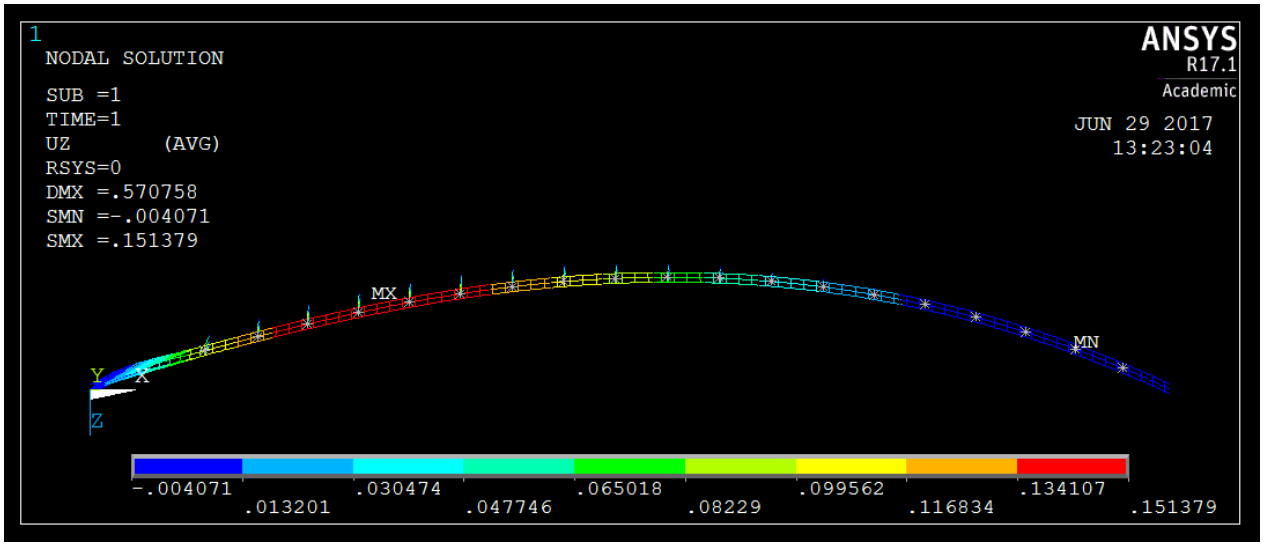

Figure 35: Deflections in the z-direction due to cable tension

Figure 36 and 37 show the distribution of bending moment and shear forces for the inner bridge beam with no external forces. The distributions correspond well to the theory in Chapter 3.3, and the hand calculations of the extreme bending moment and shear forces in the low bridge spans are shown in Table 17 below. The beams could be assumed fixed at the ends due to symmetry. The values were calculated by determining the average self-weight per unit length (274 kN/m) and using Equation 3.6 on page 33. The results were approximately the same as in Figures 36 and 37, but were over simplified and therefore only appropriate as a rough estimate. Both the hand calculations and the values found through the analyses were well within the maximum bending moments and shear forces found in NPRA's report, suggesting they were at structurally safe levels.

Table 17: Hand calculations of extreme bending moment and shear force due to self-weight

		Total bridge beam	**One bridge beam**
$M_{z,min}$	[10^8 Nm]	−9.45	−4.72
$M_{z,max}$	[10^8 Nm]	4.72	2.36
V_y	[10^7 N]	2.79	1.39

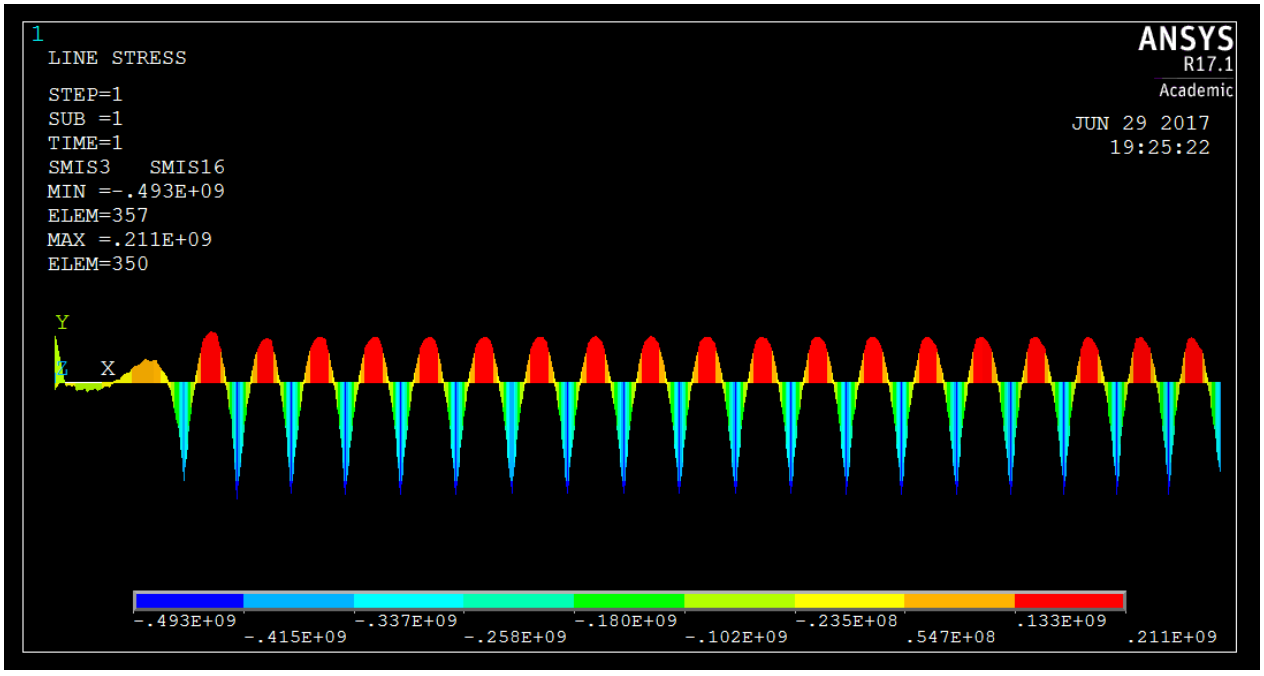

Figure 36: Bending moments in the inner bridge girder due to self-weight

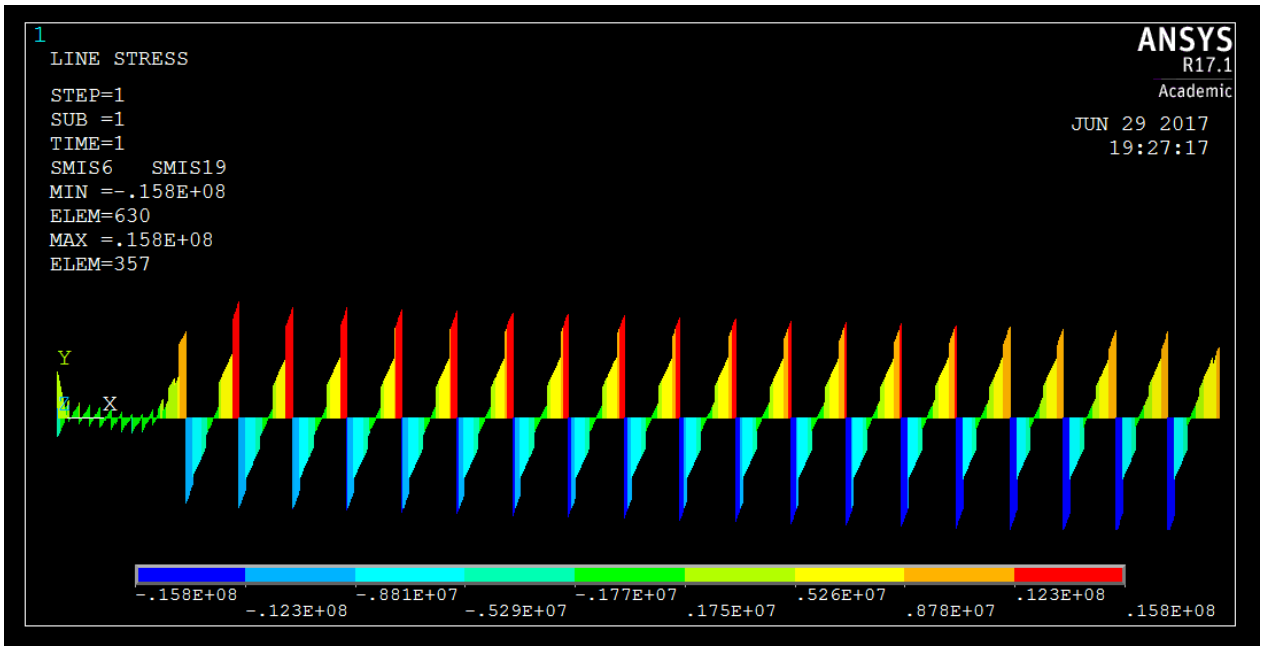

Figure 37: Shear forces in the inner bridge girder due to self-weight

The extreme values for deflection, bending moments and shear forces due to self-weight, environmental loads and traffic separately are presented in Table 18. As could be expected, increased horizontal loads had no effect on bending moments about the z-axis og vertical shear forces. Current forces increased vertical and horizontal deflections somewhat, but was nearly negligible compared to the effect of the wind forces. Although the wind and current forces were purely horizontal they had a small effect on the vertical deflection, which was most likely caused by a combination of the springs in the y-direction and small rotations about the x-axis. These rotations were well within the limits from Chapter 3.2 and therefore not looked at closer for the static analyses.

Table 18: Results from the static analysis with external loads with 1-year return period

		Self-weight	**Current**	**Wind**	**Traffic**	**Traffic with conc. load**
$U_{y,max}$	[m]	−0.5671	−0.5701	−0.5863	−1.3096	−1.4208
$U_{z,max}$	[m]	0.1514	0.1782	0.3920	0.2026	0.2031
$M_{z,min}$	[10^8 Nm]	−4.95	−4.95	−4.95	−7.20	−7.41
$M_{z,max}$	[10^8 Nm]	2.18	2.18	2.18	2.90	3.08
$V_{y,min}$	[10^7 N]	−1.58	−1.58	−1.58	−2.00	−2.05
$V_{y,max}$	[10^7 N]	1.58	1.58	1.58	2.04	2.06

Figure 38 shows the vertical deflections with distributed traffic loads at the cable bridge and the first three spans of the low bridge. Here, the maximum deflection appeared at the spans between the pontoons, and was approximately 1.30 m below zero position. This was not the relative deflection of the bridge beam, however, as the draught of the pontoons had increased due to the extra weight. The pontoons had moved down roughly 0.85 m, which resulted in a relative deflection of about 0.46 m. This was still within the limit of L/350 when L is the 203.4 m length between columns. The maximum deflection of the cable bridge was also still within the limit of 1.45 m.

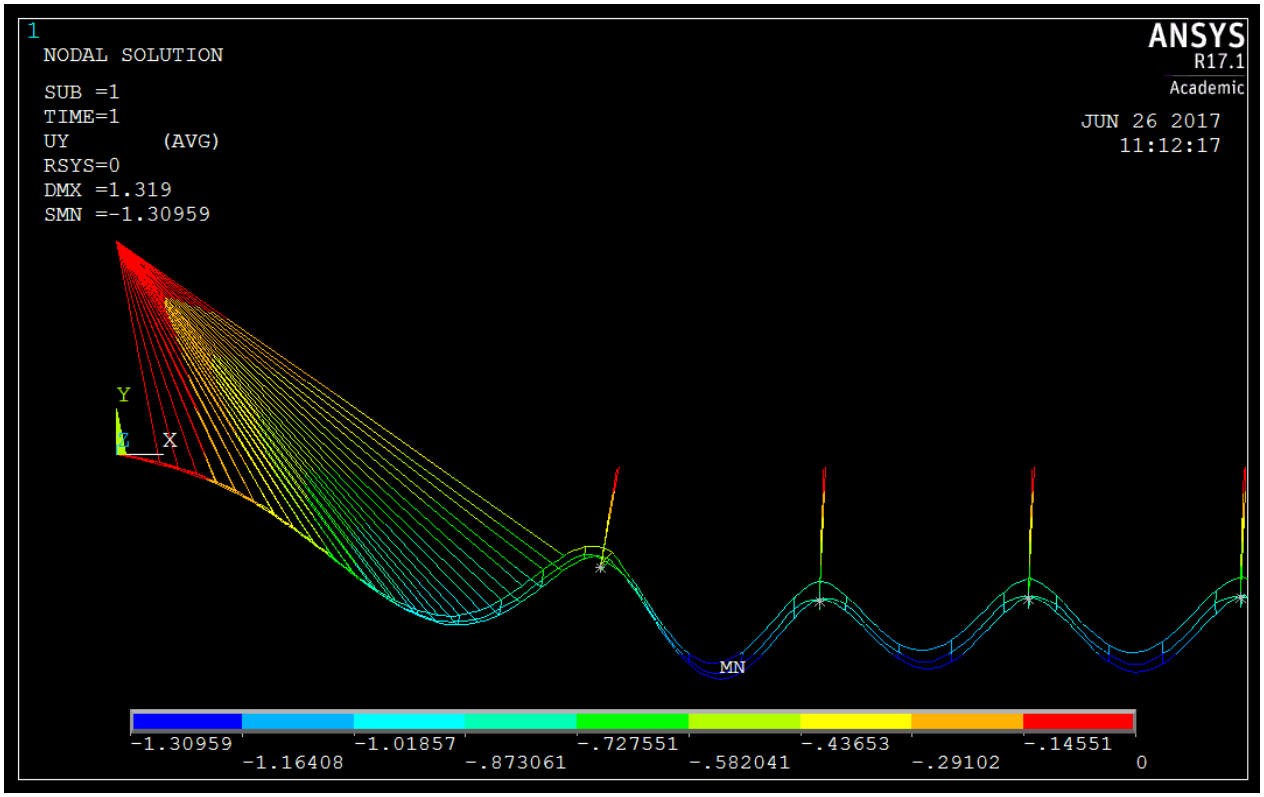

Figure 38: Deflections in the y-direction due to distributed traffic loads. The red points with zero deflection are the fixed ends of the springs

The concentrated traffic load was applied at the middle of each span and contributed to an increase in vertical deflection. This concentrated load was quite conservative in the way it was applied at every span, and it was left out for the combined static analysis. Another reason why it was not considered further was that the permitted load response criteria concerns responses when acted on by 70% of maximum traffic, which meant omitting the concentrated load would still yield conservative results.

Table 19 shows the results for the combination of environmental loads and distributed traffic loads, as well as the linear superposition of the individual results. The current and wind had no effect on the bending moments, for example, and the combined results were therefore expected to be the same as for traffic loads. This was not the case, however, and similarly the deflections were slightly larger in the z-direction and smaller in the y-direction than the linear superposition suggested. This was likely caused by the coupling of the two springs in the y-direction and the spring in x-rotation.

Table 19: Results of static loads in combination and theoretical results with linear superposition

		Combination	**Linear superposition**
$U_{y,max}$	[m]	−1.3062	−1.3318
$U_{z,max}$	[m]	0.4777	0.4700
$M_{z,min}$	[10^8 Nm]	−7.24	−7.20
$M_{z,max}$	[10^8 Nm]	2.88	2.90
$V_{y,min}$	[10^7 N]	−2.00	−2.00
$V_{y,max}$	[10^7 N]	2.04	2.04

Table 20: Results from static analysis with environmental loads with 10 and 100 years return period

		10-year	**100-year**
$U_{y,max}$	[m]	−0.5994	−0.6180
$U_{z,max}$	[m]	0.5913	0.8691
$M_{z,min}$	[10^8 Nm]	−4.95	−4.94
$M_{z,max}$	[10^8 Nm]	2.15	2.14
$V_{y,min}$	[10^7 N]	−1.59	−1.59
$V_{y,max}$	[10^7 N]	1.58	1.58

Extreme responses to static loads for 10-year and 100-year storm conditions are shown in Table 20. In these cases, no traffic loads were applied as the bridge would be closed off due to safety. The maximum deflections appeared at the same location as for the bridge with no external forces, see Figures 34 and 35. The extreme values for bending moments and shear forces were marginally different from the values for the 1-year storm, and was practically negligible when comparing the three static storm conditions.

Although no explicit response criteria applied to storms of this strength, deflections should be within reasonable limits in order to maintain structural integrity. The deflections in the y-

directions were both smaller than maxima for traffic loads and therefore assumed safe. The z-direction deflections were larger than for the other static analyses, but still assumed to be structurally safe as they were less than 1 m for a 4 km long bridge.

5.4 Regular Wave Response

Below in Table 21 are the results from the regular analyses after being adjusted for amplitude. Recall from Chapter 3.2 that maximum permitted response is 0.5 m/s^2 and 0.6 m/s^2 in vertical and horizontal accelerations and 1.5° in roll rotation. 1.5° is approximately 0.026 radians.

Table 21: Max response in regular waves, red number indicating exceedance of criteria limits

Period [s]	A_y [m/s^2]	A_z [m/s^2]	θ_x [rad]
2	0.1434	0.1572	0.0006
3	0.3585	0.1426	0.0017
4	0.1189	0.1189	0.0031
5	0.3851	0.2126	0.0132
6	0.0797	0.1640	0.0051
7	0.3218	0.3184	0.0223
8	0.1002	0.7359	0.0082
9	0.0132	0.0675	0.0014
10	0.0127	0.0834	0.0016
11	0.0121	0.0981	0.0015
12	0.0221	0.2828	0.0040
13	0.0230	0.1648	0.0053

Table 21 contains selected results only, and all values are absolute maxima, i.e. no distinction was made between the direction of response. The full table with more detailed responses can be found in Appendix E. When adjusted for wave amplitude, the responses seemed to be within the limits of the criteria, except for horizontal accelerations in waves with 8 s period. While this in itself seemed reasonable, the relationship between magnitude of applied force and magnitude of response in the different directions did not seem coherent. This could have been due to resonance in the system, but the eigenfrequencies of the bridge were not close to any of the lower frequencies, where this behaviour also appeared. Additionally, the response in the different directions did not increase and decrease harmoniously. Although the responses were not

expected to harmonise perfectly, some coherency was thought likely, and the results were not as aticipated. The vertical response was larger for waves with a 5 s period, although the heave force for this wave was smaller than for waves with 3 and 4 s periods even when adjusted for a larger amplitude. The rotations about the x-axis also seemed small compared to responses in heave and sway. Overall, the regular wave analyses yielded unexpected results.

5.5 Irregular Sea State Response

Before the analyses on irregular sea states with different phase angles were run, the same sea state was run four times to uncover any imprecision in the ANSYS calculations. The focus for this part of the analysis was on the translations and accelerations in the y and z-direction, and rotations and accelerations about the x-axis. The results showed that the responses in the z-direction were unpredictable, where one of the four simulations yielded significantly different results for translations compared to the other three. For accelerations, two simulations gave identical results and two deviated from these, see Table 22. Table 23 shows the statistical variance and standard deviation of the set, and the original data can be found in electronic appendix *seastate_response.xlsx*. The other rotational and translational responses were consistent with negligible variations only.

Table 22: Response in the z-direction for four runs of the same sea state. Sea state 1-1 and 1-3 are identical and assumed correct. Values significantly deviant from these are marked in red. Orange signifies a smaller, potentially negligible difference

		U_z	A_z
Sea state 1-1	Max.	0.4877	0.3354
	Min.	-0.1925	-0.3331
Sea state 1-2	Max.	0.3116	0.3027
	Min.	-0.1450	-0.3106
Sea state 1-3	Max.	0.4877	0.3354
	Min.	-0.1925	-0.3331
Sea state 1-4	Max.	0.4847	0.3008
	Min.	-0.1840	-0.3083

Table 23: Mean, variance and standard deviation for four data sets from the same 1-hour sea state run in ANSYS. Only the values with a standard deviation larger that 2% of the mean are shown here

		U_z	A_z
Mean, μ	Max.	0.4429	0.3185
	Min.	−0.1796	−0.3213
Variance, σ^2	Max.	5.749×10^{-3}	2.830×10^{-4}
	Min.	3.147×10^{-4}	1.403×10^{-4}
Standard deviation, σ	Max.	0.0758	0.0168
	Min.	0.0177	0.0118
σ, % of μ	Max.	17.11	5.28
	Min.	9.87	3.67

Since running the same sea state several times revealed some inconsistencies in the ANSYS results, it was important to keep this in mind when looking at results from different sea states. Figure 39 shows the maximum responses from six different sea states based on the same JONSWAP spectrum for a storm with a 1-year return period. The response in the z-direction for sea state 4 seemed incoherent, which was suspected to be due to the imprecisions previously mentioned. This particular sea state was therefore run through ANSYS again two times, and new extreme values were found. The values from these two runs were practically identical and seemed to correspond better to expectations, which can be seen in Figure 40. Based on these results the values from the rerun analyses were assumed correct and used in the further studies.

After the extreme responses had been determined for six sea states, the data was used to determine the mean, variance and standard deviations. The results are presented in Table 24. This was to determine a range within which the extreme responses were most likely to be, and establish whether the bridge would be safe for travel or not. Assuming the extreme responses are normally distributed, 95% will be within a range of $\pm 2\sigma$ of the mean. Since only the maximum extremes were of interest for this study, the mean $+2\sigma$ were found for positive extremes and mean -2σ for negative extremes.

The deflections were not of particular interest in the dynamic analysis, but should still be within the mentioned criteria. The average maximum vertical deflection for a 1-year storm was -0.63 m

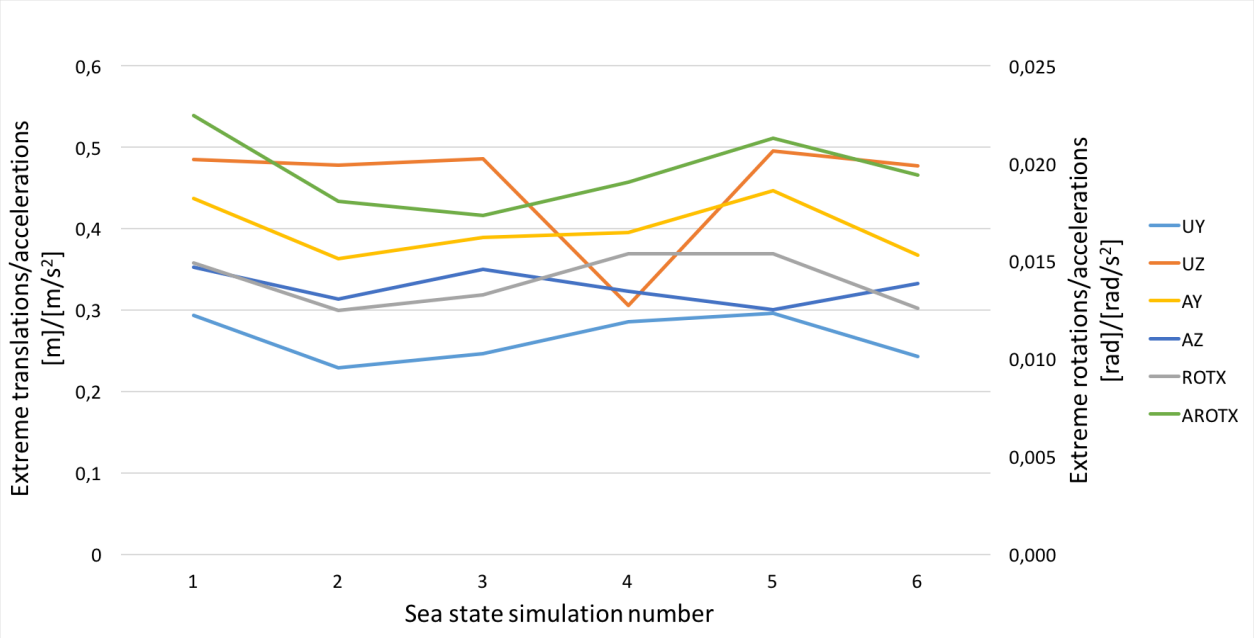

Figure 39: Max responses for six 1-hour simulations based on the same JONSWAP spectrum of a storm with 1-year return period. The results for sea state 4, in particular U_z, seem to be incoherent and potentially caused by inconsistencies in ANSYS

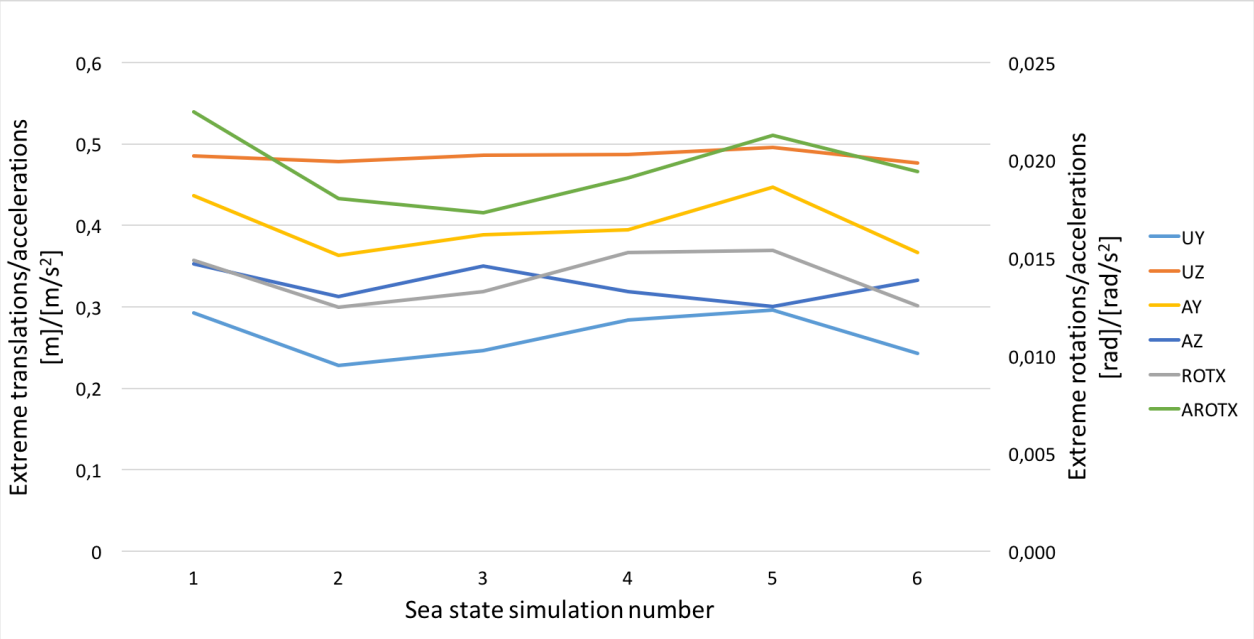

Figure 40: Max responses for the same six 1-hour simulations as in Figure 39 after rerunning the ANSYS analysis for sea state 4 and obtainingmore accurate results

Table 24: Mean, variance and standard deviations for six data sets from a 1-hour sea state with a 1-year return period

		U_y	U_z	θ_x	A_y	A_z	$\ddot{\theta}_x$
Mean, μ	Max.	0.2651	0.4846	0.0140	0.3995	0.3278	0.0196
	Min.	−0.6299	−0.2022	−0.0140	−0.3896	−0.3471	−0.0193
Variance, σ^2	Max.	7.133×10^{-4}	3.769×10^{-5}	1.538×10^{-6}	1.023×10^{-3}	3.642×10^{-4}	3.142×10^{-6}
	Min.	1.543×10^{-4}	1.910×10^{-4}	1.760×10^{-6}	9.818×10^{-4}	3.981×10^{-4}	1.641×10^{-6}
Standard deviation, σ	Max.	0.0267	0.0061	0.0012	0.0320	0.0191	0.0018
	Min.	0.0124	0.0138	0.0013	0.0313	0.0200	0.0013
σ, % of μ	Max.	10.07	1.27	8.87	8.01	5.82	9.04
	Min.	1.97	6.83	9.50	8.04	5.75	6.64

(See Table 24), and -1.08 m for a 100-year storm (See electronic appendix *seastate_response.xlsx*). Although the maxima appeared approximately at the middle of the spans, they appeared together with downward motions of the pontoons. Hence, the relative deflections were assumed to still be within reasonabe limits even for maximum dynamic responses.

Table 25 shows the mean values of the extreme responses for the 1-year return period sea states, and the mean plus/minus two standard deviations. Tables 26 and 27 show the same, using the standard deviation in percent found from the 1-year sea states. Applying the criteria from Chapter 3.2, responses during a storm with a 1-year return period were within safe limits. For a storm with a 10-year return period, the means were around the limits and extreme responses could be expected to exceed the limits. For the sea state with 100-year return period, the means were significantly higher than the safe criteria, and some of the upper limits exceeded the criteria by about 70%.

Table 25: Mean $\pm 2\sigma$ for a storm with 1-year return period

			$\boldsymbol{\mu}$	$\boldsymbol{\mu \pm 2\sigma}$
$\boldsymbol{A_y}$	[m/s^2]	Max	0.3995	0.4635
		Min.	−0.3896	−0.4523
$\boldsymbol{A_z}$	[m/s^2]	Max	0.3278	0.3660
		Min.	−0.3471	−0.3870
$\boldsymbol{\theta_x}$	[rad]	Max	0.0140	0.0165
		Min.	−0.0140	−0.0166

Table 26: Mean $\pm 2\sigma$ for a storm with 10-year return period

			$\boldsymbol{\mu}$	$\boldsymbol{\mu \pm 2\sigma}$
$\boldsymbol{A_y}$	[m/s^2]	Max	0.5336	0.6191
		Min.	−0.5590	−0.6489
$\boldsymbol{A_z}$	[m/s^2]	Max	0.4398	0.4910
		Min.	−0.4702	−0.5243
$\boldsymbol{\theta_x}$	[rad]	Max	0.0227	0.0267
		Min.	−0.0224	−0.0267

Table 27: Mean $\pm 2\sigma$ for a storm with 100-year return period

			$\boldsymbol{\mu}$	$\boldsymbol{\mu \pm 2\sigma}$
$\boldsymbol{A_y}$	[m/s^2]	Max	0.7589	0.8804
		Min.	−0.7348	−0.8530
$\boldsymbol{A_z}$	[m/s^2]	Max	0.6712	0.7493
		Min.	−0.6697	−0.7466
$\boldsymbol{\theta_x}$	[rad]	Max	0.0376	0.0443
		Min.	−0.0377	−0.0449

In addition to extreme motion response, the extreme bending moment, M_z, and shear force, V_y, were determined for the three storm conditions. To save space on the computer results were not stored for all elements, but for the elements as can be seen in Figure 41 only. The values for the remaining elements were assumed to be similar to the middle of the bridge due to symmetry, and based on the results from the static analyses. The extremes were found for one sea state in each storm condition only, and assumed to be of similar magnitude for the other sea states. As Table 28 shows, there was little difference in the bending moment and shear forces for the three sea states, and the extremes did not necessarily increase with increased storm intensity. This corresponded well to the results from the static analyses, where environmental loads applied to the pontoons or along the bridge in the z-direction had practically no effect on the bending moment about the z-axis and shear forces in the y-direction (See Table 18 on page 85).

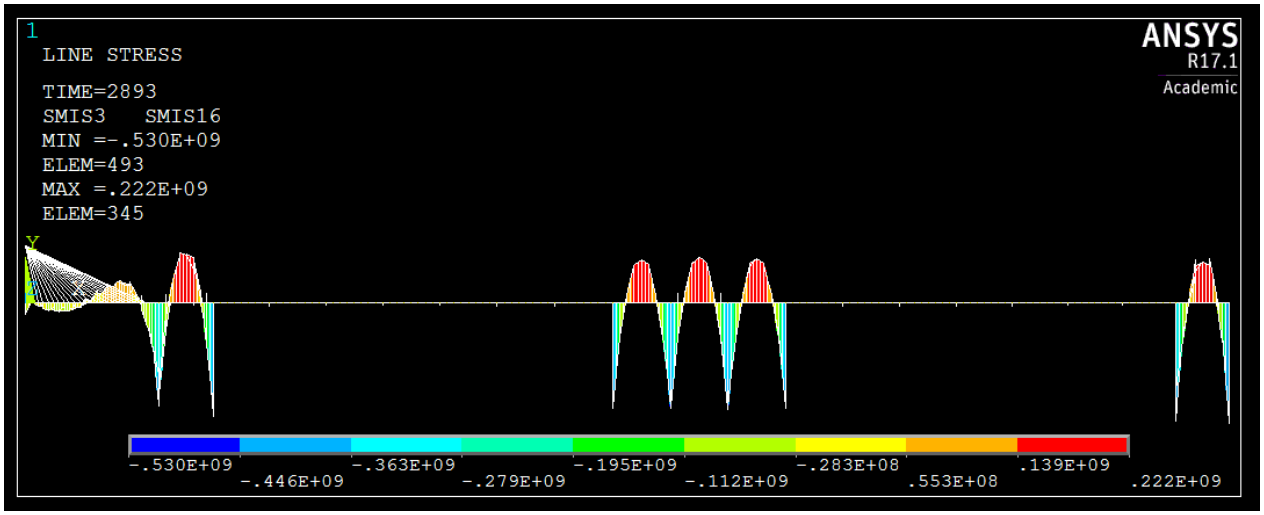

Figure 41: Bending moment about the z-axis from the irregular analysis. To save space on the computer information was only stored for these elements

Table 28: Extreme bending moment and shear forces for the three sea states

		1 year	**10 years**	**100 years**
$M_{z,min}$	[10^8 Nm]	−5.279	−5.503	−5.499
$M_{z,max}$	[10^8 Nm]	2.430	2.404	2.503
$V_{y,min}$	[10^7 N]	−1.780	−1.805	−1.859
$V_{y,max}$	[10^7 N]	1.464	1.521	1.641

The stress distribution for one span between to pontoons was found at the time of the largest bending moments for the 100-year storm, as stress is directly dependent on bending moment. The distribution in Figure 42 shows that the stresses were largest on the underside where the bridge beam joins the colums of the pontoons. This coincides with the extreme values for the bending moment, and similarly, the stresses were zero or close to zero at the zero-points of the bending moments. The maximum stress was approximately 247 MPa, which is significantly below the yield strength of the steel at 440 MPa. No stress analysis was performed for static traffic loads where the bending moments were at their maxima, but an estimate could be made based on the results from the dynamic analysis. By assuming a proportional relationship with the bending moment and assuming the maximum stress will appear at at the same location, an extreme bending moment of $-7.41 \cdot 10^8$ resulted in a stress of approximately 333 MPa, which was still acceptably below the yield stress.

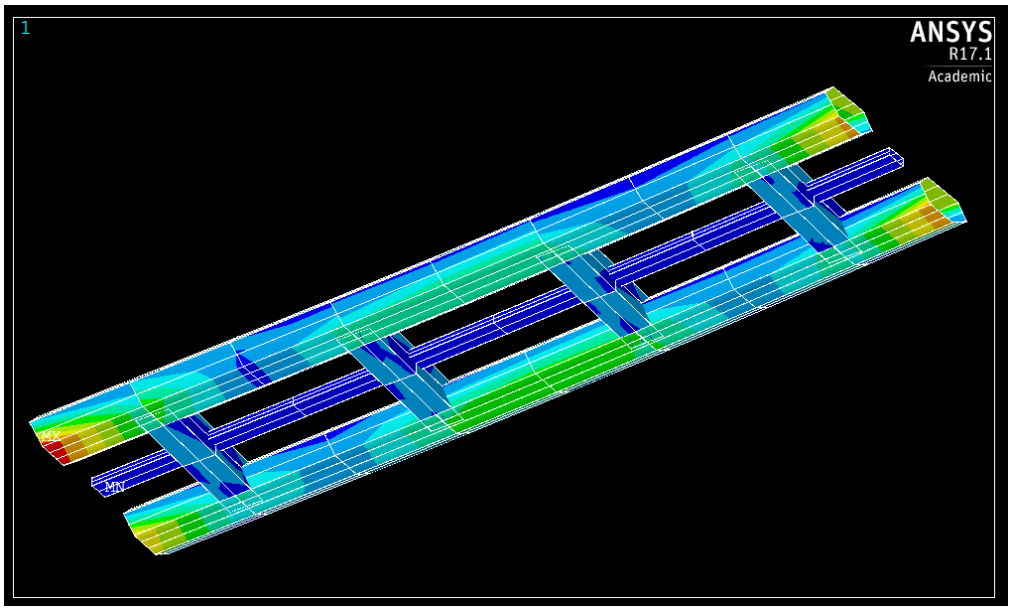

Figure 42: Von Mises stress distribution on the underside of the bridge. Dark blue indicates zero stress, red is maximum stress and green is intermediate stress levels. The results for the pedestrian bridge beam were not saved and included in the analysis and are therefore zero

Chapter 6

Discussion

The arced pontoon bridge concept suggested by the NPRA for crossing Bjørnafjorden in Norway is a very large and complex structure, with a complex set of forces acting on it both internally and externally. Although significant effort was put into creating a reasonably realistic model, it is important to acknowledge its potential shortcomings and how they may have affected the outcome of the analyses.

The model was for example assumed to deform in a linear fashion, and it was divided into relatively big elements. The convergence study showed that both of these simplifications had neglible effects on the deflections and shear forces, but the extreme bending moments in the beams were affected slightly compared to a nonlinear model with a small element size. This effect was assumed small enough to be neglected in order to save computational time. Nevertheless, the effect of nonlinearity and element size may be more noticeable for larger responses, like from a 100-year storm. In this case the forces acting on the bridge are substantially larger than for a 1-year storm, which results in larger deformations, potentially to a degree where nonlinearities will kick in. It may also be worth looking into the effect of even smaller elements at certain points in the model, for example at connections and sharp angles. These are usually points of high stresses, and potential weak spots when it comes to fatigue and failure. Since the aim of this study was to determine global responses, such effects were not analysed, but if the bridge concept is to become a realisation it is important to determine local responses as well as

global.

The time step convergence test showed that increasing the time between each load step had a significant effect on the results. Time steps of 0.4 and 0.6 s were easy to dismiss as too inaccurate, but 0.2 s was assumed to be sufficiently accurate. This was compared to the results from the analysis with time step 0.1 s, assuming these results were correct and accurate. Although likely that this was the case, a more in-depth time step convergence test with even shorter steps could have been advantageous. Additionally, looking at the time step effects for different wave periods and for irregular sea states would probably have given a more complete picture of the effect of time step length. Quantifying this effect and incorporating it in the dynamic analyses could make a significant difference, especially since the convergence test showed that longer time steps gave non-conservative results.

As previously mentioned, one of the reasons for carrying out a modal analysis was to determine if the eigenfrequencies of the structure were outside of the range of common load frequencies to avoid resonance. For the bridge structure, this was the case for most of the modes, but some of the vertical modes might coincide with external heave load frequencies during sea states with 10 and 100 year return periods. Similarly, the lower horizontal modes had long eigenfrequencies potentially close to wind oscillation frequencies. This means that the responses of the bridge in these cases could become unusually large and potentially damage the structure. Due to damping in the structure as well as radiation damping, the maximum response will likely be limited. Still, it is important to quantify the damping effect and make sure there is no risk of responses that could harm the structure even for force oscillation frequencies close to the natural frequencies of the bridge.

For the static analyses, reasonable judgement had to be shown when evaluating the results due to lack of absolute limits on deflections. When loaded with self-weight only, the maximum deflections in y-direction were within L/350, and maximum horizontal deflections were approximately 0.15 m due to pretension in the cables in the southern end. These values seemed reasonable for a structure of this size, since the most significant distributed vertical loads are the self-weight, not traffic loads (274 kN/m compared to 66.2 kN/m). Additionally, the vertical deflections of the pontoons under self-weight were all approximately zero, which indicated that

the buoyancy forces applied to the model were applied correctly.

The static analyses with external loads were somewhat simplified, as the traffic loads were modelled as evenly distributed loads and wind and current were modelled as uniform and static instead of changing with depth, height and time. Still, they were assumed reasonable estimates when looking at global responses, as well as somewhat conservative since the limits given in Chapter 3.2 referred to 70% of maximum traffic load. The static response from current, wind and traffic separately were within acceptable limits for a 1-year storm condition. This was the case even for traffic with distributed and concentrated loads, even though this load condition was larger than specified by the criteria. It was noted how the purely unidirectional forces also affected the deflections in the perpendicular direction, which was thought to be due to the springs attached to the model. This effect also became apparent when comparing the deflections due to current, wind, traffic and the combination of the three. The response from the combined loads was almost, but not entirely, a superposition of the individual results. Because the bridge was arced, and because the springs were acting in different directions, it seemed reasonable that the deflections in vertical and horizontal directions were not completely uncoupled, but rather affected one another.

For the 10 and 100-year storm conditions, the bridge was assumed to be closed to traffic, and vertical deflections were therefore smaller than for a 1-year storm with traffic loads. The difference in bending moments and shear forces compared to only self-weight were negligible and likely caused by approximations done by ANSYS. However, the horizontal deflections due to wind and current were significantly increased, as expected for increased horizontal loads. Still, the maximum deflection in the z-direction for the 100-year storm condition was less than 1 m, which seemed to be reasonable even though no definite criteria were imposed by Handbook N400 (Statens Vegvesen, 2009).

When looking at the bending moments and shear forces from the static analyses, it was evident that the distribution shape and magnitudes corresponded well to the theory and hand calculations. The maxima at the middle of the spans were slightly smaller than the hand calculations, which was reasonable since the weight at the middle of the spans was less than the average weight. Similarly, at the ends of the spans the extreme values were larger than the hand calcu-

lations (when looking at absolute value) as these ends of the bridge beam were heavier than the average. See Figure 22 on page 61 and Table 7 on page 62 for the properties and cross-section distributions in question. Only the main bridge girders were looked at for the bending moments and shear forces as they were at their largest for these beams. These beams were also the main features of the bridge, and where most of the loads are applied. Still, more local studies should be performed where bending and shear in cross beams, columns and pedestrian beams are looked at more closely.

Since the focus for this study was the dynamic response to waves, no more detailed analyses of static loads were deemed necessary. Should the concept be considered as the solution for crossing Bjørnafjorden, more in-depth analyses of static loads will be important, and static and dynamic loads in combination. Local analyses of joints and other irregularities in the structure will also have to be carried out, as stresses might be high in these areas.

One observation from the regular wave analyses, was the large accelerations in the z-direction. Although only one value exceeded the criteria, the accelerations in this direction were significantly larger than the accelerations in the y-direction. Compared also to the results from the irregular wave analyses, these responses seemed excessive. This, together with the uncovered inconsistencies in the results from ANSYS, may point towards an error or inadequate simplification of the model. Since the pontoons are floating on water, creating realistic boundary conditions that mimicked the behaviour of the pontoons in water was a challenge. Approximations and simplifications in the model may have affected the behaviour of the bridge, and it is possible these effects were particularly prominent for long, regular waves. For such waves, the force oscillates slowly, which means large forces keep working unidirectionally over several seconds. Hence, the structure has time to react and respond, as opposed to when it is influenced by an irregular wave or a wave with shorter periods. In addition, the amplitude of the force is generally larger for longer waves, which means the responses will likely be larger too. However, this does not explain the large response for some of the lower periods, which indicates that something else might be causing the irregular results. There could potentially be something wrong with the input code or forces, as these were manually implemented and hard to monitor closely during the process. Using a time delay between the pontoons instead of a phase angle may have

had some effect, though it seems unlikely that this alone could have caused the unexpected results. Ultimately, no definite reason could be found for the regular wave responses. The effect seemed to be on the conservative side, hence the results from the irregular sea state analyses should still be valid.

The first part of the irregular sea state analyses involved running the same sea state four times and comparing the results. The differences between the responses were negligible with exception of maximum deflection and acceleration in the z-direction. For two of the simulations, the response values were practically identical, and it seemed likely this was the more accurate result. Still, with only four data sets it was not possible to say with certainty which results were the more reliable. As for the regular wave analysis it was difficult to ascertain what caused the errors, and it could have been caused by input errors or flaws in ANSYS. Since no obvious source of the inconsistency could be found, the chosen course of action was to keep using the model as intended, but be aware of potential errors in other results. This seemed to be an acceptable choice, and another irregular sea state simulation seemed to show the same kind of error. The discovered error was significantly different from the expected value, but there is a chance smaller, less significant errors may have been overlooked. To identify smaller errors, each sea state could have been run again, and the more conservative value utilised. Due to time considerations this was not done, but should be considered for future work.

When examining the results from the irregular wave analyses of six different sea states, they seemed more reasonable than the ones from the regular analyses. The relative magnitude of the extreme responses in different directions correlated well (See Figure 40 on page 91), and the variance between the different data sets was small. Additionally, the outer limits ($\mu \pm 2\sigma$) were within the motion criteria presented in Chapter 3.2 for a sea state with a 1-year return period. This is favourable, as having to close down the bridge once a year because of severe weather is undesirable. For the two greater storms, the responses were larger than permitted for safety and comfort of travellers. For storms of this strength, the bridge will be closed as wind speeds are likely to exceed 25 m/s, hence the safety criteria do not apply directly. Nevertheless, responses should not be too extreme, as this may cause damage to the structure. The upper limits for the storm with 100-year return period were up to about 70% larger than the permitted responses for

safe travel. While this did not seem unreasonably large for a storm of this intensity, the long-term effects of such responses should be looked into further as there might be risk of fatigue damage.

The extreme bending moments and shear forces found in the irregular dynamic analyses were within the limits of the extreme values from the static traffic load analyses. The results were therefore deemed safe, which the stress analysis supported. Although no stress analysis was carried out for the static loads, the estimation made based on the results from the dynamic analysis was assumed accurate enough to determine structural safety. The stress seemed to remain significantly below the yield strength of the steel at all times.

Although the results from the 1-year irregular sea state analyses seemed to suggest that the bridge would be safe for traffic, these results were obtained from an analysis without any applied traffic loads. It is therefore likely that the behaviour of the bridge would be affected by different traffic load conditions, and possibly exceed response limit criteria even for a 1-year storm. Since the traffic load situation could potentially affect both static and dynamic behaviour, more detailed studies should be carried out on the effect of traffic loads during storms. There might be a need to regulate the amount of traffic allowed onto the bridge at the same time in order to maintain safe and comfortable driving conditions.

Chapter 7

Conclusion

When looking simply at the final results from the static and irregular analyses, the bridge responses seemed to be within satisfactory limits. For the 1-year sea state, responses were within the safety criteria posed by the Eurocodes and the NPRA, and the bridge would be safe for traffic when not closed due to winds stronger than 25 m/s. The bridge should also remain structurally safe for all three storm conditions based on the analyses. Additionally, shear forces, bending moments and stresses were of reasonable magnitudes and corresponded well to hand calculations. Based on these analyses, the bridge concept was deemed safe for traffic and/or structurally intact for the relevant sea states.

Although the results from the static and irregular analyses were reasonable, the results from the regular simulations as well as the inconsistensies in the responses for the irregular sea states suggested deficiencies in the analyses. Whether the flaws were caused by the model or by errors in the software was unclear, and regardless this meant the results should be used with some caution. More studies should be performed with regular and irrefgular waves to quantify the error and possibly adjust the results.

Even despite the aforementioned shortcoming in the analyses, this study in itself is not sufficient to finally conclude that the proposed bridge concept is safe in all storm conditions. Instead the study resulted in reasonable estimates suggesting the concept is viable, and uncovered the need for more detailed analyses like local stress and fatigue analsyses.

Chapter 8

Future Work

As mentioned, this study was not sufficiently detailed to decisively condlude that the bridge concept from the NPRA would be safe in all storm conditions. It may be an acceptable beginning, but should the concept be chosen and planning moved forward, several improvements should be implemented and analyses performed.

Improvements on the model and applied loads should include individual spring stiffnesses for each bridge cable, as well as modelling the entire cable-stay bridge with more detailed boundary conditions at the tower. Wind, current and traffic should be applied as dynamic loads, and in combinations with wave loads. Other traffic scenarios should be looked at where the loads are not constant along the length of the bridge, but rather placed at areas resulting in unfavourable loading conditions. Wind, current and wave loads from different directions, as well as short-crested waves should also be analysed.

After enhancing the model, more in-depth analyses should be performed, including local and global stresses and fatigue. Looking at the effects of smaller element sizes, especially at connections and sharp angles could be of interest and uncover weak spots in the structure. Running longer simulations than 1-hour simulations should also be considered, as this may yield more consistent and reliable results.

References

American Wood Council (2007). Beam design formulas with shear and moment diagrams. Retrieved from http://www.awc.org/pdf/codes-standards/publications/design-aids/AWC-DA6-BeamFormulas-0710.pdf.

Arda, T. S., Yardimci, N., and Eyrekci, O. (1996). Rehabilitation of two floating bridges, Turkey. *Structural Engineering International*, 6(1):17–18.

Ashton, I., Johanning, L., and Linfoot, B. (2009). Measurement of the effect of power absorption in the lee of a wave energy converter. *Proceedings of the 28th International Conference on Offshore Mechanics & Arctic Engineering, Honolulu, Hawaii, OMAE*.

Askheim, S. and Thorsnæs, G. (2016). Sognefjorden. *Store norske leksikon*. Retrieved from https://snl.no/Sognefjorden.

Bergdahl, L. (2009). *Wave-induced loads and ship motions*. Chalmers University of Technology, Göteborg.

British Standards (2004). *BS EN 10025-3:2004. Hot rolled products of structural steels - Part 3: Technical delivery conditions for normalized/normalized rolled weldable fine grain structural steels*. BSI.

British Standards (2008). *UK National Annex to Eurocode 1: Actions on structures - Part 2: traffic loads on bridges*. BSI.

Broer.no (n.d.). Nordhordlandsbrua. Retrieved from http://broer.no/bro/index.php?ID=43.

Brown, D. J. (1993). *Bridges: three thousand years of defying nature*. Octopus publishing, Great Britain.

CEN (1991). *Eurocode 1: Actions on structures - Part 2: Traffic loads on bridges*. European Standard, 2 edition.

Chandrasekaran, S. (2015). *Dynamic analysis and design of offshore structures*, volume 5. Springer, New Delhi.

Chopra, A. K. (2007). *Dynamics of structures: theory and applications to earthquake engineering*. Prentice-Hall, New Delhi, 2nd edition.

DNV (2010). *Environmental conditions and environmental loads*. Recommended practice DNV-RP-C205. Det norske veritas, Norway.

Falk-Petersen, D., Enger, E., Dimmen, A., and Gustavsen, T. M. (2016). Utvkiklingsstrategi for ferjefri og utbetra E39. Technical report, Nasjonal Transportplan.

Faltinsen, O. (1993). *Sea loads on ships and offshore structures*. Cambridge university press.

Fjeld, A. (2013). Mulighetsstudie for kryssing av Sognefjorden. Retrieved from http://www.vegvesen.no/_attachment/513902/binary/828560?fast_title=Mulighetsstudie+for+kryssing+av+Sognefjorden+-+Neddykket+r%C3%B8rbru.pdf.

Fjord1 (n.d). Sandvikvåg-halhjem. Retrieved March 3, 2017, from http://www.fjord1.no/ferje/ruteoversikt-for-ferje/hordaland/sandvikvag-halhjem.

Fréchot, J. (2006). Realistic simulation of ocean surfave using wave spectra. *Proceedings of the first international conference on computer graphics theory and applications (GRAPP 2006)*, pages 76–83.

Google Maps (n.d.). Lake Washington. Retrieved from https://www.google.no/maps/@47.6140615,-122.242848,17650m/data=!3m1!1e3?hl=en.

He, J. and Fu, Z. F. (2001). *Modal Analysis*. Butterworth-Heinemann, Oxford.

Henriksen, S. and Hilmo, O. (2015). Norsk rødliste for arter 2015. *Artsdatabanken*.

History.com (2010). Lacey V. Murrow memorial bridge sinks to the bottom of Lake Washington. Retrieved from http://www.history.com/this-day-in-history/lacey-v-murrow-memorial-bridge-sinks-to-the-bottom-of-lake-washington.

Jakobsen, S. E. (2013). *Hovedrapport: Sognefjorden mulighetsstudie flytebru.* Statens Vegvesen, revised edition.

Jakobsen, S. E. and Larsen, P. N. (2012). Mulighetsstudie for kryssing av Sognefjorden med flytebru - presentasjon brukonferansen 2012. Retrieved from http://www.vegvesen.no/_attachment/397743/binary/683490?fast_title=Ferjefri+E39+-+Flytebru.pdf,%20http://www.vegvesen.no/.

Johansen, I. L. (2016). Vurdering og sammenligning av brukonsepter for kryssing av bjørnafjorden: oppetid. Retrieved from https://www.vegvesen.no/_attachment/1623828/binary/1148214?fast_title=Vurdering+og+sammenligning+av+brukonsept+Bj%C3%B8rnafjorden.+Oppetid%2C+april+2016.pdf.

Johs.holt (n.d.). Bergsøysundet flytebru. Retrieved from http://www.johsholt.no/wp-content/uploads/Norsk-Bergsoysundet-1.pdf.

Langen, I. and Sigbjörnsson, R. (1979). *Dynamisk analyse av konstruksjoner*. Tapir, Trondheim.

Larsen, P. N. (2016a). Curved bridge - navigation channel in south. Retrieved from http://www.vegvesen.no/_attachment/1605060/binary/1145259?fast_title=Bj%C3%B8rnafjorden+Endeforankret+flytebun+-+Oppsumering+av+analyser.pdf.

Larsen, P. N. (2016b). Straight bridge - navigation channel in south. Retrieved from http://www.vegvesen.no/_attachment/1605065/binary/1145263?fast_title=Bj%C3%B8rnafjorden+Sideforankret+flytebru+-+oppsumering+av+analyser.pdf.

Lindeman, A. (1965). The pontoon bridge at Marquette. *The Annals of Iowa*, 37(7):615–618.

Lwin, M. M. (2000). Floating bridges. In Chen, W.-F. and Duan, L., editors, *Bridge Engineering Handbook*. CRC Press, Boca Raton.

Lwin, M. M. (93). The Lacey V. Murrow Floating Bridge, USA. *Structural Engineering International*, 3(3):145–148.

Moan, T. (2003). Nonlinear analysis. In *Finite element modellign and analysis of marine structures*, chapter 12. Marine technology centre, Trondheim, Norway.

Moaveni, S. (2015). *Finite Element Analysis- Theory and application with ANSYS*. Pearson, fourth edition.

Moe, G. (1997). Design philosophy of floating bridges with emphasis on ways to ensure long life. *Journal of Marine Science and Technology*, 2(3):182–189.

Myrhaug, D. and Lian, W. (2009). *Marine Dynamics. Lecture notes*. Department of Marine Technology, Faculty of Engineering Science and Technology, NTNU.

Norled (n.d.). Sogn of fjordane - rutetider. Retrieved May 7, 2017 from https://www.norled.no/kart-og-rutetider/ferje/sogn-og-fjordane/.

Norman, E. B. and Norman, V. D. (2012). Mørebyen? virkninger for arbeidsmarkedet og verdiskapning av ferjefri e39 fra nordfjord til kristiansund. Retrieved from http://www.vegvesen.no/_attachment/446266/binary/741179?fast_title=SNF+2012+-+Virkninger+for+arbeidsmarkeder+og+verdiskapning+av+ferjefri+E39+fra+Nordfjord+til+Kristiansund.pdf.

Ottosen, N. S. and Petersson, H. (1992). *Introduction to the finite element method*. Prentice-Hall.

Russell, B. R. and Thrall, A. P. (2013). Portable and rapidly deployable bridges: historical persepctive and recent rechnology development. *Journal of bridge engineering*, 18(10):1074–1085.

Shixiao, F., Weicheng, C., Xujun, C., and Cong, W. (2005). Hydroelastic analysis of a nonlinearly connected floating bridge subjected to moving loads. *Marine Structures*, 18(1):85–107.

So, K. S., Orazem, P. F., and Otto, D. M. (2001). The effects of housing prices, wages and commuting time on joint residential and job location choices. *American Journal of Agricultural Economics*, 83(4):1036–1048.

Statens Vegvesen (1994). Nordhordlandsbrua/the nordhordaland bridge. Retrieved from http://web.archive.org/web/20060209233657/http://www.vegvesen.no/region_vest/prosjekter/nordhordlandsbrua/brosjyre_1994.pdf.

Statens Vegvesen (2009). *Bruprosjektering. Håndbok N400*. Vegdirektoratet.

Statens Vegvesen (2011). Mulighetsstudie - kryssing av Sognefjorden - oppsummering av idéfasen. Retrieved from http://www.vegvesen.no/_attachment/207480/binary/399909?fast_title=Mulighetsstudie+-+kryssing+av+Sognefjorden%2C+mars+2011.pdf.

Statens Vegvesen (2015a). Brudata frå Bjørnafjorden. Retrieved from http://www.vegvesen.no/vegprosjekter/ferjefriE39/Nyhetsarkiv/brudata-fr%C3%A5-bj%C3%B8rnafjorden.

Statens Vegvesen (2015b). Statusrapport ferjefri e39. Retrieved from http://www.vegvesen.no/_attachment/926185/binary/1041502?fast_title=Statusrapport+Ferjefri+E39+mai+2015.pdf.

Statens Vegvesen (2016a). Bjørnafjorden suspension bridge - K1 & K2 design summary. Retrieved from http://www.vegvesen.no/_attachment/1607159/binary/1145772?fast_title=Bj%C3%B8rnafjorden+Supension+Bridge+%28TLP%29+K1+%26K2+Design+Summary.pdf.

Statens Vegvesen (2016b). Fjordkryssing - bjørnafjorden. Retrieved from http://www.vegvesen.no/Europaveg/e39stordos/fjordkryssing-bj%C3%B8rnafjorden.

Statens Vegvesen (2016c). Fjordkryssing bjørnafjorden. Retrieved from http://www.vegvesen.no/Europaveg/e39stordos/fjordkryssing-bj%C3%B8rnafjorden.

Statens Vegvesen (2016d). Forsking. Retrieved from http://www.vegvesen.no/vegprosjekter/ferjefriE39/forsking.

Statistics Norway (2013). Samlet areal, arealfordelinger og kystlinjens lengde, etter fylke. Retrieved from https://www.ssb.no/a/aarbok/tab/tab-019.html.

Todt, C., Haugsøen, H. E., Tverberg, J., Eilertsen, L., and Johnsen, G. H. (2015). *Kartlegging og verdisetting av marint biologisk mangfold E39 Stord-Os. Virkninger for naturmangfold, fiskeri og havbruk*. Rådgivende Biologer AS.

Ulstein, H., Skogstrøm, J. F. B., Aalen, P., and Grünfeld, L. A. (2015). Produktivitetseffekter av ferjefri E39. Retrieved from Menon Business Economics website: http://www.vegvesen.no/_attachment/918913/binary/1039669?fast_title=MENON+2015+-+Makro%C3%B8konomiske+effekter+av+ferjefri+E39.pdf.

Vermont Agency of Transportation (n.d.). Bridge prosjects. Retrieved from http://vtrans.vermont.gov/highway/structures-hydraulics/accelerated-bridge-program/bridge-projects.

VtransTV (2015). Brookfield floating bridge part 2 - the new bridge [video file]. Retrieved from https://www.youtube.com/watch?v=aIaoHVqp1dk.

Washington State Archives (n.d.). Building the first Lake Washington floating bridge. Retrieved from https://blogs.sos.wa.gov/FromOurCorner/index.php/2011/01/building-the-first-lake-washington-floating-bridge/.

Watanabe, E. and Utsunomiya, T. (2003). Analysis and design of floating bridges. *Progress in Structural Engineering and Materials*, 5(3):127–144.

Watanabe, E., Wang, C. M., Utsunomiya, T., and Moan, T. (2004). Very large floating structures: applications, analysis and design. *CORE report*, 2.

Weisstein, E. (n.d.). Standard deviation. Retrieved from http://mathworld.wolfram.com/StandardDeviation.html.

WSDOT (1990). World's first concrete floating bridge seattle-mercer island, washington. Retrieved from https://www.sos.wa.gov/_assets/office/clipping-file-2.pdf.

WSDOT (2003). Uniquely northwest. Retrieved from https://web.archive.org/web/20061007130146/http://www.wsdot.wa.gov/NR/rdonlyres/46D92108-DD55-442F-81B8-285AA25F34EE/4712/quarterly_Summer2004.pdf.

WSDOT (2016). SR 520 - floating bridge facts. Retrieved from http://www.wsdot.wa.gov/Projects/SR520Bridge/About/BridgeFacts.htm.

Zallen, R. M. (2008). Beam and arch action. A structural primer for non-engineers. *Zallen Engineering - Forensic Engineering in Construction*, (15).

Appendices

List of appendices

LIST OF APPENDICES

Appendix A

Sectional Properties from the NPRA

Sectional properties of girder		H1	H2	H3	S1	F1
Used in analysis		High bridge cable 6-20	High bridge Cable 1-6	High bridge Axis 2	support section Axis 3-22	Span section Axis 3-22
Equivalent plate thicknesses	mm					
Top plate	Plate 1	25	37	46	36	25
Inner inclined web (top)	Plate 2	20	23	29	20	20
Outer inclined web (top)	Plate 3	20	28	35	36	25
Outer inclined web (bottom)	Plate 4	20	28	35	36	25
Inner inclined web (bottom)	Plate 5	20	23	29	20	20
Bottom plate	Plate 6	20	37	46	36	25
Total width of twin box	m	53	53	53	55	55
Section height	m	5	5	5	6.5	6.5
Properties (twin box)						
Area	m2	1.46	2.10	2.63	2.50	1.85
Iz (weak axis)	m4	6.10	9.38	11.72	18.34	13.16
Iy (strong Axis)	m4	554.2	809.1	1011.4	1037.0	737.9
It (torsion)	m4	17.5	24.5	30.7	45.8	35.9
Sectional modulus						
Weak axis in top plate (A)	m3	2.90	4.30	5.37	5.99	4.27
Weak axis in bottom plate (B)	m3	2.11	3.33	4.16	5.33	3.85
Strong axis in top plate (A)	m3	22.62	33.03	41.28	42.33	30.12
Strong axis in bottom plate (B)	m3	25.78	37.63	47.04	46.09	32.79
Weight						
Steel weght twin box	ton/m	11.4	16.5	20.6	19.6	14.5
Transverse stiffener	ton/m	1.8	1.8	1.8	1.8	1.8
Vierendel	ton/m	3.3	3.3	3.3	3.0	3.0
Pedestrian lane	ton/m	1.6	1.6	1.6	1.6	1.6
Total steel	ton/m	18.1	23.2	27.3	26.0	20.9
Permanent loads						
Total girder weight in kN/m	kN/m	178	228	268	255	205
Asphalt, railings etc	kN/m	57	57	57	57	57
Total permanent load	kN/m	235	284	325	312	262

Appendix B

Damping and Added Mass Values for Regular Waves

Damping values in heave (d_h), sway (d_s) and roll (d_r)

T [s]	d_h [N/(m/s)]	d_s [N/(m/s)]	d_r [Nm/(rad/s)]
1	0	1.50×10^5	0
2	0	3.00×10^5	1.00×10^7
3	0	9.50×10^5	3.50×10^7
4	3.00×10^5	2.10×10^6	2.80×10^8
5	5.00×10^5	3.20×10^6	5.20×10^8
6	3.50×10^5	3.90×10^6	5.00×10^8
7	1.00×10^4	3.51×10^6	2.80×10^8
8	2.60×10^5	3.40×10^6	1.00×10^8
9	1.00×10^6	2.95×10^6	2.00×10^7
10	1.68×10^6	2.22×10^6	1.00×10^7
11	2.26×10^6	1.52×10^6	2.00×10^7
12	2.70×10^6	1.00×10^6	3.00×10^7
13	2.92×10^6	6.70×10^5	3.50×10^7

Added mass values in three directions and three rotations

T [s]	$M_{a,x}$ [kg]	$M_{a,y}$ [kg]	$M_{a,z}$ [kg]	$I_{a,xx}$ [kg·m^2]	$I_{a,yy}$ [kg·m^2]	$I_{a,zz}$ [kg·m^2]
1	6.00×10^6	3.70×10^7	1.90×10^6	1.12×10^{10}	1.20×10^9	2.88×10^9
2	5.10×10^6	3.71×10^7	1.60×10^6	1.12×10^{10}	1.00×10^9	2.86×10^9
3	3.40×10^6	3.69×10^7	1.15×10^6	1.11×10^{10}	7.00×10^8	2.77×10^9
4	1.80×10^6	3.67×10^7	7.00×10^5	1.10×10^{10}	4.00×10^8	2.61×10^9
5	1.10×10^6	3.67×10^7	7.00×10^5	1.12×10^{10}	3.00×10^8	2.56×10^9
6	1.20×10^6	3.67×10^7	1.80×10^6	1.14×10^{10}	5.00×10^8	2.65×10^9
7	2.10×10^6	3.60×10^7	2.70×10^6	1.16×10^{10}	2.00×10^9	2.80×10^9
8	7.50×10^6	3.50×10^7	3.70×10^6	1.17×10^{10}	4.50×10^9	3.15×10^9
9	1.70×10^7	3.43×10^7	5.00×10^6	1.16×10^{10}	4.70×10^9	3.60×10^9
10	2.52×10^7	3.39×10^7	6.00×10^6	1.15×10^{10}	4.30×10^9	3.90×10^9
11	2.89×10^7	3.40×10^7	6.40×10^6	1.15×10^{10}	3.80×10^9	3.96×10^9
12	2.87×10^7	3.45×10^7	6.50×10^6	1.15×10^{10}	3.60×10^9	3.89×10^9
13	2.71×10^7	3.54×10^7	6.40×10^6	1.15×10^{10}	3.30×10^9	3.81×10^9

Appendix C

Regular Wave Forces in Roll and Sway for Unit Amplitude

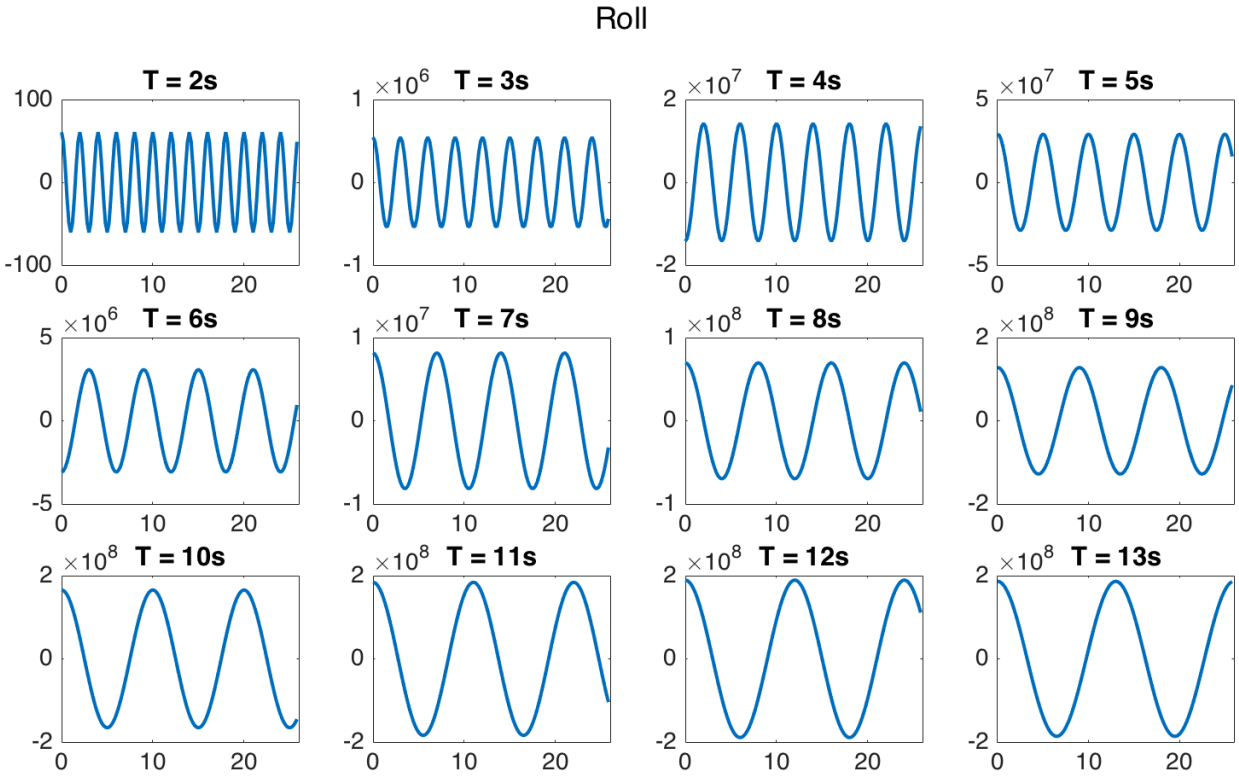

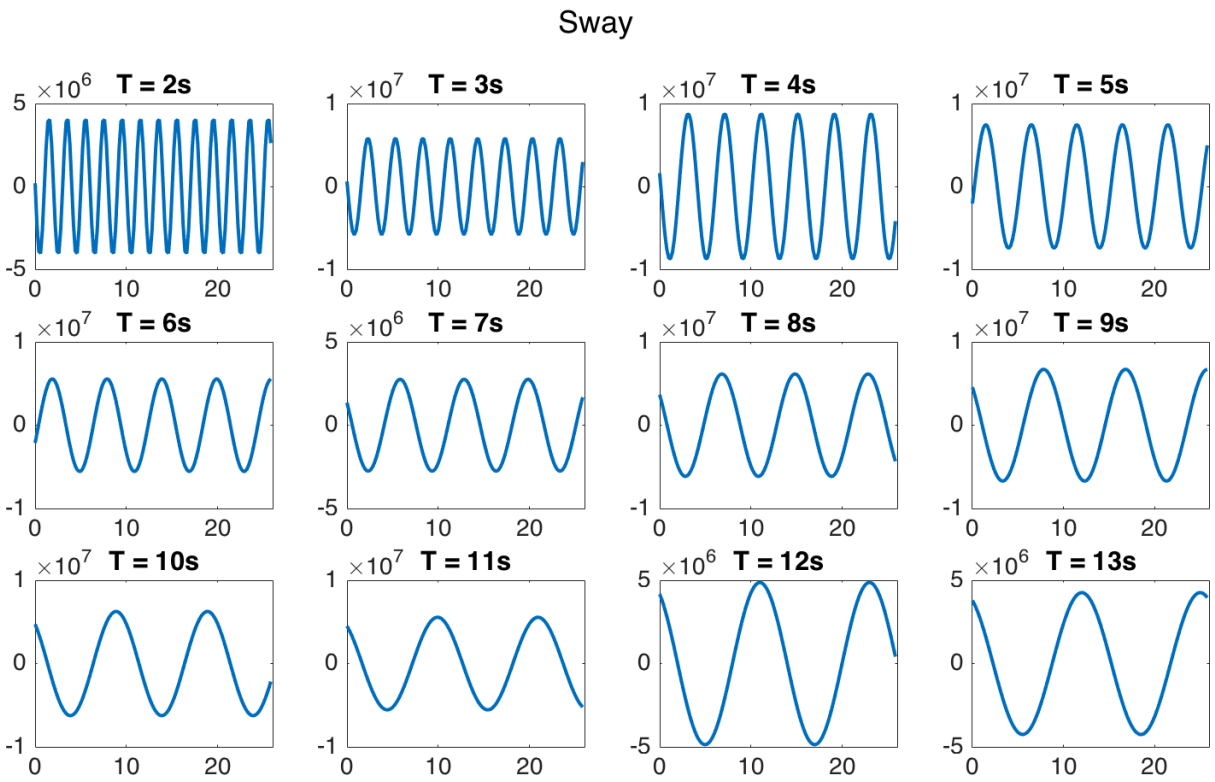
Sway
×10^6 T = 2s
×10^7 T = 3s
×10^7 T = 4s
×10^7 T = 5s
×10^7 T = 6s
×10^6 T = 7s
×10^7 T = 8s
×10^7 T = 9s
×10^7 T = 10s
×10^7 T = 11s
×10^6 T = 12s
×10^6 T = 13s

Appendix D

Mode Shapes and Frequencies

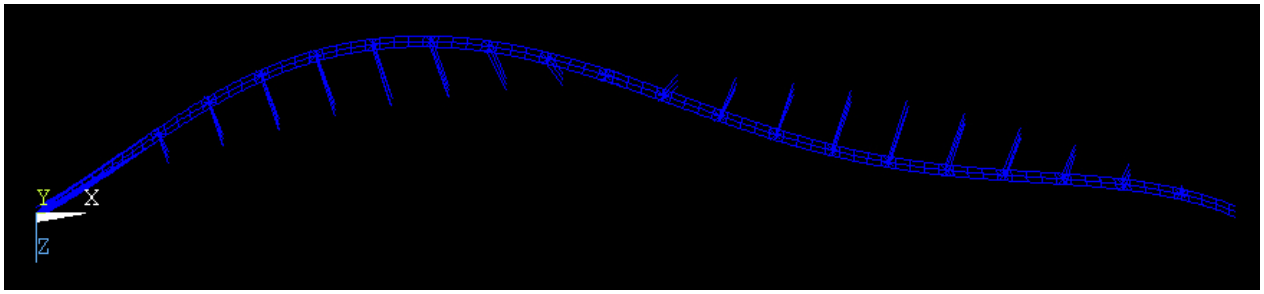

Mode 1

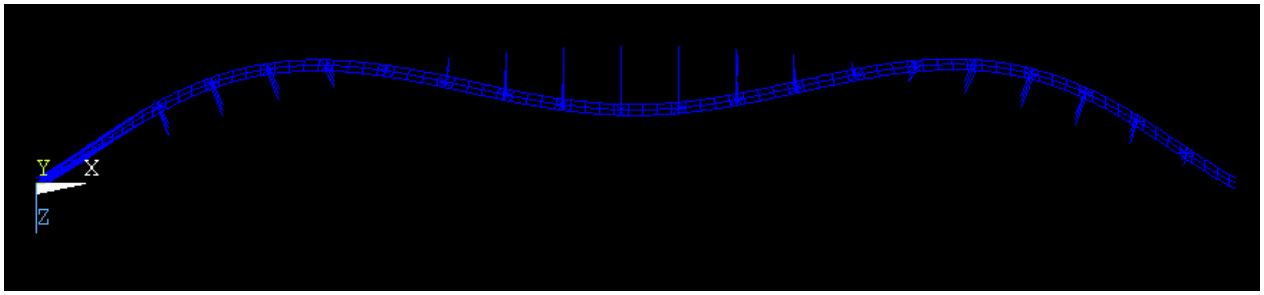

Mode 2

The lines in the table indicates a change in added mass used in the analysis

Mode number	**Eigenfrequency,** $\mathbf{F_n}$ [1/s]	**Eigenperiod,** $\mathbf{T_n}$[s]	**Circular freq.,** $\boldsymbol{\omega_n}$[rad/s]
1	0.0187	53.596	0.117
2	0.0322	31.053	0.202
3	0.0559	17.896	0.351
4	0.0649	15.415	0.408
5	0.0832	12.020	0.523
6	0.0930	10.752	0.584
7	0.0930	10.752	0.584
8	0.0931	10.747	0.585
9	0.0932	10.732	0.585
10	0.0935	10.698	0.587
11	0.0940	10.636	0.591
12	0.0949	10.537	0.596
13	0.0962	10.391	0.605
14	0.0981	10.191	0.617
15	0.1014	9.862	0.637
16	0.1047	9.551	0.658
17	0.1070	9.347	0.672
18	0.1088	9.195	0.683
19	0.1135	8.811	0.713
20	0.1188	8.415	0.747
21	0.1237	8.085	0.777
22	0.1293	7.732	0.813
23	0.1318	7.590	0.828
24	0.1321	7.572	0.830
25	0.1360	7.353	0.854
26	0.1370	7.300	0.861
27	0.1383	7.230	0.869
28	0.1487	6.727	0.934
29	0.1513	6.609	0.951
30	0.1649	6.065	1.036

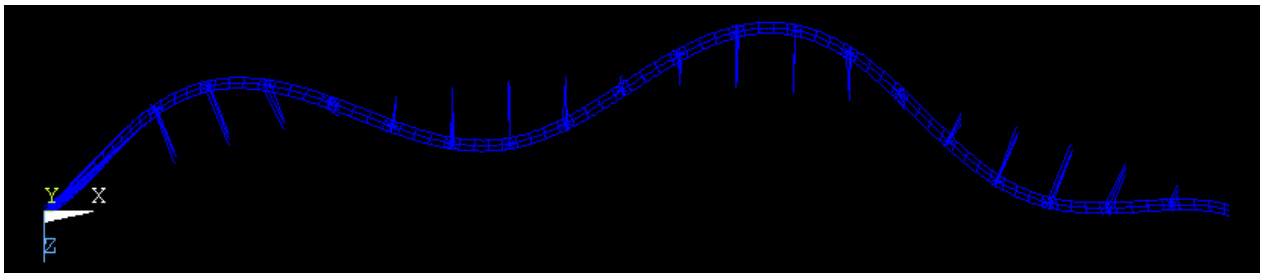

Mode 3

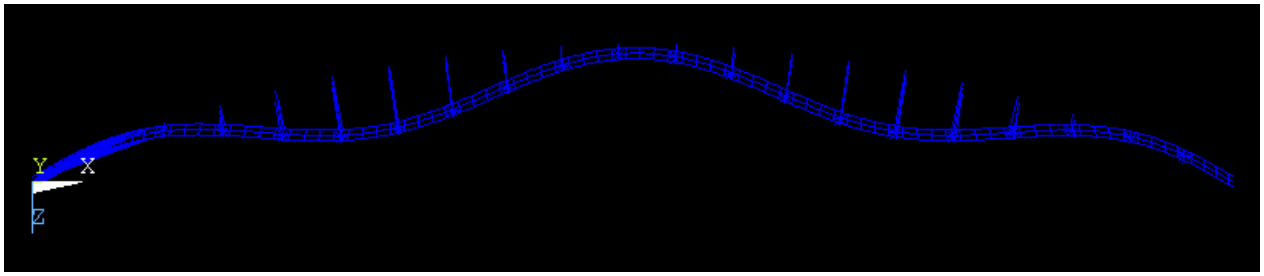

Mode 4

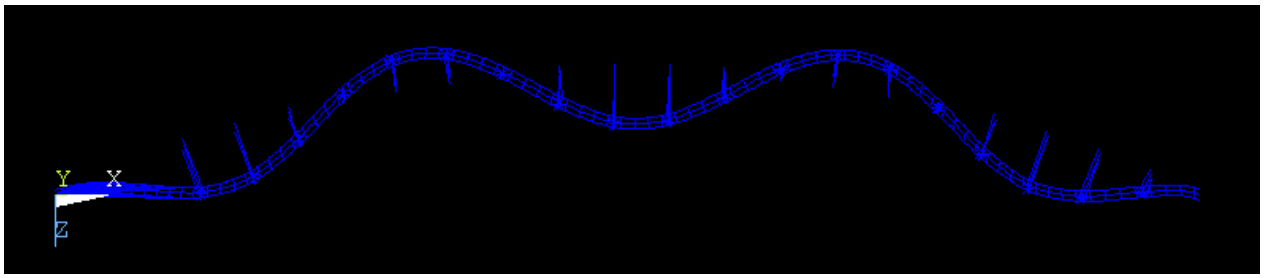

Mode 5

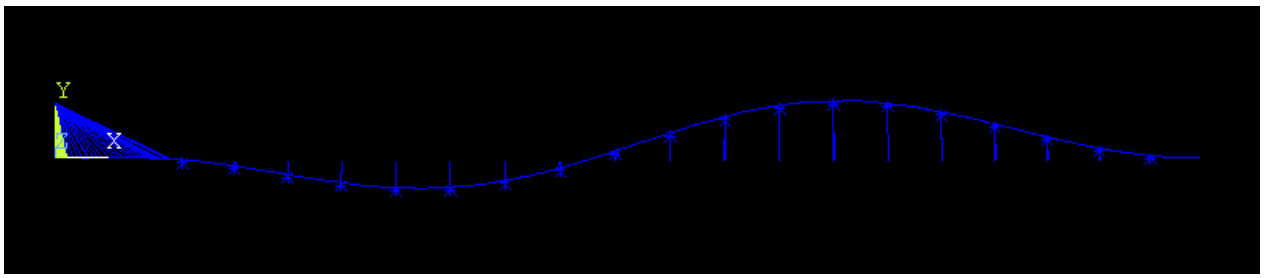

Mode 6

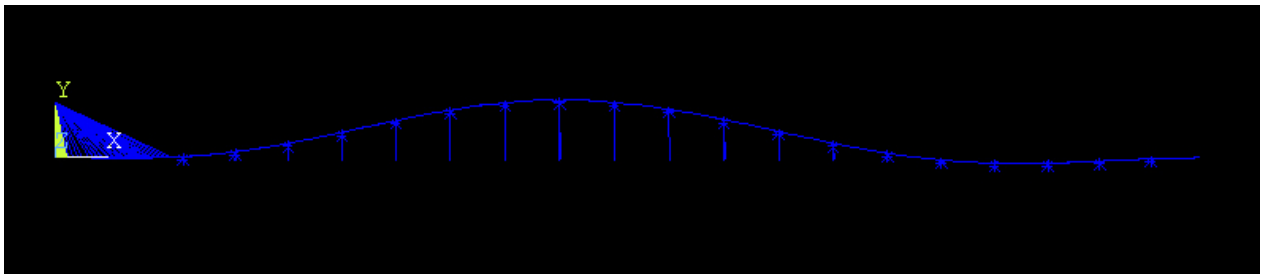

Mode 7

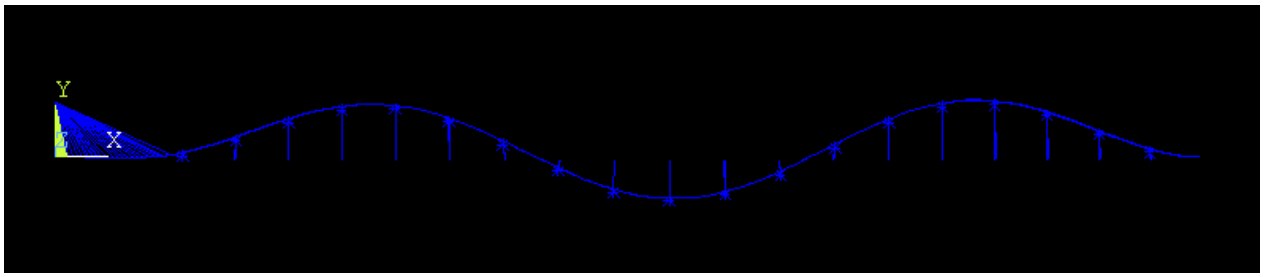

Mode 8

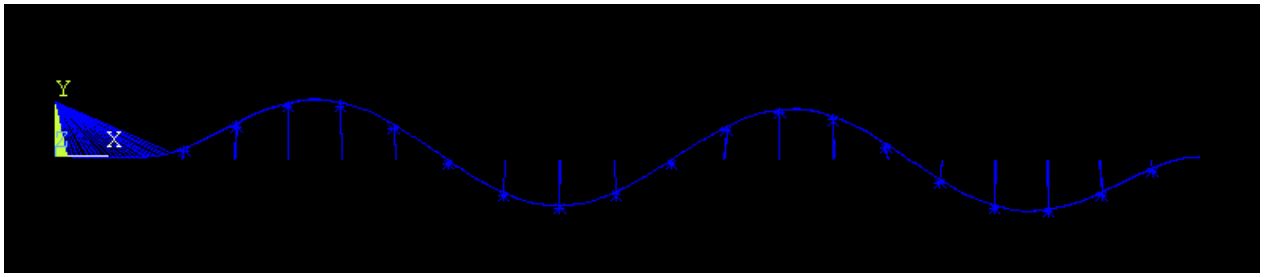

Mode 9

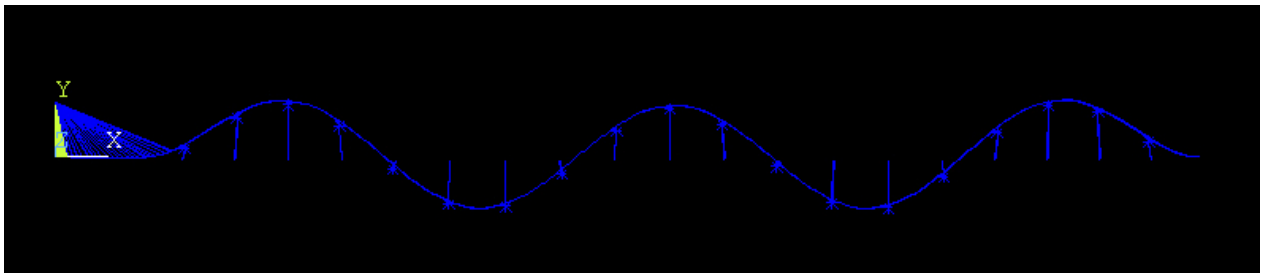

Mode 10

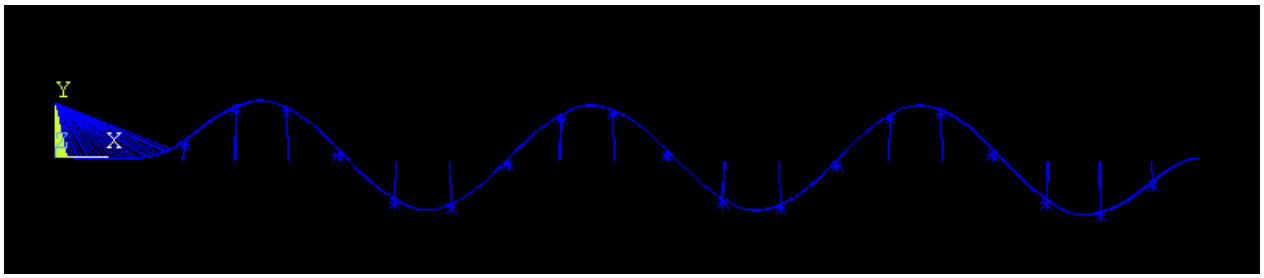

Mode 11

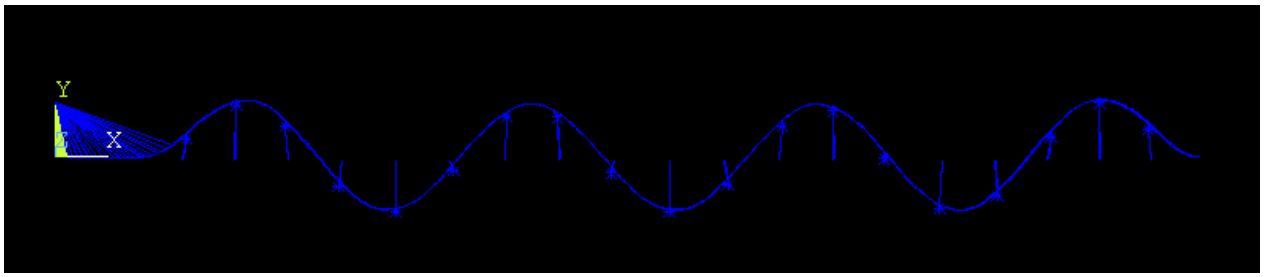

Mode 12

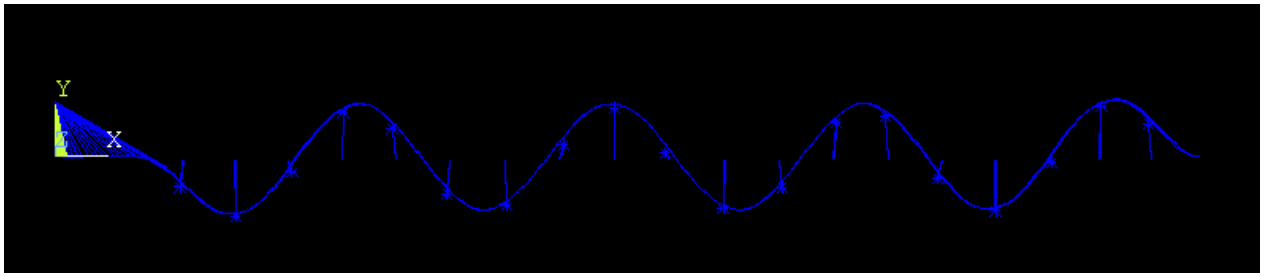

Mode 13

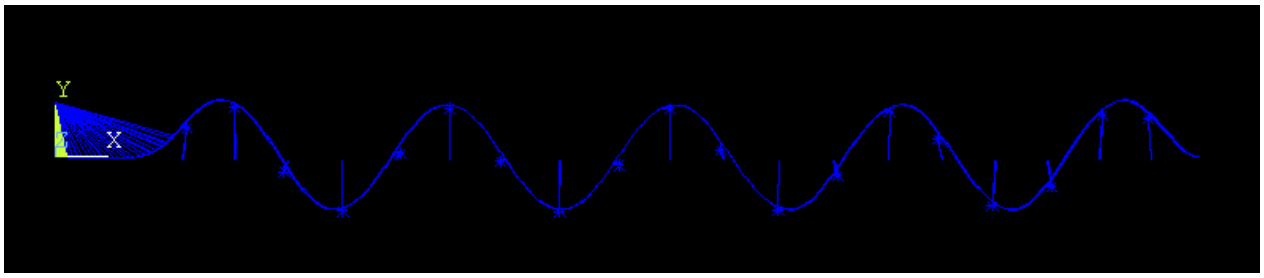

Mode 14

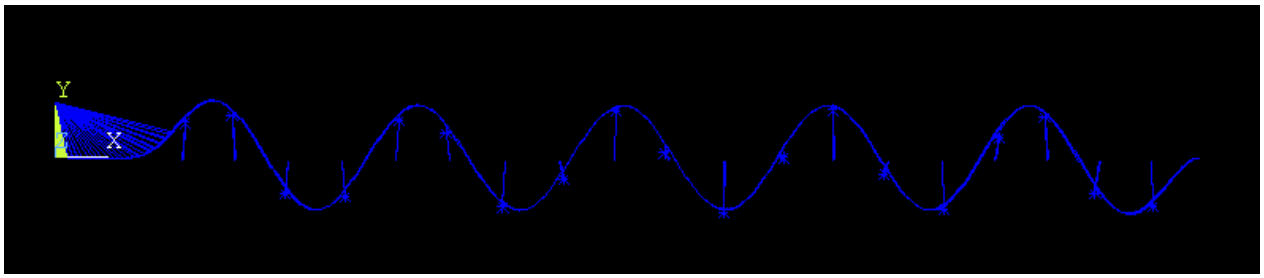

Mode 15

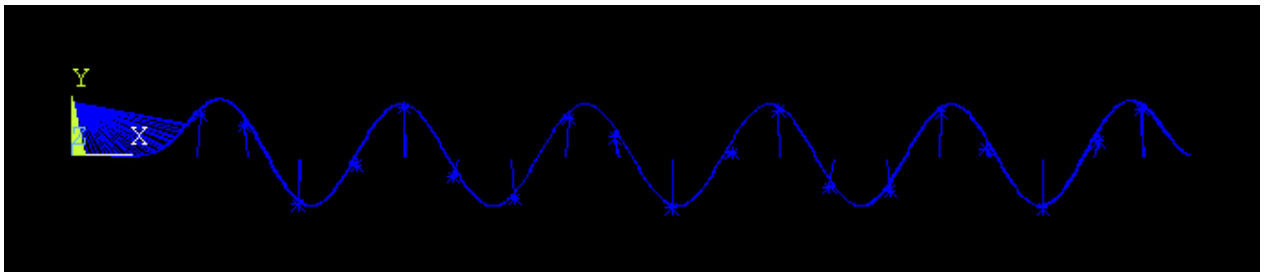

Mode 16

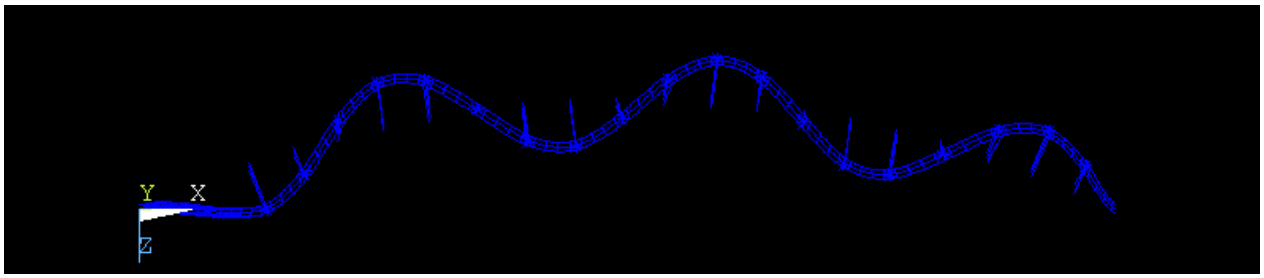

Mode 17

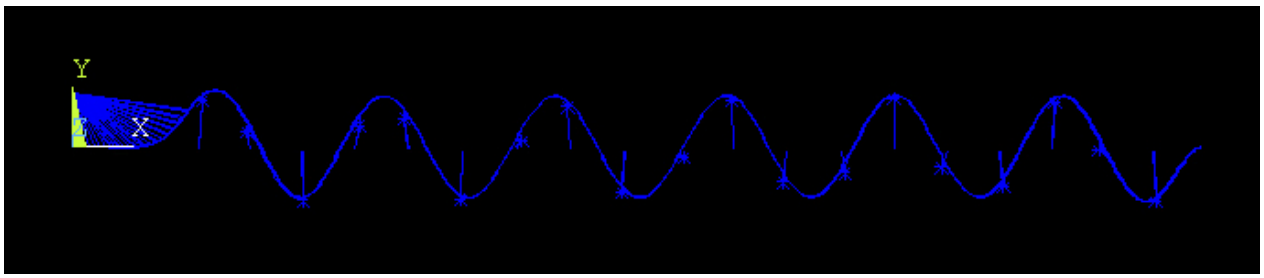

Mode 18

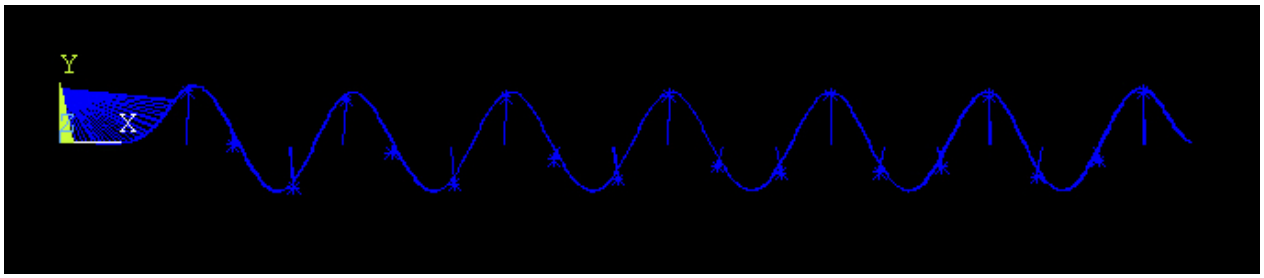

Mode 19

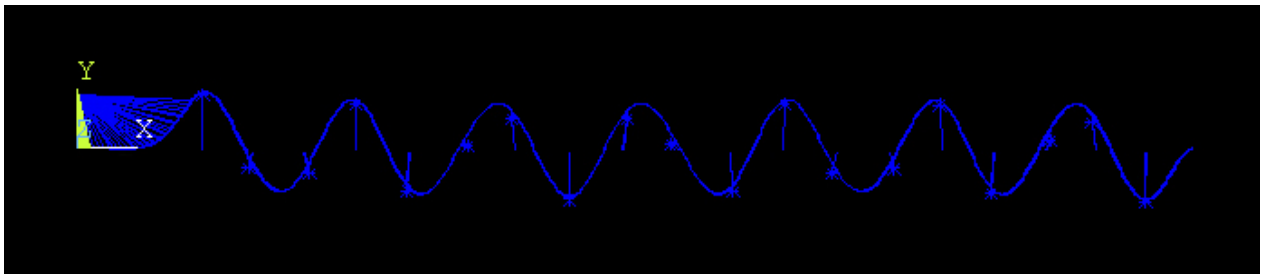

Mode 20

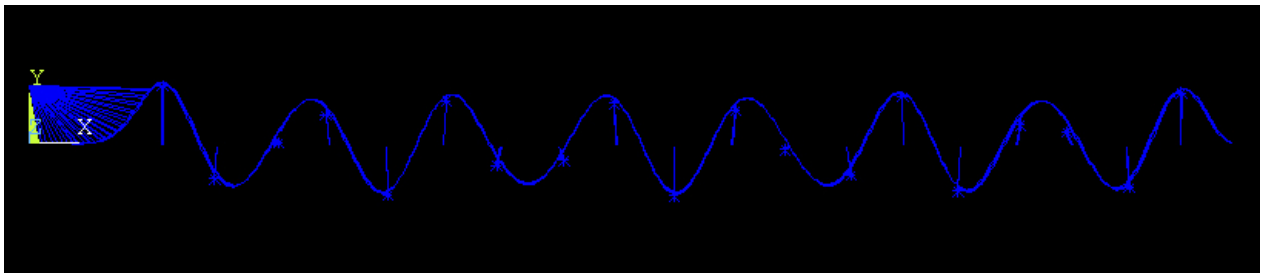

Mode 21

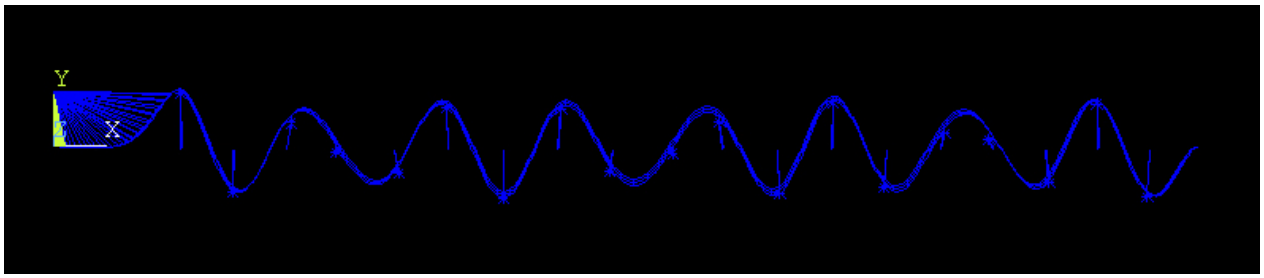

Mode 22

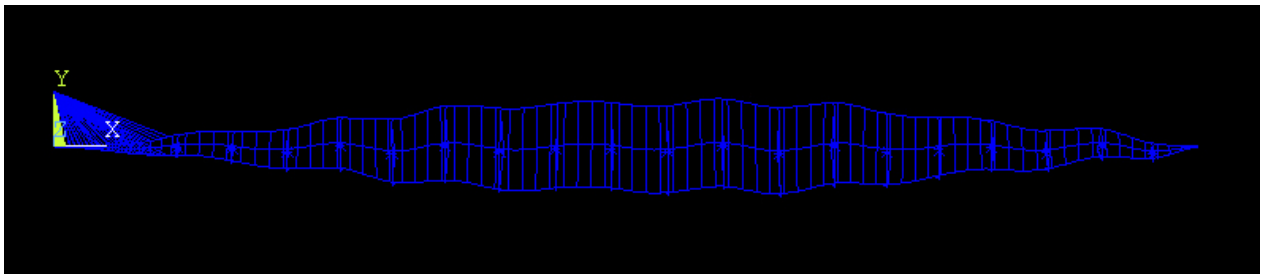

Mode 23

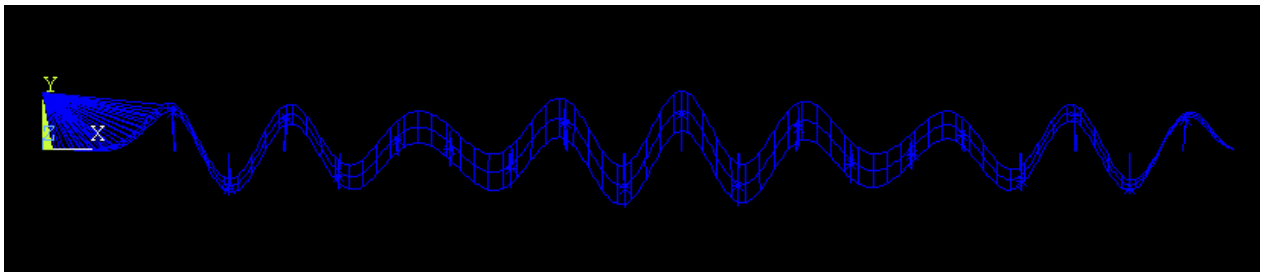

Mode 24

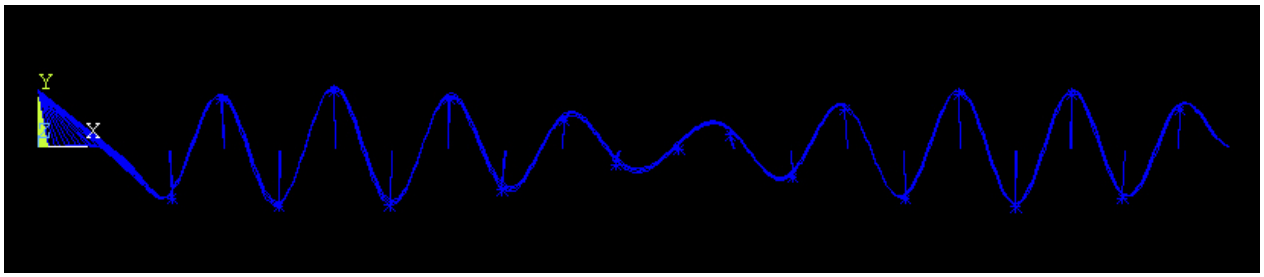

Mode 25

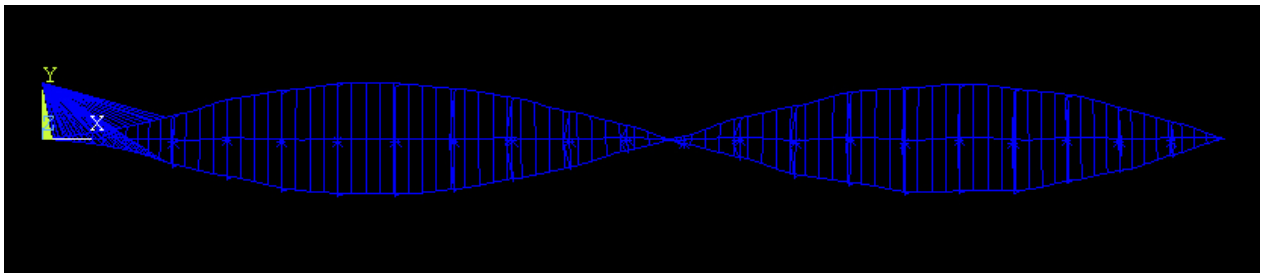

Mode 26

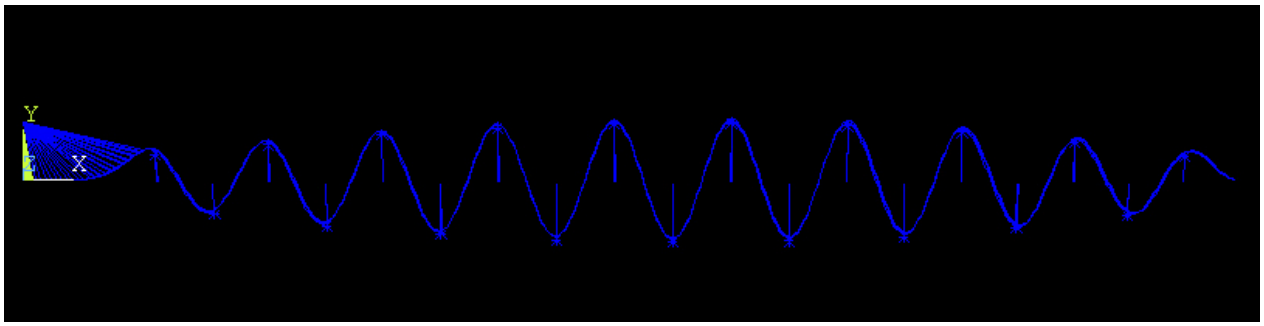

Mode 27

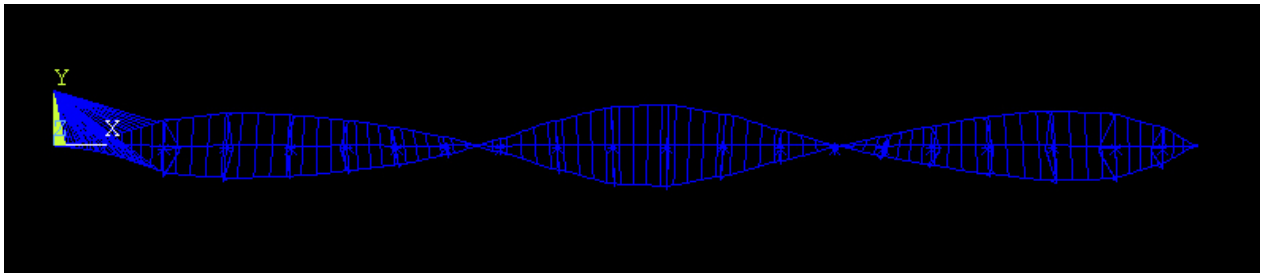

Mode 28

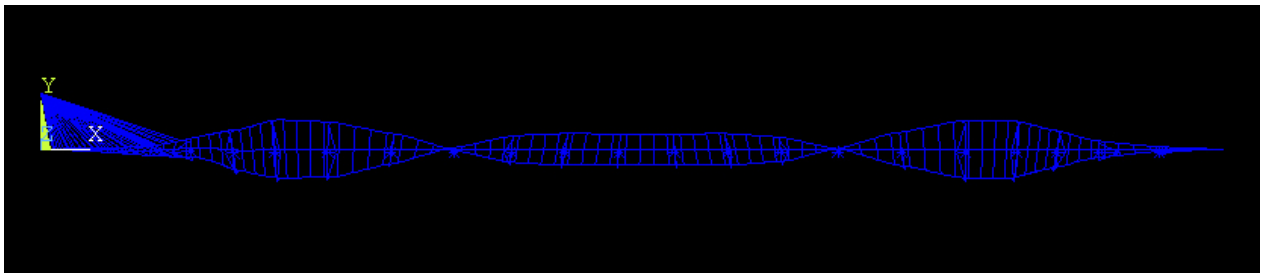

Mode 29

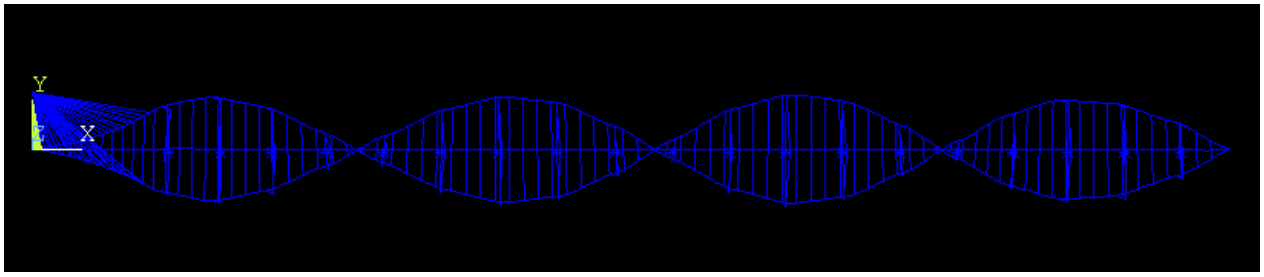

Mode 30

Appendix E

Results from Regular Wave Analysis with Unit Amplitude

Period		U_y	U_z	θ_x	A_y	A_z	$\ddot{\theta}_x$
2	min	−0.4709	−0.0974	−0.0022	−0.7172	−0.7060	−0.0113
	max	0.0384	0.2475	0.0029	0.6472	0.7861	0.0124
3	min	−0.6302	−0.1089	−0.0052	−1.1950	−0.4657	−0.0213
	max	0.1131	0.2598	0.0057	1.1457	0.4755	0.0216
4	min	−0.4938	−0.0890	−0.0061	−0.2378	−0.2378	−0.0124
	max	0.1086	0.2448	0.0058	0.2374	0.2374	0.0125
5	min	−0.6164	−0.1339	−0.0160	−0.4789	−0.2653	−0.0252
	max	0.3114	0.3002	0.0165	0.4813	0.2658	0.0250
6	min	−0.4522	−0.0953	−0.0043	−0.0724	−0.1491	−0.0038
	max	0.0713	0.2247	0.0047	0.0721	0.1490	0.0038
7	min	−0.6342	−0.2769	−0.0155	−0.2298	−0.2274	−0.0120
	max	0.2955	0.3899	0.0159	0.2297	0.2269	0.0119
8	min	−0.4652	−0.7035	−0.0051	−0.0668	−0.4844	−0.0025
	max	0.1049	0.8811	0.0055	0.0663	0.4906	0.0025
9	min	−0.6189	−1.3009	−0.0133	−0.1304	−0.6747	−0.0064
	max	0.2633	1.4631	0.0137	0.1319	0.6697	0.0063
10	min	−0.6750	−2.0327	−0.0155	−0.1273	−0.8335	−0.0060
	max	0.3281	2.2120	0.0157	0.1273	0.8335	0.0060
11	min	−0.7248	−2.9322	−0.0148	−0.1211	−0.9795	−0.0047
	max	0.3623	3.1032	0.0148	0.1210	0.9807	0.0047
12	min	−0.7495	−5.0877	−0.0194	−0.1106	−1.4138	−0.0053
	max	0.3924	5.2659	0.0201	0.1099	1.4133	0.0053
13	min	−0.8458	−3.5398	−0.0260	−0.1151	−0.8241	−0.0060
	max	0.4936	3.5702	0.0264	0.1150	0.8225	0.0060